Journal of Materials Chemistry A

REVIEW

View Article Online
View Journal | View Issue

Cite this: J. Mater. Chem. A, 2018, 6, 21747

Recent advances in the preparation, characterization, and applications of two-dimensional heterostructures for energy storage and conversion

Pratteek Das, [ac] Qiang Fu, [ab] Xinhe Bao [ab] and Zhong-Shuai Wu *[a]

Graphene and other two-dimensional materials (2DMs) have attracted intensive interest for use in energy storage and conversion systems because of their unique structure and remarkable properties. Although significant progress has been made in this field, certain intrinsic limitations obstruct the achievement of desired properties. 2D heterostructures, upon stacking or stitching different 2DMs in well-defined sequences or patterns, could significantly entail drastic changes in their properties, and thereby synergistically combine the merits of individual 2DMs while eliminating their related drawbacks. Herein, we provide a topical review of recent advances in the preparation and characterization of 2D heterostructures for energy-related applications. Firstly, an introduction is given to the definition and importance of 2D heterostructures, followed by their typical categories of vertically stacked heterostructures and horizontal in-plane heterostructures reported so far. Secondly, the state-of-the-art synthesis approaches to fabricate 2D heterostructures, including mechanically aligned transfer, chemical vapor deposition, liquid exfoliation and self-assembly, and layer by layer self-assembly, are introduced in detail. Then, the current status of advanced characterization techniques like scanning probe-, electron-diffraction-, X-ray-, and spectroscopy-based techniques that are critical for the accurate identification of 2D heterostructures and understanding of the performance-enhancing mechanisms of devices is systemically summarized. Furthermore, recent applications of 2D heterostructures in energy storage

Received 17th May 2018
Accepted 8th August 2018

DOI: 10.1039/c8ta04618b

rsc.li/materials-a

[a]Dalian National Laboratory for Clean Energy, Dalian Institute of Chemical Physics, Chinese Academy of Sciences, 457 Zhongshan Road, Dalian 116023, China. E-mail: wuzs@dicp.ac.cn

[b]State Key Laboratory of Catalysis, Dalian Institute of Chemical Physics, Chinese Academy of Sciences, 457 Zhongshan Road, Dalian 116023, China

[c]University of Chinese Academy of Sciences, 19 A Yuquan Rd, Shijingshan District, Beijing, 100049, China

Pratteek Das received his MSc degree from the Indian Institute of Technology, Kharagpur in 2016. He worked on several projects on a wide range of topics like nanogenerators and crystallography in India, China and Germany before joining the 2D Materials & Energy Devices group at the Dalian Institute of Chemical Physics, Chinese Academy of Sciences (CAS) in 2017 as a PhD student, supervised by Prof. Zhong-Shuai Wu, under the sponsorship of CAS-TWAS President's Fellowship. His research interest involves the preparation and application of 2D heterostructures for energy storage devices like batteries and supercapacitors.

Qiang Fu obtained his BS in 1996 from the Beijing Institute of Technology and his PhD in 2000 from the same university. Subsequently, he joined the Max Planck Institute for Metal Research for his postdoctoral studies under the sponsorship of the Max Planck Fellowship. In 2005, he moved to the Fritz Haber Institute of the Max Planck Society. In 2006, he took a position at the Dalian Institute of Chemical Physics, CAS and became a full professor in 2008. His research interests concentrate on surface and interface catalysis.

(*e.g.*, lithium/sodium ion batteries, lithium sulfur batteries, supercapacitors, and micro-supercapacitors) and conversion (*e.g.*, hydrogen/oxygen evolution reactions and photocatalysis) are exemplified to highlight their positive synergistic effect. Finally, future challenges and prospective solutions that may direct the growth of 2D heterostructures and their energy-related applications are proposed.

1. Introduction

The term heterostructure was initially defined, originating from multiple heterojunctions, which commonly referred to the interfaces that occur between any two layers or regions of dissimilar crystalline materials with different properties.[1] This kind of engineered heterostructure has aided the realization of some astounding applications and shows immense potential that is yet to be tapped,[2–4] and becomes very interesting in particular when we reduce one of the dimensions to the nanoscale. In this review, a 2D heterostructure refers to the system of stacking or stitching two or more distinct two-dimensional materials (2DMs) that form a well-defined interface/junction called a heterointerface/heterojunction, which synergistically combines the advantages of individual 2DMs while eliminating their related drawbacks.

Discovered by the prestigious Nobel Prize awardees Novoselov and Geim, the synthesis of 2DMs started with the mechanical exfoliation of graphite using scotch tape to obtain monolayer and few-layer graphene.[5] This method was simple but it was the experiment that changed the course of scientific research and ushered the era of intensive studies on graphene and its unique properties.[6] Within a short period of over a decade, there are over 110 000 publications on graphene recorded by the web of science. Currently, a large pool of other 2DMs have also been synthesized and their properties are being explored intensively. Therefore, it is not difficult to imagine the magnitude of research dedicated to 2DMs. One outcome of this intensive research is the study related to the synthesis and applications of 2D heterostructures.

The discovery of graphene and other 2DMs obtained from metal oxides (MOs), transition metal dichalcogenides (TMDCs),[7] MXenes,[8,9] phosphorene,[10,11] *etc.* and the subsequent study of stacking these 2DMs has made 2D heterostructures the buzzword in the present scientific community. As we know, individual 2DMs no matter how good they are tend to show characteristic weaknesses in certain applications. But, as soon as they are rationally stacked with two or more 2DMs, synergistic effects become evident and as a whole, a robust material with enhanced performance is observed. Owing to this, a myriad of applications that include spintronics,[12] superconductivity,[13] catalysis,[14] energy storage,[15] and optoelectronics[16] have been widely explored (Fig. 1).

This review will delve into the depths of 2D heterostructures and provide a comprehensive overview of the main preparation methods (*e.g.* mechanical exfoliation and aligned transfer, chemical vapor deposition (CVD), liquid exfoliation and self-assembly, and layer by layer (LBL) self-assembly), advanced characterization techniques (*e.g.* scanning probe-based, electron-diffraction-based, X-ray based, and spectroscopy-based techniques) that are useful for the accurate identification of 2D heterostructures, and their applications in energy storage (*e.g.*, lithium/sodium ion batteries, lithium sulfur batteries, supercapacitors, and micro-supercapacitors) and conversion (*e.g.*, hydrogen/oxygen evolution reactions and photocatalysis). Also, the challenges that have not yet been overcome and some critical scope for future studies will be discussed. This review will

Xinhe Bao received his PhD in physical chemistry from Fudan University, China, in 1987. He moved to Germany in 1989 and worked as an Alexander von Humboldt Fellow at the Fritz-Haber Institute in Berlin. In 1995 he came back to China and joined the Dalian Institute of Chemical Physics as a full professor. He is a member of the Chinese Academy of Sciences, and a Fellow of the Royal Society of Chemistry. His research activities focus on the fundamental understanding of catalysis by nanotechnologies and in situ characterization techniques, and their applications to the development of new nanocatalysts and novel catalytic processes related to energy conversion and storage.

Zhong-Shuai Wu received his PhD from the Institute for Metal Research, CAS in 2011, and worked as a postdoctoral fellow at the Max-Planck Institute for Polymer Research in Germany during 2011–2015. Then he became a full Professor and group leader of 2D Materials & Energy Devices at the Dalian Institute of Chemical Physics, CAS. His research interest involves graphene and 2D materials for supercapacitors, batteries, and flexible and micro-scale energy storage. He has published 70+ articles in Energy Environ. Sci., Adv. Mater., Nat. Commun., J. Am. Chem. Soc., ACS Nano etc., with a total citation of >14600 times. He is a guest editor of Energy Storage Materials, and a guest editor and section editor of the Journal of Energy Chemistry and international advisory board of Materials Research Express and J. Phys Energy.

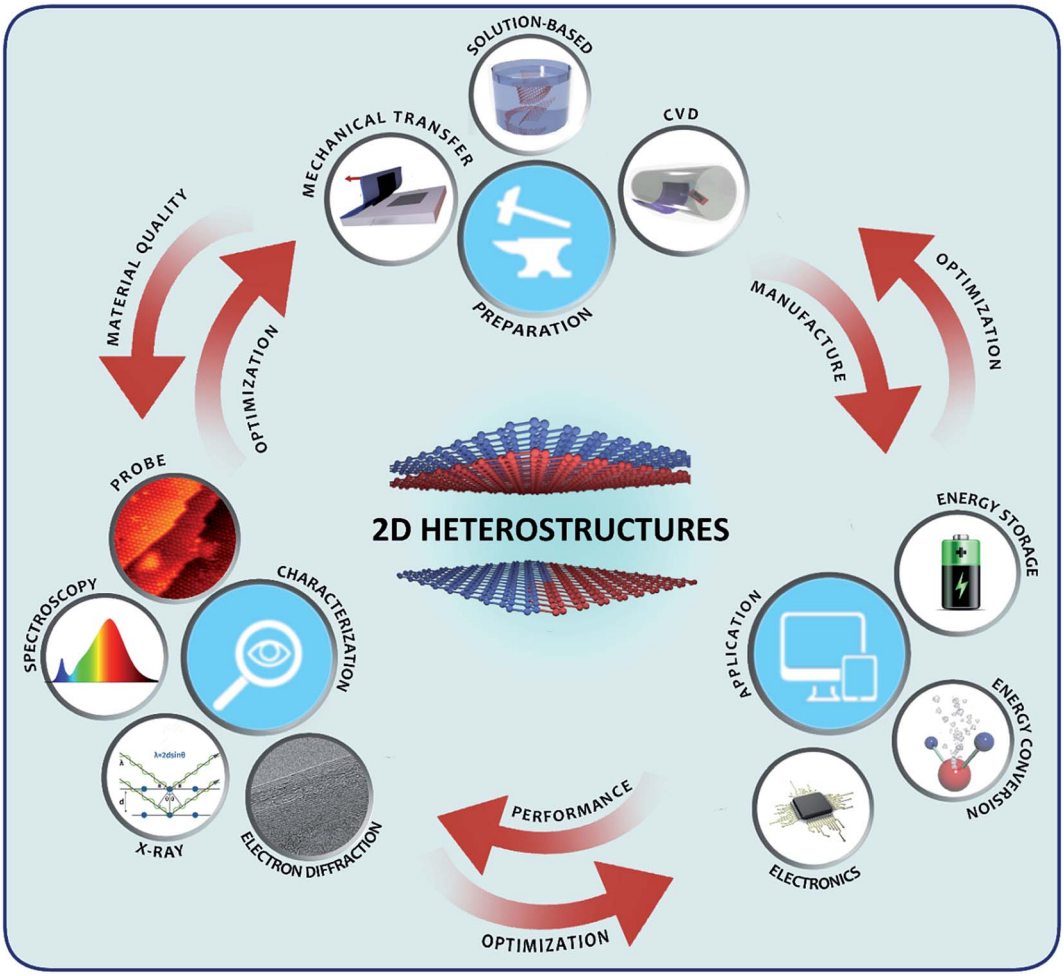

Fig. 1 Scheme of the preparation, characterization, and applications of 2D heterostructures.

distinctly consider only 2D heterostructures where alternate stacking of individual 2DMs has been achieved giving rise to a well-defined heterojunction/heterointerface involving strong interactions. It is very different from conventional composites to create individual 2DMs with nanoparticles or simply mix different 2DMs existing as separate phases such that the degree of synergy is quite limited. This difference and the added advantages of 2D heterostructures will be discussed in detail along with providing a toolbox for identifying them and understanding mechanisms using several characterization techniques in the subsequent sections. We focus on an important emerging class of materials which holds great potential to solve the related shortcomings of individual 2DMs and their composites. We hope that this review will offer a clear bird's eye view on the current status and future directions of 2D heterostructures.

2. Importance of 2D heterostructures

The study of 2D heterostructures is of great importance because individual 2DMs have certain intrinsic shortcomings that they cannot overcome on their own. As a typical example, graphene is a wonder 2D material with superior electrical conductivity[17] and mechanical strength[18] that rivals metals and shows promising applications in electronics,[19,20] transparent conducting films,[21] and energy storage and conversion.[8,22–24] But it is difficult for graphene to be directly used in transistors because it doesn't have a bandgap. It is well known that graphene has a Dirac cone band structure which gives it incredible charge carrier mobility,[25] but without a bandgap that transistor won't switch off, making it impossible to apply graphene-based transistors in logic gates.[26] Several strategies have been employed to create an artificial bandgap in graphene. One method is to apply electric fields perpendicular to the sheet stacking direction, mechanically stress the material, and engineer graphene nanoribbons.[27] Although it was met with success it comes nowhere near replacing the silicon-dominated industry with such performance. Also, such a method cannot be practically applied in real mass-produced devices. Similarly, for energy storage devices, graphene with a large surface area and superior conductivity offers a good solution for improving the power density and energy density of supercapacitors compared to the previously used nanocarbons.[28] However, it is also observed that graphene obtained from reduced graphene oxide (rGO) with serious agglomeration doesn't show as high conductivity and capacitance as pristine graphene.[29–31]

TMDCs are another class of 2DMs with wide-ranging applications, such as energy storage and optoelectronics. But the solution processability of TMDCs presents a major challenge as it is hard to obtain high quality depositions using scalable solution-based methods, thus reducing electronic performance.[32] In TMDC-based energy storage devices, the initial charge–discharge capacity is high, but they usually suffer from poor structural stability during large ion intercalation and de-intercalation.[33] Also, monolayer to few-layer TMDCs are semiconducting in nature, which is a significant drawback taking into account electrode conductivity.[34]

It should be emphasized that the combination of graphene and TMDCs in the form of heterostructures led to some unprecedented observations in MoS_2 electrodes for lithium ion batteries (LIBs). As demonstrated by Chang *et al.*, MoS_2 and graphene formed heterostructures, making it possible to vary the interlayer spacing by changing the ratio of TMDC to graphene, which in turn mitigated the volume change inherent to TMDCs (Fig. 2a and b). It also facilitated the fast diffusion of lithium ions along the 2D channels, leading to a great improvement in electrochemical performance. Furthermore, the power density was also significantly enhanced due to the conductive nature of graphene.[35] So it is quite evident that forming 2D heterostructures can diminish the shortcomings of individual 2DMs, and is particularly attractive for energy storage application.

As another example, it is known that the mechanism of catalytic activity of any material depends on the surface potential, relative position of conduction and valance bands, and electron density (Fig. 2e).[39] Of great importance is that 2D heterostructures could precisely tune these properties because the electronic properties of 2DMs change when they are brought into near proximity with each other. Also, the region between two layers can act as a nanoreactor[40] (Fig. 2d). More significantly, this concept can be extended to 2D heterostructures. Furthermore, 2D heterostructures have also been the subject of computational simulation. Computational analysis of MnO_2/graphene/MnO_2 heterostructure shows an interfacial charge transfer from graphene to MnO_2, which induces half-metallicity in the latter. Also, there is spin splitting at the Dirac point creating a non-trivial gap between the opposite spin bands, which is important in guiding research in spintronics.[41]

These are just a few examples of 2D heterostructure synergy that can result from such a nanoscale architecture. By careful

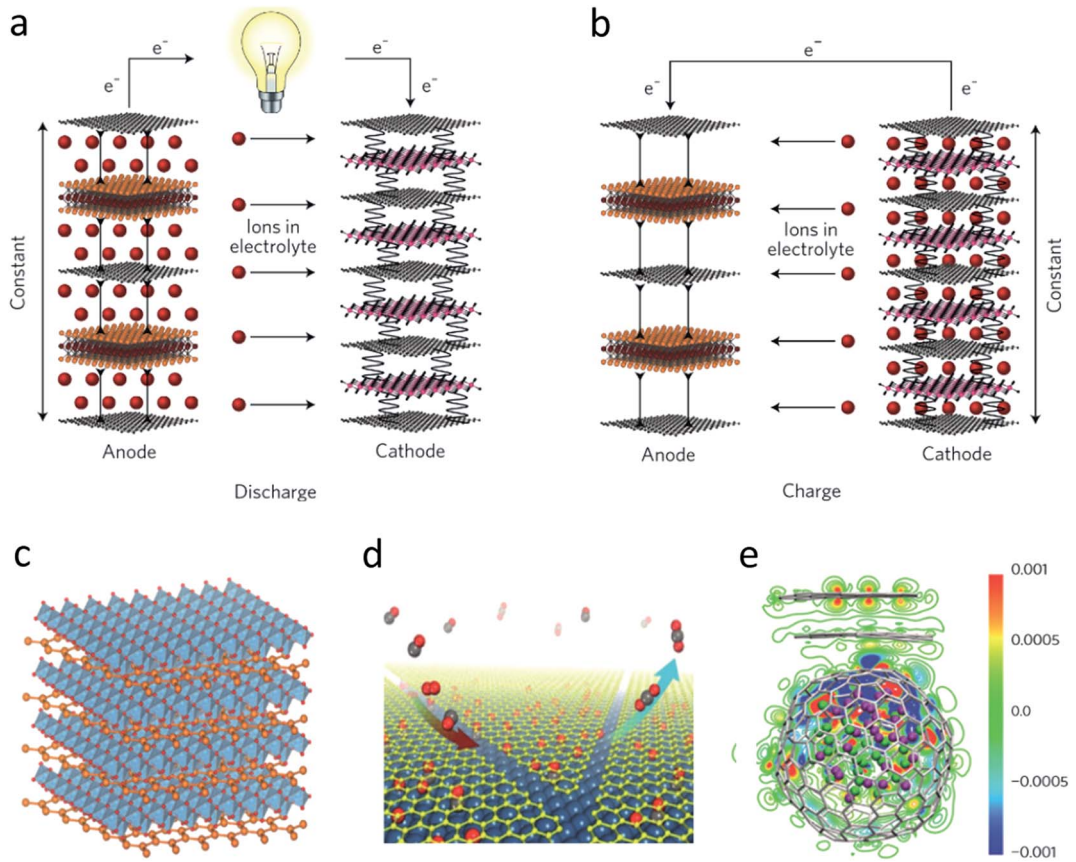

Fig. 2 (a) The discharge and (b) charge process of a LIB with heterostructured electrodes, showing the preservation of the interlayer distance that suppresses the volume change inherent to intercalation, thus improving the cycling stability of LIBs. Black connectors between the layers represent pillaring molecules that are components of the heterostructure.[36] Copyright 2017, Nature Springer. (c) Schematic of graphene based heterostructures applicable for catalysis (red layer is graphene).[37] Copyright 2015, American Chemical Society. (d) Nanoreactor at the 2D interface.[38] Copyright 2014, National Academy of Sciences. (e) Co–Ni nanocluster encapsulated by graphene layers, resulting in the redistribution of electron densities (red represents high and blue represents low density).[39]

and rational rearrangement of the composition, ratio, order and size of 2D heterostructures, more novel features could come to light. Therefore, this calls for the urgent need to turn our attention towards 2D heterostructures.

3. Types of 2D heterostructures

Before going into the details, it is of utmost importance to have a basic understanding of the types of 2D heterostructures. This is invaluable because the synthesis approach and the subsequent application can vary depending on the types of heterostructures. Typically, there are two broad categories of heterostructures, corresponding to the wide domain of applications – vertically stacked heterostructures (Fig. 3a) and horizontal in-plane heterostructures (Fig. 3b).

Vertically stacked heterostructures are those in which two or more 2DMs have interfacial contact which may be either due to strong (covalent) or weak (van der Waals) interaction. The identifier is the formation of a well-defined heterointerface between the faces of different 2DMs. The order of stacking is important because it may change the properties accordingly; therefore, the properties can be tuned by rationally choosing the stacking order. Ideally, any number of layers can be stacked in any order, but as will be discussed in the subsequent sections this has been a rather difficult task so far, and has been achieved by only mechanically stacking 2DMs. Horizontal in-plane heterostructures have at least two different 2DMs stitched together at the edge. This stitching is a result of strong bonding between the atoms at the edge sites. In most cases, one 2DM is grown at the edge site of another 2DM and the identifier is a well-defined heterojunction between the edges of different 2DMs. The term heterojunction may also be used instead of heterointerface in the case of vertically stacked 2D heterostructures but in this review we will use heterojunction in relation to horizontal in-plane heterostructures. Recently, other heterostructures with unique designs have been reported,[42] for example, a vertically aligned 2DM on the surface of another 2DM (Fig. 3c). This can be considered a heterostructure because there is a well-defined junction between the two materials, which affects the properties in ways differing from conventional composites as will be discussed further in the subsequent sections. There are also possibilities of imagining new-generation heterostructures that may have unprecedented applications, as visualised in Fig. 3d.

4. Methods of synthesis

The surprisingly simple method of mechanically peeling 2DMs out from their bulk layered parent materials also applies to synthesizing 2D heterostructures of the highest quality. But as will be discussed later, there are certain shortcomings related to its scalability. Therefore, it is necessary to consider other approaches like CVD and solution-based methods. As we know, no method is completely versatile. Each has its own advantages and disadvantages, and thereby the aim of this section is to scrutinize and illuminate the strengths and weaknesses of each method. The method used to obtain 2DMs determines their morphology and structure, such as thickness, layer number, lateral size, and grain boundaries, which consequently decide other physiochemical properties like electronic band structure, ion intercalation, and charge carrier mobility.[43–46] In the following, we begin with the method of mechanical exfoliation that started this 2D revolution. A table considering several aspects of different methods has been given for comparison of the advantages and disadvantages, as shown in Table 2.

4.1. Mechanical exfoliation and aligned transfer

This method, involving mechanical exfoliation, controlled transfer of a 2DM, and subsequently fabricating heterostructures, is also known as a deterministic placement

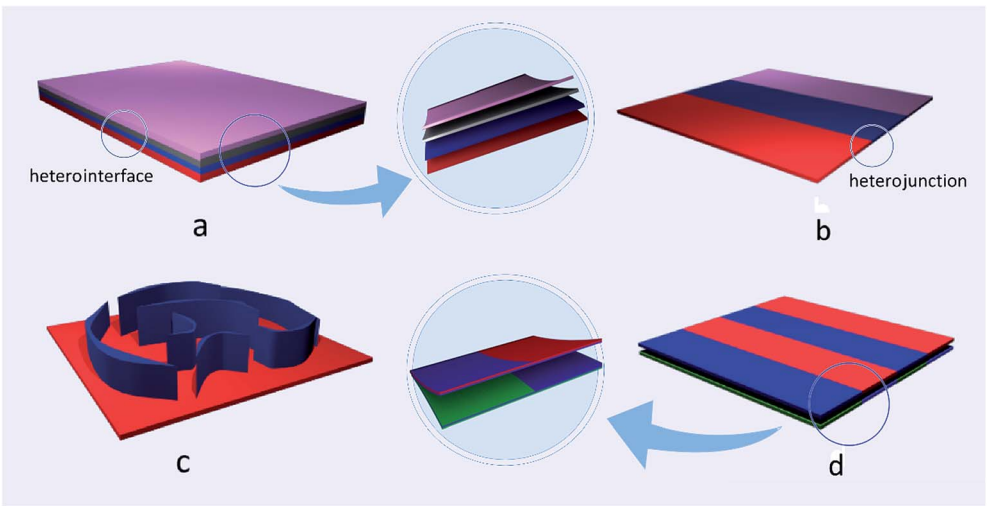

Fig. 3 Schematic representation of 2D heterostructures, (a) a vertically stacked heterostructure (with a heterointerface), (b) a horizontal in-plane heterostructure (with a heterojunction), (c) a special heterostructure with a vertically aligned 2DM on another 2DM, and (d) a new-generation complex heterostructure (with both a heterointerface and a heterojunction).

Table 1 Effect of different growth promoters on the morphology and quality of 2D MoS_2 films[92]

Growth promoter[a]	Vaporization temperature[b] (°C)	Approx. domain size (μm)	Overall quality
PTAS	>600	60	Excellent
F_{16}CuPc	>430	60	Excellent
PTCDA	>450	Continuous	Good
CuPc	>430	30	Good

[a] PTAS – perylene-3,4,9,10-tetracarboxylic tetrapotassium salt, F_{16}CuPc – copper(II) 1,2,3,4,8,9,10,11,15,16,17,18,22,23,24,25-hexadecafluoro 29*H*,31*H*-phthalocyanine, PTCDA – 3,4,9,10-perylene-tetracarboxylic acid-dianhydride, and CuPc – copper phthalocyanine. [b] Vaporization temperature of the growth promoter.

technique. Pioneered by Dean and co-workers,[47] this method was developed to place a graphene layer on hexagonal boron nitride (h-BN). Prior to that a Si/SiO_2 substrate was commonly used to prepare graphene-based electronics. Due to the highly disordered nature of such a substrate, the characteristics of graphene material were far inferior to predicted values. Hence, a suitable alternative was found in h-BN since its surface is atomically smooth and is devoid of any dangling bonds or charge traps. The observed properties of the graphene/h-BN heterostructure in this study were indeed superior to prior findings.[5,48–53] This is considered as the first demonstration of the promising application of 2D heterostructure. The method used by Dean *et al.* has come to be known as the PMMA (poly-methyl methacrylate) transfer method (Fig. 4a). The basic strategy is to transfer a 2DM onto a hydrophobic polymeric layer like PMMA coated over a Si/SiO_2 substrate which is covered with a water-soluble layer like poly-vinyl alcohol (PVA). Once the transfer has taken place, the assembly is immersed in water, leading to the dissolution of the water-soluble PVA layer. This causes PMMA to float in water with the graphene layer attached to it. The PMMA layer can then be carried onto a glass slide. The next step is to transfer that layer onto another 2DM that has been mechanically exfoliated onto another substrate. It is important to note here that this transfer process requires precise alignment and control that cannot be done accurately by hands. Therefore, the systems like optical microscopes for locating and micromanipulators for aligning the flakes are used in conjunction manually to carry out the task. The use of optical microscopes and micromanipulators is an essential step but the process of separating the flake from its initial substrate may vary. For example, a technique known as the wedging transfer method (Fig. 4b) was used by Schneider *et al.*[54] who used water intercalation to transfer a flake sandwiched between a hydrophobic polymer and hydrophilic substrate. The intercalation of water delaminates the polymer from the parent substrate, making it float. Later by using micromanipulators, it can be placed on top of the target 2DM exfoliated onto another substrate. Subsequently, the polymer is dissolved with acetone, leaving us with the 2D heterostructure. There is yet another method that uses a sacrificial polymer of Elvacite, which is melted away by heating the target substrate before placing the transfer assembly onto it.[55]

One feature common to all the methods discussed above is the use of a sacrificial layer and wet chemistry. The use of sacrificial layers and other chemicals add another parameter to the experiment, which somewhat reduces control over the morphology and chemistry of 2D heterostructures. These might be useful for certain applications while remaining an obstacle for others. For instance, the wedging method mentioned above can lead to the formation of wrinkles due to capillary forces. While the wrinkled features are useful for applications like energy storage or lasing,[56] it is highly undesirable for certain applications such as high-speed field effect transistors (FETs), optical switches and corrosion inhibition.[57] Even though control over wrinkles can be achieved by varying substrate properties (hydrophobic substrate) as reported by Calado *et al.*,[58] it is still desirable to have dry techniques for faster transfer and higher yield. One such method of PDMS dry peeling was demonstrated by Castellanos-Gomez *et al.*[59] In this approach, they first exfoliated a 2DM onto a PDMS layer. This PDMS layer acts as a stamp for transferring the 2DM onto the target substrate containing the target 2DM. Once the two come in contact, the "PDMS stamp" can be gently peeled leaving

Table 2 Comparison of different methods for obtaining 2D heterostructures

Method	Quality/defects/ impurities	Number of layers	Hetero-structure yield	Typical applications	Cost	Type of hetero-structures	Flake size/structure
Mechanical exfoliation and aligned transfer	High quality, mechanical defects, polymer residues	Virtually any number of layers	Low	Fundamental research of all types	Low	Vertical	Several to tens of micrometers/flat or wrinkled flakes
CVD	High quality, chemical impurities, polymer residues	2∼ few layers	Moderate to high	Electronics, optoelectronic, spintronics	High	Vertical and in-plane	Continuous films of wafer size/flat, porous, complex
Liquid exfoliation and self-assembly	Unintentional functionalization, composites instead of heterostructures may be formed	Few layers and more (LBL allows a lower number of layers)	High	Energy storage, energy conversion	Low to moderate	Vertical (in-plane very difficult)	Hundreds of nanometers to several micrometers/flat, wrinkled, porous, complex

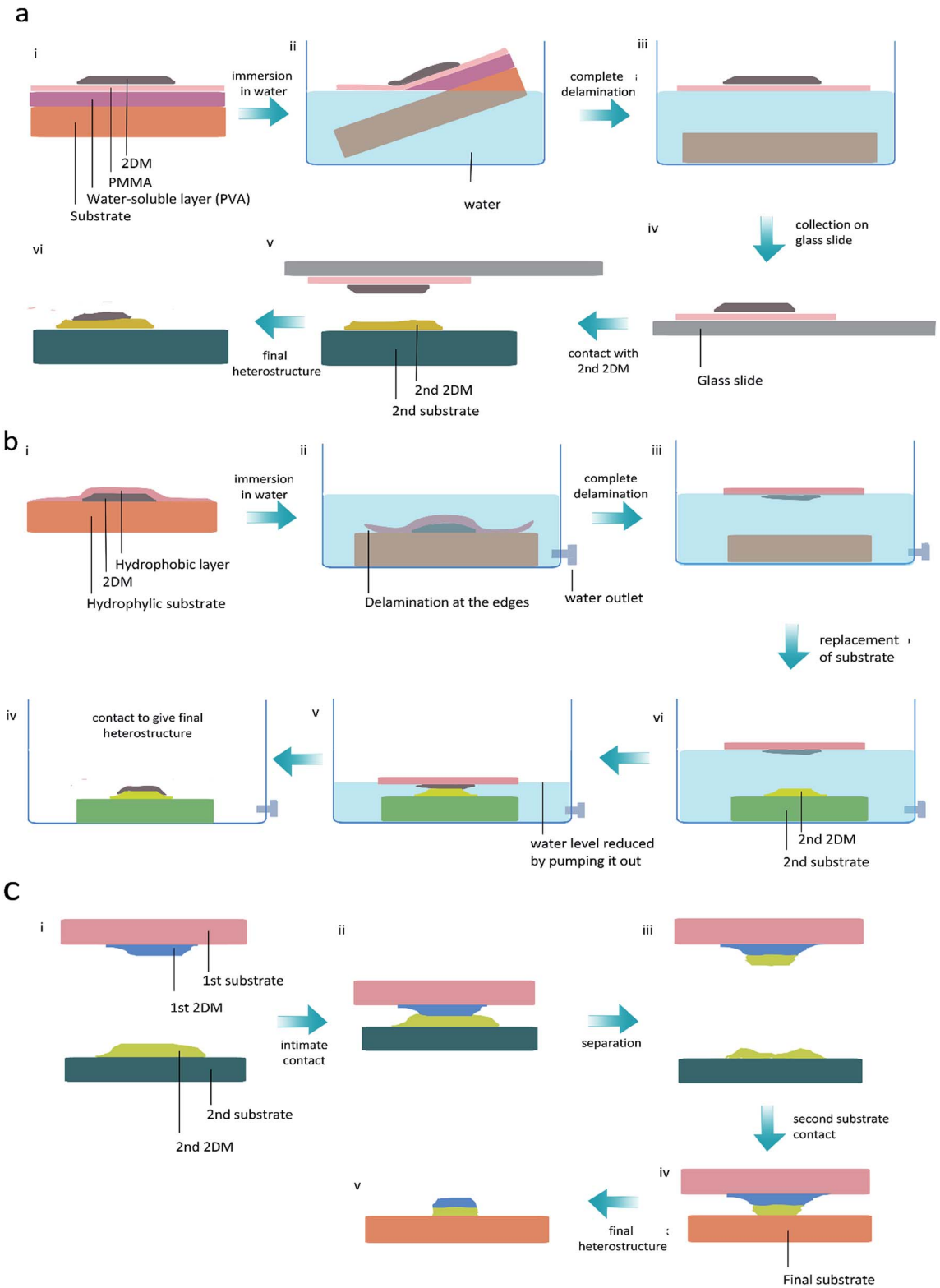

Fig. 4 Schematic showing different mechanical transfer and aligning methods for creating 2D heterostructures: (a) PMMA transfer method, (b) wedging method, and (c) van der Waals lift and transfer method.

a heterostructure on the target substrate. It should be noted that a 2D nanosheet will have strong van der Waals interaction with another 2D nanosheet (Fig. 4c). The ease of peeling the polymer depends on the adhesion strength between the 2DM and substrate. This van der Waals interaction can also be used as an effective method for a dry peel-transfer method, which doesn't bring polymer peeling into the scene.[60] Everything in this method is the same as the previous method except the fact that

h-BN mounted on PDMS is used as the "peeler". Since h-BN itself is atomically thin and can form a large contact area with other 2DMs, it has strong van der Waals interaction with them. Therefore, when pressed against another 2DM, it lifts the material off from the parent substrate. Subsequently, the other 2DM will also behave like h-BN in terms of van der Waals interaction, leading to the formation of vertically stacked heterostructures. This method has been used to form heterostructures of h-BN and graphene,[60] h-BN and TMDCs[16] *etc.* It is the cleanest method among all the methods discussed above which leaves neither chemical nor polymer residue. At first sight it may appear that these methods could not possibly find any place in energy related applications. But it should be noted that these methods can produce the highest quality heterostructures with minimal defects and a simple morphology. This ultimately makes mechanically stacked heterostructures an attractive platform for studying the mechanisms of electrochemical systems. This is discussed in Section 7.[248]

The choice of method depends on the end result that the researcher expects to obtain or the properties that are to be studied. If minimal contamination is required, then van der Waals lift and transfer is recommended. But this method is time consuming. If the rapid production and higher yield of heterostructures with an atomic level of flatness is desired, then PDMS based dry peeling is the method of choice. For studying the lasing or energy storage mechanism of wrinkled heterostructures, the modified wedging technique should be chosen since it allows a certain degree of control over wrinkle formation and orientation.[58] But it is a more complicated approach compared to the others.

To summarize the above discussion, mechanically stacking 2DMs to obtain 2D heterostructures generally enables the synthesis of a flat morphology with high quality (low structural defects)[55] and having significant changes to the properties like carrier mobility and conductivity change[47] which may be used to study the mechanisms of energy storage devices. On the other hand, it may also be used to create certain structural features like wrinkles[58] that may serve as a platform for studying lasing and possibly energy storage systems. A more comprehensive summary and comparison with other methods is presented in Table 2.

Although these methods produce some of the highest quality 2D heterostructures and have aided the advancement of fundamental science, the obvious drawback is that they are not scalable for the mass production of the designed devices. To achieve this we must look at the ways that can provide us rapid production and high yield while maintaining the quality of such 2D heterostructures. The next section takes on one of the challenges of the mechanical exfoliation technique – high yield with good quality 2D heterostructures grown *via* the CVD strategy.

4.2. CVD growth

CVD is a method for producing good quality 2DMs with a large area (at least wafer size), making it an important method for fundamental research. CVD growth is a big and vibrant field in itself of which 2D heterostructure synthesis is only a part. In this section, specific focus will be given to studies that deal with 2D heterostructure synthesis rather than just 2DMs. Nevertheless, it is important to understand the parameters that affect the growth of 2DMs in general by using this method for understanding the mechanism and optimizing heterostructure synthesis, thus making it a good stepping stone to start off the discussion.

4.2.1. Parameters of CVD growth. As the name suggests CVD is a method of depositing chemical vapors on a substrate, and therefore it goes without saying that the starting material and substrate are both important parameters in the entire process. And since vapors (gases) are involved, it is intuitive that the temperature and pressure also play an equally important role in the quality and rate of deposition. In this section, we will discuss these parameters briefly to get an idea about what factors affect the final properties of the films obtained and subsequently we will discuss how they are useful in preparing 2D heterostructures.

4.2.1.1. Starting material. The starting material, also known as the precursor, is the chemical reactant, which decides to a large extent how the final film will look like. It can be gaseous, liquid or solid. A gaseous starting material is often more advantageous compared to solids and liquids in the sense that they are easy to deal with and a steady flow can be ensured throughout the process of CVD. This results in accurate control of the morphology, structure and size of the final 2DM. Liquid and solid starting materials on the other hand are converted into the vapour state by applying heat, and thus the concentration of this vapour may vary depending on the physical conditions to which it is subjected to. For example, the temperature at the precursor source can greatly affect the vapour pressure of solid material precursors.[61] This can create a concentration gradient in the span of CVD, leading to undesirably non-uniform deposition.

It is quite fortunate that graphene can be grown from gaseous precursors of CH_4 and H_2.[62–65] But for TMDCs, a solid or liquid state precursor is the trend.[66–68] The role of the precursor in determining the size of the 2D film deposited is evident from several studies. These studies suggest that a low nucleation density is important for large size crystal growth.[69,70] A method demonstrated by Lee *et al.* used liquid MoO_3 and solid sulfur precursors to create a unique solution processed precursor deposition.[71] This resulted in a low super-saturation state of the vapour reactants, which in turn reduced the nucleation density. The as-obtained single crystals were as large as 400 micrometers and predominantly monolayers. The precursor also determines the operating temperature. For instance, with a common gaseous precursor CH_4, the operating temperature is around 950 °C, while if benzene,[72] naphthalene[73] or pyridine[74] is used, the temperature may be reduced to less than 600 °C and even to 300 °C. By varying the ratio of precursors, a balance can be struck between the growth and etching, resulting in a different morphology and pattern of the final film.[75] Another important 2DM, h-BN, which is a good dielectric and shows superior mechanical properties also uses the sublimation of a solid precursor like ammonia borane.[76]

Quite recently, the metal–organic CVD technique has been demonstrated for the deposition of TMDCs.[77,78] Metal–organic precursors are solid[77] or gaseous,[78] but both of them are found to be more advantageous for the growth of large scale and uniform 2D TMDCs. Also, the composition and morphology of the resulting 2D layers can be tweaked conveniently in this case. These experiments also demonstrate the direct correlation between the precursor control and resultant 2D layer.

4.2.1.2. Substrate. The substrate is an important parameter in the CVD growth process because it affects not only the growth of a 2DM but also its final properties. A substrate may simply be a platform for growing the material or may assist the process of growth with catalytic effects. The most commonly used substrates for graphene growth are copper (Cu),[79–81] nickel (Ni),[82] and cobalt (Co),[83] but Cu trumps the list due to its low cost. A growth route utilizing van der Waals force instead of catalytic growth was demonstrated by Hwang *et al.*[84] The substrate used was a metal-catalyst-free sapphire. A detailed study by them has led to the understanding of the mechanism of such a catalyst-free growth and the importance of other parameters in conjunction with the sapphire substrate for the optimal growth of graphene. Interestingly, substrate properties have a profound effect on the number of layers and uniformity. This inference comes from the study of graphene growth on a Cu substrate with varied substrate conditions.[85]

TMDCs on the other hand are mostly grown on non-catalytic Si/SiO_2 substrates,[71] allowing for the easy fabrication of electronic and optoelectronic devices. Apart from this, CVD on sapphire, gold and silicon nitride substrates have also been reported.[86–88] The complete characterization of nucleation centres of TMDCs grown on a Si/SiO_2 substrate has led to some important insights into the mechanism of growth.[89] The growth of TMDCs was carried out using the standard method that is abundantly found in the literature.[90] The investigation was performed using aberration corrected transmission electron microscopy (TEM) and energy dispersive spectroscopy (EDS) mapping. It is revealed that the core–shell structure with a MoS_2–$MoSe_2$ TMDC fullerene inside it acted as the nucleation centre from where the monolayer grew (also known as the seed structure). This mechanism was found to be independent of the transition metal used, and thus can be extended to other TMDCs as well. Another detailed study with a different route of experimentation validated a similar seeding mechanism but with nanoparticles instead of fullerenes.[91] This illumination about the mechanism may be used for substrate engineering to grow TMDCs with varying physical and chemical properties.

Growth promoters or seeding promoters have proven to be an effective way of synthesizing high-quality TMDCs, in particular MoS_2. The substances used by Lee *et al.* were perylene-3,4,9,10-tetracarboxylic acid tetra-potassium salt (PTAS), perylene-3,4,9,10-tetracarboxylic dianhydride (PTCDA) and rGO.[90] This study systematically presents the effect of different growth promoters on the formation of a monolayer, but does not present a mechanism of how they work. Ling *et al.* took this one step further by discussing the effect of concentration of these growth promoters by varying the position of the substrate with respect to the growth promoters.[92] They also experimented with new aromatic growth promoters in different concentrations to judge the optimal conditions. Table 1 lists the growth promoters effective in producing large domain monolayers and their effect on the final film morphology. Also, since the smoothness of the substrate is emphasized in every CVD experiment, it is expected that the substrate surface morphology must play an important role in some aspects of the growth. Indeed, it was observed that the nucleation and orientation of the as-grown TMDC film could be guided along the atomic level terraces on the sapphire substrate on the *c*-plane.[93] Density functional theory and first principles calculations have shown that such effects on the nucleation and orientation of MoS_2 on a gold substrate[94] and graphene on a Cu substrate[95] are essentially due to the facet-dependent binding energy of the 2DMs concerned.

4.2.1.3. Temperature. The 2DM growth by the CVD process is temperature dependent. This is evident from the observation of temperature dependent nucleation and growth rate of graphene on a Cu substrate. Higher temperature enables higher growth rates while lowering nucleation density.[96] Subsequently, it affects the growth kinetics, which can be inferred from the morphology study of the obtained graphene layers. Temperature also affects the doping of 2DMs. In fact, under the same flow rates of NH_3 and CH_4, temperature overrides the doping precursor parameter. A reduction in temperature by 100 °C results in a five-fold increase in dopant concentration.[97] Similarly, under lower temperature the growth rate of N-doped graphene is lower, confirming the general trend of temperature dependence of the growth rate.[96]

Temperature becomes an important parameter for the TMDC growth *via* CVD because most common routes use solid precursors. Temperature affects the saturation pressure of sublimated solid precursors which may change the concentration of vapour. This can greatly influence the growth rate and quality. A systematic study of the effect of temperature on various properties like the yield, number of layers, flake size and flake shape provides some key insights into TMDC growth *via* CVD.[98] Interestingly, this experiment shows that temperature can change the regime of growth from thermodynamic to kinetic because it affects the sublimation speed and thus also changes the concentration and diffusion of active species. It was also observed that the monolayers were chemically unstable at higher temperatures resulting in abundance of few-layer growth. Not only the source temperature but also the substrate temperature is important. For instance, it has been observed that the reduction in substrate temperature results in lower mobility of carbon adsorbed on a copper substrate and decreases the lateral size of islands grown, leading to multilayer formation.[99]

4.2.1.4. Chamber pressure. There are several types of CVD processes, like atmospheric pressure CVD, low pressure CVD, and ultrahigh vacuum CVD, categorized by pressure in the growth chamber. Pressure directly controls the velocity of mass transport. The lower the pressure, the higher the velocity of mass transport. The advantage of operating at low pressure is the higher degree of exposure that the substrate receives, resulting in more uniform deposition. A direct relation between

the chamber pressure and final morphology of h-BN grown on copper foil was studied by Koepke *et al.*,[100] who observed that pressures lower than 2 torr resulted in uniform and highly crystalline growth whereas higher pressure led to the formation of amorphous non-uniform deposits although the growth rate was higher in the latter case. Such a behaviour was attributed to the incomplete thermolysis of the precursors at higher pressures (Fig. 5).

4.2.2. CVD growth of 2D heterostructures. An important part of 2D heterostructure fabrication is the ability to tune the properties for different applications by varying external parameters. However, one-step CVD growth doesn't allow the precise control over spatial and size distribution. Particularly for TMDC based heterostructures, there is a possibility of contamination between the transition metal precursors which hinders the achievement of a clear interface or boundaries. Moreover, there might be some inherent problems in the growth of specific heterostructures that might be overcome by tweaking the parameters discussed above. For example, Gao *et al.*[101] reported a switching between graphene/h-BN vertical and horizontal in-plane heterostructures by using temperature as a switching parameter (Fig. 13a). This was a consequence of h-BN etching by CO_2 above a particular temperature (900 °C). Though this method led to the discovery of never-seen-before control over the type of heterostructure, it had a slow growth rate. It is difficult to grow graphene on h-BN using CVD because h-BN isn't a suitable substrate for the growth of graphene, using the common gaseous precursors like CH_4. This is due to the fact that unlike Ni, Cu, and Co substrates, the CH_4 decomposition rate on hBN is lower. Also, h-BN is catalytically inert.[102] By rationally varying a parameter (in this case the precursor), Li *et al.* used nickelocene to achieve 8–10 times faster growth rates of graphene on h-BN.[102] This was a consequence of Ni deposition on h-BN, providing a catalytic effect for fast decomposition of the carbon precursor. These examples clearly show that the parameters discussed in the previous sections allow control over the fabrication of heterostructures using CVD.

There have been several reports about CVD being used as a step in conjunction with other techniques such as mechanical alignment to fabricate 2D heterostructures. There are still fewer reports concerning all CVD-grown heterostructures mainly due to the fact that not all 2DMs can be grown on top of one another. The next section will be a discussion about several important heterostructures fabricated using CVD techniques, and will focus on the parameter dependent optimization and tuning of heterostructure properties.

4.2.2.1. CVD growth of vertically stacked heterostructures. It is easily noticeable that in vertically stacked heterostructures the

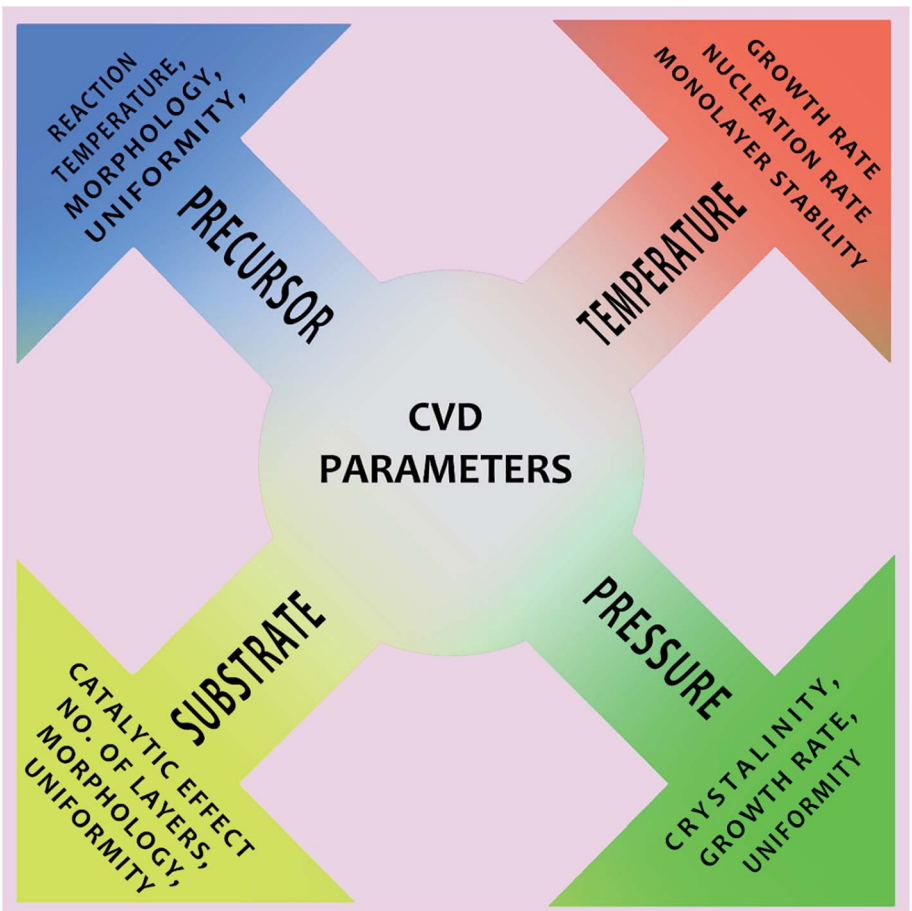

Fig. 5 Summary of CVD parameters and their effects on the different characteristics of the as-grown films.

interlayer distance can be considered as another parameter for varying the properties of the assembly. This has been substantiated in a recent study by Xu *et al.*[103] In this work the dependence of indirect recombination in TMDC heterostructures of CVD-grown WSe_2 and MoS_2 on the thickness of the insulating h-BN layer between them has been studied. The h-BN layer thickness has been adjusted by stacking multiple numbers of monolayers. The results of this experiment clearly show that dipole–dipole interactions between WSe_2 and MoS_2 are strongly dependent on the insulating layer thickness while keeping the input excitation constant. However, the method for stacking the CVD-grown h-BN is the mechanical alignment technique and not an all-CVD process. The one-step CVD growth was reported as early as 2014 in which the authors suggested a temperature-selective growth mechanism of WS_2 on MoS_2.[104] In a one-step process the simultaneous growth of both 2DMs takes place but due to the difference of vapour pressure of each precursor the nucleation rates differ. As a result, a vertically stacked heterostructure is formed. However, one-step CVD doesn't allow good control over the size of 2D heterostructures, which is limited to smaller than 20 μm flake size. To gain control over the size, a two-step CVD growth was used. Again, in this experiment, the temperature was an important parameter for the growth of different kinds of heterostructures. Nevertheless, this attempt makes a promising case for the fabrication of complicated heterostructures.[105]

A quite unique method of growing well-defined heterostructures was demonstrated by Xue and co-workers,[106] who used a photo-resist with rectangular patterns before depositing Mo over CVD-grown WS_2 layers, resulting in impressively ordered units of vertically stacked heterostructures. This work demonstrates the fabrication of multiple electronic device arrays using heterostructures grown on a single flexible substrate (Fig. 6d). Although the photodetection capability of this assembly was modest, this could pave the way for creating ordered heterostructures that might find applications in other fields. Notably, not only the shape but also the stacking sequence of different layers in 2D heterostructures can be precisely controlled. This was demonstrated with MoS_2/WS_2 heterostructures with stacking sequences A–A and A–B mediated by temperature,[107] which gives the possibility of flexibility in fundamental studies as well as with different stacking sequences. However, the number of layers in the stack is still limited.

TMDC/TMDC materials are not the only important class of heterostructures. A TMDC on graphene is also an interesting heterostructure thanks to its metal–semiconductor interface that enables the optoelectronic and electronic performance. Although the most studied method for such an architecture is mechanical exfoliation and alignment with applications ranging from FETs to DNA hybridization,[109–111] several CVD techniques have also been reported. Most notable among them is the large scale growth of MoS_2 on graphene with an effective device size of 4 cm^2 and integration of several FETs on a single substrate (Fig. 6a–e).[108] They used a patterned mask to establish graphene as an interconnect in FETs with properties superior to metals (Fig. 6f).[106] Even with the relative success of this class, TMDC/graphene heterostructures have been marred with certain limitations. The heterostructure area coverage remained quite small compared to the flake size of the individual 2DMs.[112] This hindered the successful integration of heterostructures into commercially viable electronic devices. However, recently there seems to be renewed hope. An all-CVD process was reported by Chen *et al.* in which they synthesised a 1 cm^2 continuous layer of MoS_2 on graphene.[113] Normally the MoS_2 domain size grown on graphene is at a submicron level due to the high temperature and longer duration required for MoS_2 growth under which graphene tends to degrade. However, it was observed that, with the introduction of H_2, larger domains could be obtained because H_2 mitigated the reactive oxygen

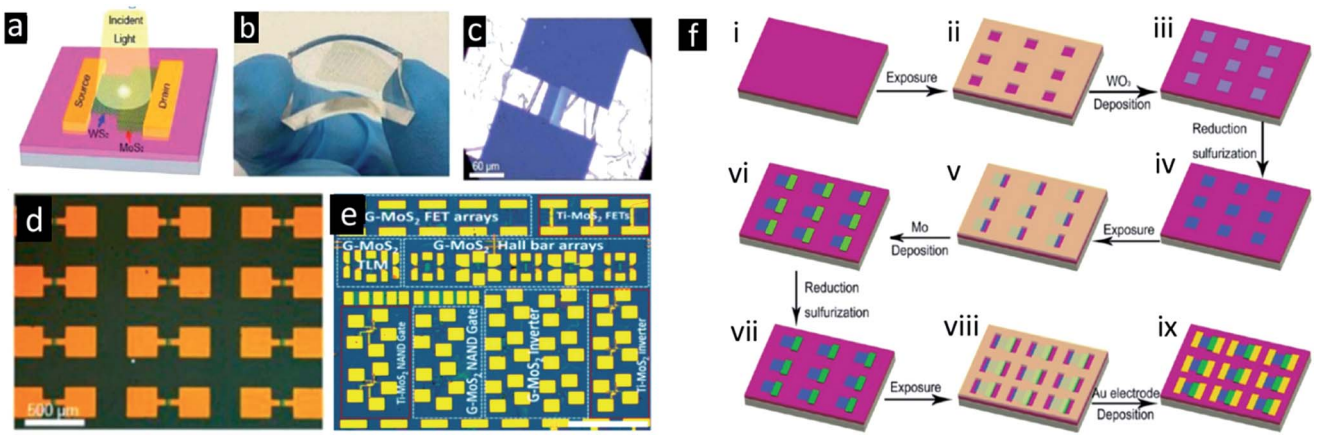

Fig. 6 (a) Schematic of a MoS_2/WS_2 vertical heterointerface phototransistor. (b) Photograph of arrays of devices fabricated from MoS_2/WS_2 vertical heterointerfaces on a PDMS substrate. (c) Optical image of a single MoS_2/WS_2 vertical heterointerface device on the PDMS substrate. (d) MoS_2/WS_2 vertical heterointerface device arrays on the SiO_2/Si substrate.[106] (e) Optical micrograph of a large-scale chip of MoS_2 devices using CVD-grown graphene as an electrode and interconnects as well as control devices and circuits using Ti/Au adjacent electrodes.[108] (f) Schematic for the preparation of MoS_2/WS_2 vertically stacked heterostructures and corresponding fabrication of devices.[106] Copyright 2016 and Copyright 2014, American Chemical Society.

evolved during MoO_3 decomposition, which would otherwise react with graphene and degrade it.

h-BN based vertically stacked heterostructures have exhibited many novel properties. For example, h-BN/graphene was able to show Hofstadter's butterfly and fractal quantum hall effects,[114] and WSe_2/h-BN showed an interlayer electron–electron interaction and electron–phonon coupling,[115] as well as effective passivating properties.[116] These studies used the mechanical exfoliation technique but there have been reports about combining it with CVD.[117] To overcome the disadvantages of this mixed method, an all-CVD process was developed by Fu *et al.*[116] Their detailed study demonstrates the growth of MoS_2 on h-BN on a wafer scale (5.08 cm) and subsequent fabrication of FET arrays.[106] The key novelty of this work lies in the operation in the thermodynamic regime to control the epitaxial alignment of the MoS_2 layer, resulting in the seamless merging of the grains to form a continuous and uniform film.

4.2.2.2. CVD growth of horizontal in-plane heterostructures. Horizontal in-plane heterostructures come with their own advantage of a larger, more vivid effective surface area, because both 2DM faces are exposed, while still having a covalent heterojunction, allowing us to fabricate complex heterostructures (Fig. 7h–j). Achieving lateral horizontal in-plane heterostructures is a much more complicated task than fabricating vertically stacked heterostructures, because unlike their vertical counterpart they require strict lattice matching and cannot just use van der Waals interaction to sustain themselves. This means that only bottom-up techniques can be used for their synthesis. And even then, not all materials can be stitched together because different 2DMs may have different lattice parameters. Therefore, only a few combinations of 2DMs have been tried so far. Out of the known bottom-up techniques, CVD is the most popular and intensively studied approach. In this sub-section, we will discuss the progress in achieving novel horizontal in-plane heterostructures.

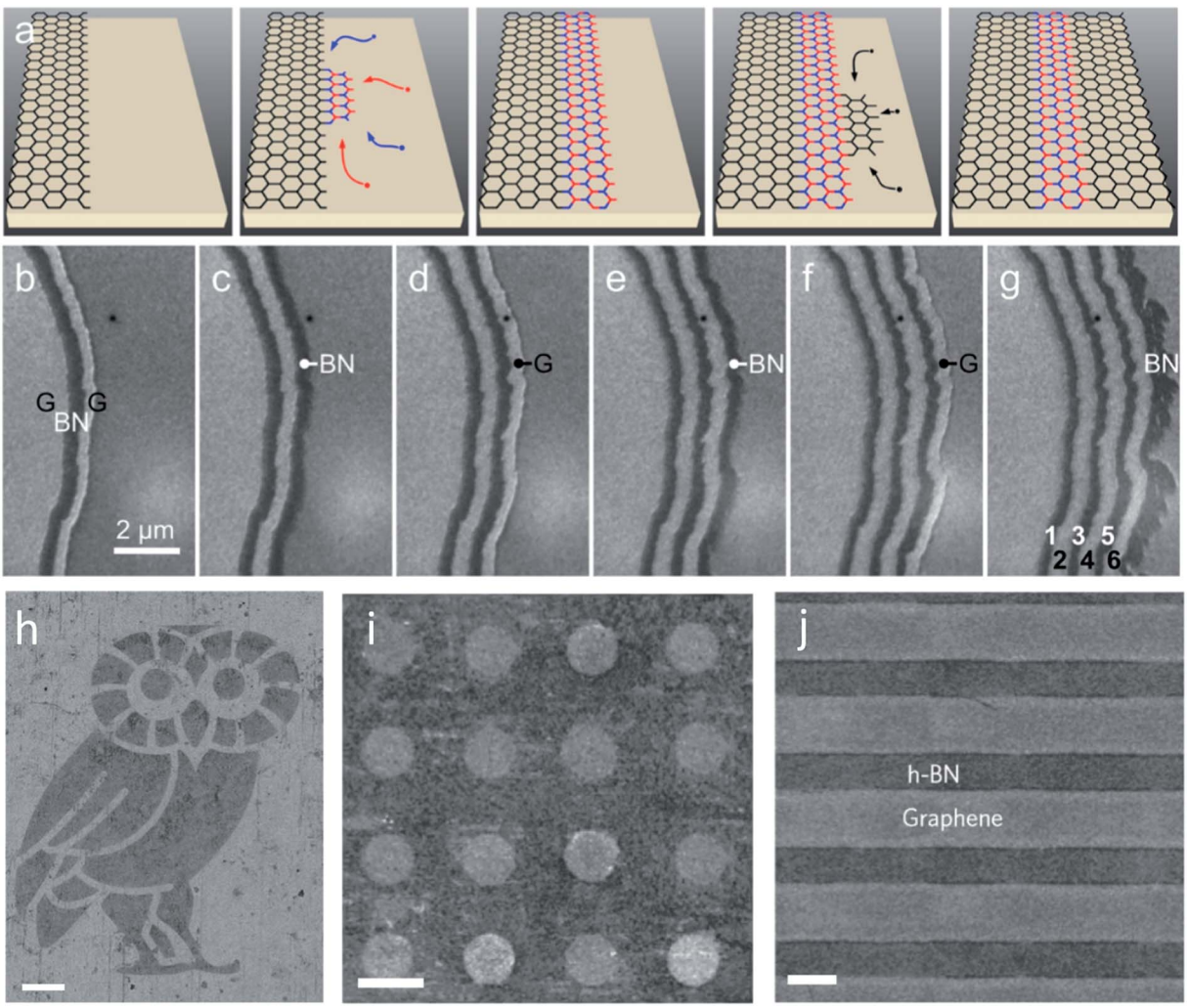

Fig. 7 (a) Schematic diagram for step by step growth of a horizontal graphene–h-BN in-plane heterostructure. (b–g) Real time imaging of horizontal in-plane hetero-epitaxial growth of alternating graphene and h-BN stripes.[118] Copyright 2014, American Chemical Society. (h–j) Complex horizontal in-plane heterostructures synthesized by mask assisted pattern etching and subsequent growth. Darker regions represent h-BN while lighter regions show graphene. Scale bars for (h–j) are 100, 50, and 10 μm, respectively.[119] Copyright 2013, Macmillan Publishers Limited.

Graphene and h-BN have striking similarity in lattice constants and structures;[47] this not only helps h-BN to act as a superior substrate for graphene but also makes it a suitable candidate for forming horizontal in-plane heterostructures. The first report of such heterostructures was made by Ci *et al.*,[120] who demonstrated that separated graphene and h-BN domains had a unique band structure and electronic properties in contrast to B- or N-doped graphene. The method involved the introduction of ammonia borane (with varying ratios to methane) into the usual CVD growth of graphene on a copper substrate. This work paved the way for more research and in 2 years a formation mechanism was proposed. It was observed that when graphene was nucleated on the edge sites of h-BN, horizontal in-plane heterostructures were formed, while a nucleation on a copper substrate resulted in the formation of a vertically stacked heterostructure. In this regard, Gao *et al.*[101] already demonstrated switching between vertical and in-plane graphene/h-BN heterostructures in their experiment, supporting the above-mentioned mechanism.[121] It is noted that this marks a milestone in our understanding about how such heterostructures can be rationally controlled.

Compared to graphene/h-BN, TMDC/TMDC horizontal in-plane heterostructures hold more promise for device application. Generally, a one-step CVD process is employed when a single chalcogen with differing transition metals is required. As discussed previously, the different growth rates of different chalcogenides lead to the formation of heterostructures using one-step CVD growth. In most of the reports for graphene/h-BN heterostructures, the interface was observed to be atomically sharp with a width of around 1 nm;[101,119,122–124] however, in TMDC/TMDC horizontal in-plane heterostructures obtained by a one-step CVD process often mixed interfaces with a width of more than 30 nm were observed. To create atomically sharp junctions, multi-step processes have been explored in which focused ion beam patterning of one type of TMDC promoted the growth of a second TMDC on the active edge of the former (Fig. 8).[125,126] It was observed that the Se atoms of WSe_2 at the edge were replaced by S atoms and that marked the junction from where MoS_2 grew.[125] In another study,[126] focused ion beam etching was performed to confirm that the edge sites were active for second TMDC growth, and depending on the etching conditions there could be alloying, partial coverage or complete coverage.

For both classes of horizontal in-plane heterostructures, the substrate plays an important role. Sutter *et al.* showed that a substrate good for growing high-quality graphene may not necessarily be a good choice for growing graphene based horizontal in-plane heterostructures (Fig. 7a–g).[118] Hydrogenation catalysts like Pt and Ni induce etching and reduce control over the overall growth of heterostructures. This understanding may be extended to TMDC based horizontal in-plane heterostructures.

Apart from the growth of whole 2DMs on the edge, the substitution of atoms has been reported for forming in-plane $MoSe_2/MoS_2$ heterostructures.[127] With a variety of patterns incorporated on a $MoSe_2$ film and subsequent conversion of those patterns into MoS_2, this work demonstrates the flexible designing capability of this method. This kind of conversion process where the chalcogen can be replaced by other atoms has been the inspiration of newer compositions such as $MoTe_2/MoS_2$ where the use of anchor atoms (*e.g.*, Na atoms) has been demonstrated to aid the substitution.[128]

To summarize the above discussion, the CVD growth of heterostructures depends on parameters like temperature, pressure, starting material, substrate and interaction between 2DMs. It has so far been the only growth technique that can achieve horizontal in-plane heterostructures with high quality. However, care must be taken to adjust parameters to avoid the formation of alloys instead of 2D heterostructures. CVD growth not only enables the fabrication of flat continuous films for electronic application, but it can also be used to synthesize porous structures for energy storage and conversion applications like supercapacitors,[255] batteries[257] and catalysis.[215,256] This aspect will be discussed in more detail in Section 6. A comprehensive summary and comparison with other methods is made in Table 2. Additionally, CVD growth is an important method for large scale uniform coverage of 2D heterostructures over wafers which may be useful for the integration of different applications on a single chip.

4.3. Liquid based techniques

For probing the depths of fundamental science and for electronic applications, CVD techniques are no doubt the best choice since they give high quality, smooth and uniform films. But when it comes to addressing the ever-growing demand for energy storage devices that require bulk electrodes to be built from 2DMs, liquid based techniques (LBTs) prove to be a better choice. Energy storage is not the only area where LBTs have found application. In fact, LBTs have been observed to modify electronic properties in a controlled manner.[108]

If there is any technique which possesses the ability to realize the large-scale industrial production of energy storage devices on virtually any surface, then it has to be LBTs. Fig. 9 stands testimony to this statement. So this topic is indispensable during the discussion about heterostructures. In LBTs, the requirement of a large film size (as in CVD) is relaxed. Here, the primary focus is on increasing the yield and forming heterostructures at the flake level. In this section, we will focus on 2D heterostructures that form well-defined heterointerface/junctions and not just nanoparticles suspended in 2DMs. Under LBTs, we have two types of approaches of (i) liquid based exfoliation and self-assembly and (ii) LBL self-assembly.

4.3.1. Liquid exfoliation and self-assembly. While in a CVD process, different 2DMs were stacked for tuning and discovering new properties, in LBTs heterostructures serve another purpose as well. Heterostructures have become invaluable in liquids because 2DMs have a high surface energy and generally tend to restack in different solvents. In energy storage and catalytic application where a high surface area is the vital parameter to improve the quality of electrodes, the restacking of 2DMs prohibits the access of a large proportion of active sites, resulting in subpar performances. As discussed above, making heterostructures mitigates the weakness of one 2DM and the synergistic effect allows us to utilize the untapped potential of two 2DMs or more.

The most widely studied heterostructure in the last decade has been graphene/TMDC. Graphene provides a conductive

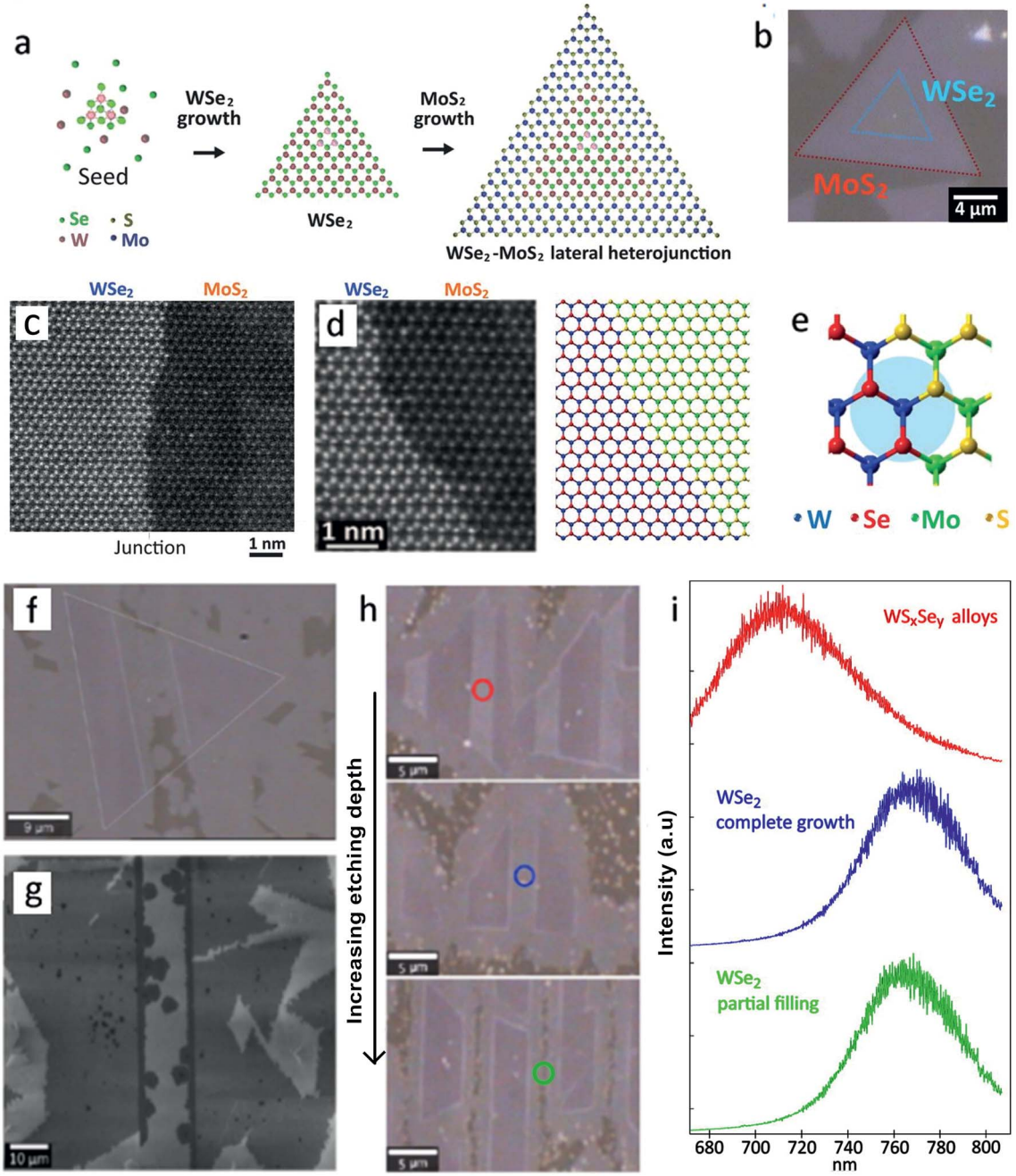

Fig. 8 (a) Schematic of the sequential growth of a monolayer WSe_2/MoS_2 in-plane heterostructure. (b) Optical image of WSe_2 and MoS_2, as distinguished by their optical contrast. (c and d) STEM images of the WSe_2/MoS_2 in-plane heterostructure. (e) Junction model of the WSe_2–MoS_2 heterostructure.[125] Copyright 2015, The American Association for Advancement of Science. (f) Optical and (g) SEM images showing partial filling of WSe_2 on the region over-etched by the focused ion beam after the second growth. (h) Optical images of WS_2–WSe_2 heterostructures. (i) Photoluminescence spectra of the second TMDC material grown on the etched region corresponding to the circle marks in (h).[126] Copyright 2016, American Chemical Society.

framework and mechanical support while the TMDC addresses several electrochemical problems by virtue of its excellent chemical properties. Unlike CVD we do not need continuously large 2DMs to form an interface; in LBTs we just need the interface formation at the lowest flake size. The most common route for achieving a graphene/TMDC heterostructure is highly straightforward. In principle, graphene and TMDC monolayers (or few layers) are obtained from different liquid phase chemical exfoliation techniques, and then mixed following certain procedures to obtain heterostructures of different morphologies. There are several routes for obtaining these 2DMs. For graphene the most commonly used method is a modified Hummers method,[131] producing graphene oxide (GO) which is subsequently reduced to form rGO. Another promising method to obtain graphene is electrochemical exfoliation of graphite, which doesn't usually involve strong

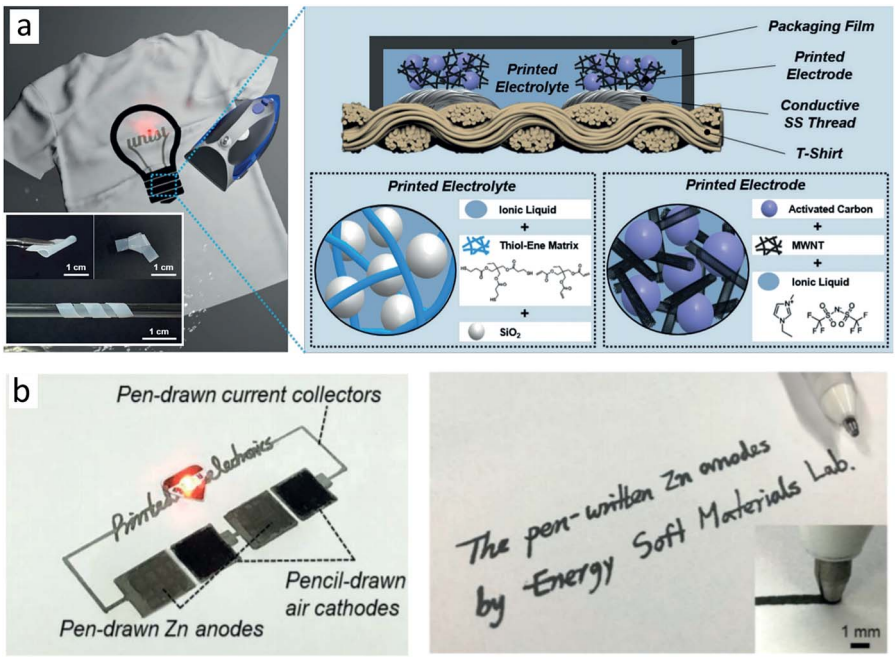

Fig. 9 (a) Schematic of supercapacitors prepared by a solution-based method and printed on a t-shirt. Inset shows the material realized so far in this direction.[129] Copyright 2018, Wiley-VCH Verlag GmbH & Co. KgaA. (b) Zinc anode ink used for preparing hand-drawn electronics.[130] Copyright 2018, Wiley-VCH Verlag GmbH & Co. KgaA.

oxidation and complicated steps.[132–135] To stabilize graphene, a certain surfactant or polymer coating has been used.[136] Similarly, TMDC nanosheets have also been obtained from chemical reactions[137] or exfoliation of MoS_2 bulk using intercalation.[138] To build a heterostructure, two types of 2DMs may then be mixed together in a suitable solvent with the assistance of ultrasonication[139] or *via* a hydrothermal process.[140] The hydrothermal process uses a sealed autoclave in which the chemical precursors are added and allowed to react at high temperatures, generally between 180 and 200 °C. Higher temperature allows greater interaction between the different 2DMs. The hydrothermal process is often assisted by a stabilizing chemical (*e.g.*, L-cysteine), which also acts as a sulfur donor in sulfur based TMDCs leading to the formation of nanoplates on graphene nanosheets (Fig. 10c and d).[141] Besides this, there have been reports of targeted growth of one 2DM on another using microwave treatment.[142] For instance, GO can interact strongly with microwaves resulting in localized heating and reduction, which generates hotspot areas on GO that improve the growth kinetics of MoS_2 and inhibits the restacking of multi-layer MoS_2 nanosheets.[143] The consequence is the formation of steps and folded edges of MoS_2 on rGO (Fig. 10a and b). It is interesting to note that it is not necessary to start with TMDC nanosheets to fabricate heterostructures. A functionalization followed by reduction can achieve the same results of 2D heterostructures. For example, Chang *et al.* demonstrated that a graphene basal plane can be functionalized by MoO_4^{2-}, which then was reduced to MoS_2 nanosheets using NH_2CSNH_2 in a hydrothermal process.[144]

An interesting study by Zhao *et al.*[138] demonstrated the formation of alternating stacks of 2DMs. This method was novel in the sense that it intercalated lithium (Li) species between the layers of MoS_2 that caused exfoliation, and subsequently the addition of dopamine (DOPA)-HCl destabilized the dispersion to form DOPA-intercalated MoS_2. The reduction of DOPA during polymerization resulted in the formation of graphene sandwiched between MoS_2 layers (Fig. 11e–g).

Porosity is an important feature of energy storage systems because highly nanoporous materials can accommodate more ions per unit area of electrode.[145] Therefore, it is desirable that the porosity should be a controllable feature of 2D heterostructures *via* a liquid exfoliation and self-assembly process. It has been validated that the porosity can be controlled by varying the MoS_2 content.[146] Not only this, but also by using monolayer dispersions of each 2DM, the interaction between them can be significantly enhanced and a better heterointerface can be formed, thus greatly suppressing the restacking. In this case, the freeze-drying process performed also helps to achieve a better porous morphology with low agglomeration.[147] It is noticeable that most of the heterostructures discussed above are based on MoS_2. This is because MoS_2 is obtained in a relatively easy manner compared to other TMDCs and it also shows most of the representative features of the TMDC family. The methods applied to MoS_2 can be extended to other TMDCs by choosing suitable precursors and conditions.[148]

MO_x (*e.g.*, RuO_2, MnO_2, NiO, and Co_3O_4) are another class of important 2DMs that exhibit high capacitance due to their pronounced faradaic mechanism. The hetero-stacking of MO/graphene can not only greatly enhance the distance between graphene sheets for easy penetration of electrolyte ions and full utilization of MO nanosheets for pseudocapacitive contribution, but also the graphene layers can serve as highly conductive

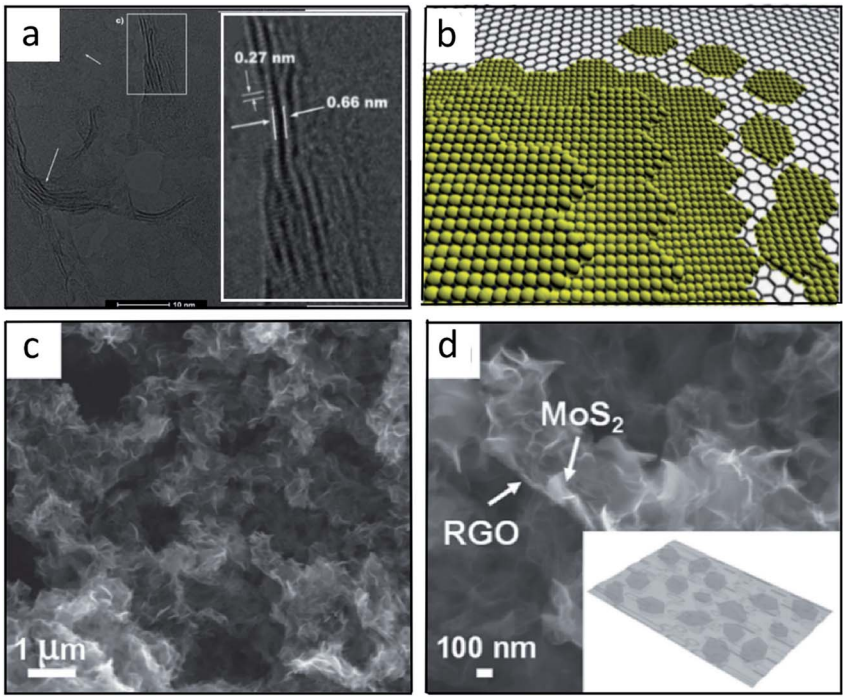

Fig. 10 (a) HRTEM image of a MoS_2/rGO vertically stacked heterostructure fabricated by a microwave assisted sol–gel method. Inset shows a magnified image of the same with dark fringes. These dark fringes are folded edges or "steps" of MoS_2 deposited. (b) Schematic of MoS_2 on rGO vertically stacked heterostructures.[143] Copyright 2012, The Royal Society of Chemistry. (c and d) HRTEM image and corresponding magnified image of MoS_2 nanoplates on rGO nanosheets. Inset shows the schematic.[141] Copyright 2015, Wiley-VCH Verlag GmbH & Co. KgaA.

pathways for improving the power capability. For instance, MnO_2/graphene heterostructures have been synthesised by mixing dispersions of water-exfoliated MnO_2 and rGO nanosheets.[149] It is observed that the electrolyte ions don't move across the planes but rather follow the in-plane paths. Recently, a MnO_2/C_3N_4 heterostructure, prepared by the liquid exfoliation and self-assembly method, demonstrated a new way to obtain MO by *in situ* growth of MO on a C_3N_4 surface. It showed enhanced photocatalytic activity and charge carrier extraction upon photo-excitation.[150] The research on MnO_2 incorporated 2D heterostructures has witnessed the creation of alternate stacking of more than two 2DMs. For instance, a ternary heterostructure of C_3N_4/rGO/MnO_2 has been reported,[151] in which covalently coupled C_3N_4/rGO was formed by a ring opening reaction, and subsequently MnO_2 was grafted onto the interface of C_3N_4/rGO by an *in situ* redox reaction. This kind of unique structure could find applications in a wide variety of fields, particularly energy storage, conversion and sensing.

A quite recent addition to the 2DM family is MXenes,[152] which are transition-metal carbide or nitride based nanosheets. MXenes have high electrical conductivity, excellent mechanic strength and large pseudocapacitance.[153] The first report of MXene based 2D heterostructures appeared in the early 2018, in which layers of MoS_2 were formed on a MXene surface.[154] The approach is quite ingenious. First, sulfur was mixed with TiC_2 in the liquid phase to incorporate sulfur atoms between its interlayers. Upon heating in an inert atmosphere, MoO motifs led to the creation of MoS_2 layers. This heating process also leads to the removal of excess sulfur. The heterostructures were used as anode materials validating the enhancement in the electrochemical performances of LIBs. MXenes have also been used to construct remarkably interconnected porous vertically stacked heterostructures,[15] in which ordered mesoporous carbon (OMC) and MXene derived carbon (MDC) were used. Specifically, $Ti_3C_2T_x$ layers were first intercalated with F127 tri-polymer (PEO-PPO-PEO) which forms micelles in the presence of resol *via* hydrogen bonding, and provides the template for forming the final OMC/MDC heterostructure. It is mentioned that OMC was obtained by thermal treatment that converted micelle@resol into OMC and the carbon from $Ti_3C_2T_x$ was used to create a uniquely porous 2D layer by etching the metal out.

Black phosphorus is a bulk material that has been known for a long time but recently entered the limelight when 2D phosphorene exfoliated from it showed unprecedented applications. The first report of liquid exfoliation of phosphorene came from Brent *et al.*, who used sonication of bulk black phosphorus to obtain few-layer phosphorene.[11] Since then its chemical properties and effect of different solvents in the exfoliation have been studied extensively.[155,156] From these investigations, it has been revealed that oxygen is highly detrimental to phosphorene,[157] because it forms oxides that then interact with water, leading to further degradation. It was demonstrated that a phosphorene/graphene film was able to show superior electrochemical performance to most previous reports.[10] This would have been impossible if there was degradation of phosphorene. Therefore, creating heterostructures may be one way of protecting the quality of phosphorene while showing new synergistic effects. Presently, there are several reports of 0D/2D

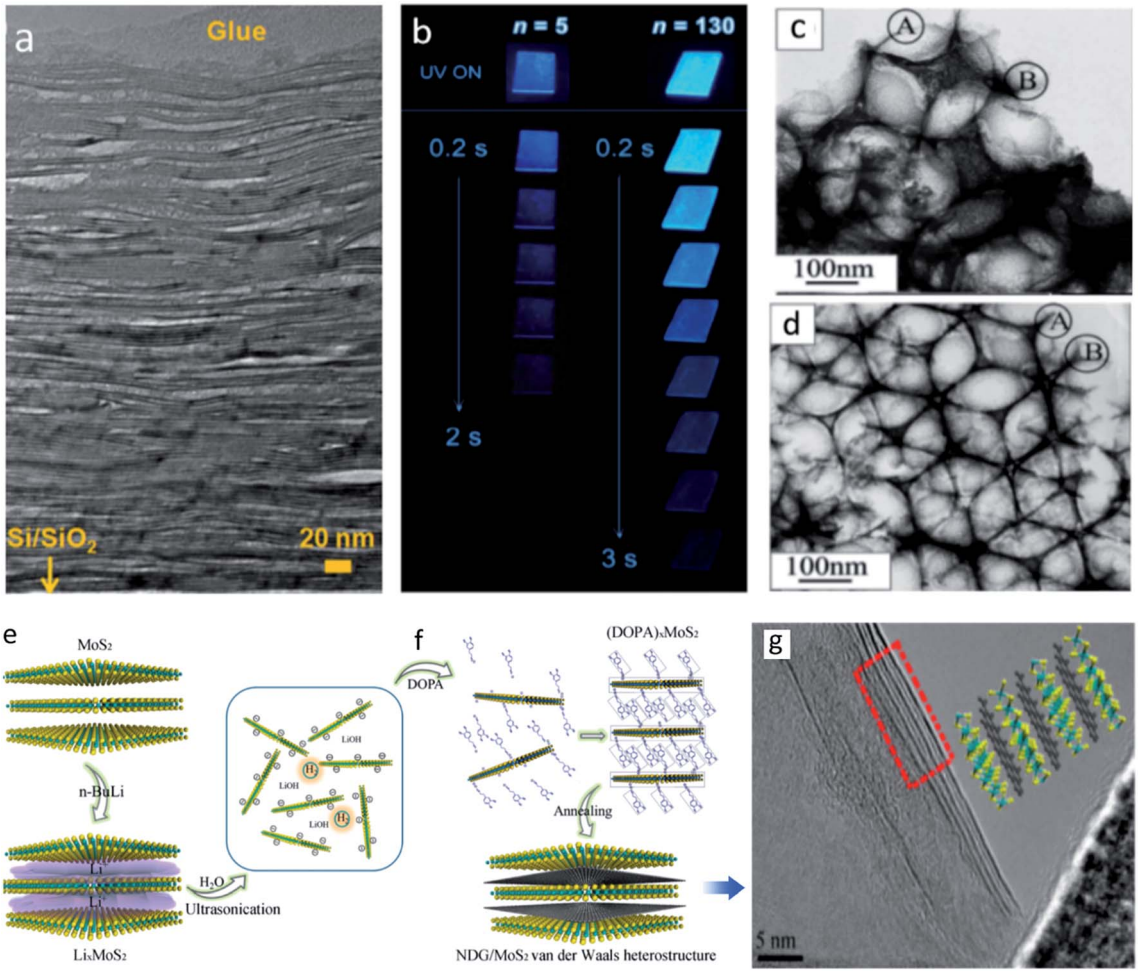

Fig. 11 (a) Bright field HRTEM image of the cross section of a 100 bilayer (LDH/perovskite) film obtained by LBL assembly.[174] Copyright 2013, American Chemical Society. (b) Photographs of room temperature phosphorescent films with different numbers of layers *n* under ambient conditions taken at different time intervals before and after the UV source was turned off.[175] Copyright 2018, Nature Springer. (c and d) TEM images of (c) SnO_2/In_2O_3 and (d) SnO_2/Fe_2O_3 heterostructured porous films, obtained by LBL deposition.[176] Copyright 2009, The Royal Society of Chemistry. (e) Li intercalation into MoS_2 gives exfoliated layers, and (f) self-assembly of $(DOPA)_xMoS_2$, followed by annealing. (g) HRTEM image of a N-doped graphene/MoS_2 heterostructure.[138] Copyright 2013, American Chemical Society.

heterostructures with the phosphorene component;[158,159] however there are currently very few reports of 2D/2D heterostructures *via* liquid exfoliation and self-assembly methods. Perhaps this is because the methods to obtain large and stable phosphorene sheets by liquid phase exfoliation are still underdeveloped. Very recently, a remarkable in-plane heterostructure based on phosphorene was reported.[160] In this work, di-cobalt phosphide was grown on the edge defects of phosphorene by simply mixing cobalt ions with black phosphorus crystals in the presence of dimethylformamide (DMF) in a solvothermal process. This is not a 2D/2D heterostructure in strict sense because Co_2P forms nanoparticles on the edge of phosphorene instead of forming a 2DM. However, this is significant progress and goes on to show that obtaining truly 2D/2D in-plane heterostructures of highly stable phosphorene in the near future might not be that difficult.

4.3.2. Layer by layer self-assembly. LBL self-assembly is an adsorption-based technique in which a wide variety of charged materials are deposited onto a surface by dipping a substrate in alternate chemicals. The technique itself predates the discovery of 2DMs and was used to deposit multilayers of charged organic/inorganic species with charged polymeric layers.[161,162] This method becomes particularly useful while considering the exfoliation of ionically bonded layered materials. The mechanical exfoliation of such layered materials is not the best route and chemical means must be employed. Geng *et al.* have shown gigantic swelling in protonated titanates in various amines. This swelling is a result of ammonium ion intercalation, which is affected by the pH of the solution and the osmotic pressure balance between the gallery and the solution.[163] There are three methods that encompass the LBL technique, namely flocculation, Langmuir–Blodgett (LB) self-assembly, and electrostatic LBL deposition (eLBL).

The method of flocculation is the fastest and simplest method that proceeds *via* the destabilisation of differently charged colloidal components that are thermodynamically unstable. However, this method due to its fast, irreversible kinetics doesn't allow much flexibility in the layer structure or

quality of the interface.[164] Several heterostructures have been reported derived from double hydroxides, perovskites and titanates with applications mostly pertaining to catalysis.[165–168] However, some other applications like energy storage and electronics remain elusive due to its shortcomings. These shortcomings aren't apparent in the LB self-assembly. In fact, using the LB method, the layer thickness and packing density can be tuned precisely, resulting in superior quality interfaces. This method employs the assembly and deposition of charged species on the surface of water. The packing density can be adjusted by the pressure applied. The LB method is generally used for the deposition of ambiphilic molecules with inherent or acquired ambiphilicity.[169] The use of hydrophobicity (without the use of ambiphilic additives) for the deposition of titanate layers has also been demonstrated.[170] This method has not only been used to obtain the popular MoS_2/graphene heterostructure, but also applied to obtain a supercapacitor electrode with a high specific capacitance of 241 F g^{-1} and good cycling performance (>90% retention after 1000 times).[171] Despite the good quality of heterostructures obtained using this method, the main disadvantage of this method lies in the slow rate of production, which hinders its scalability to industrial levels. Therefore, a method with a fast production rate of heterostructures with a high quality interface is highly desired.

The eLBL deposition is a reasonable trade-off between speed and quality. This method employs alternate immersion in cationic and anionic colloidal solutions. The adsorption between the component nanosheets is strictly electrostatic; therefore, the assembly has to be washed several times to remove non-electrostatic adsorbates. eLBL deposition allows a high level of control over the film sequence.[172] To deposit multiple like-charged layers, electrostatic glue in the form of a polymeric electrolyte is employed.[173] However, heterostructures obtained without the use of such a polyelectrolyte have also been reported.[174] In this work, positively and negatively charged nanosheets (layered double hydroxide (LDH) and perovskite) were used to cause direct electrostatic adsorption without the requirement of an alternate polyelectrolyte. Precise control of the layer sequence up to nearly bulk dimensions (200 layers) has also been demonstrated. Fig. 11a shows the HRTEM image of 100 layered LDH/perovskite vertically stacked heterostructures. Prior to the exfoliation, the LDH ($[Mn_2Al(OH)_6]^+$) was swollen by using formamide, and perovskite nanosheets were dispersed using intercalation assisted exfoliation. Careful analysis revealed that the solvent employed for dispersing the nanosheets has a critical effect on the structure and composition of the resulting heterostructures.[174]

Quite recently this method has been used for fabricating 2D heterostructures with novel properties like room-temperature phosphorescence in thin films with higher sensitivity than the pristine powder form,[175] demonstrative of great potential in applications of optical anti-counterfeiting and information security (Fig. 11b). The heterostructures were composed of inorganic 1,2,4,5-benzenetetracarboxylic acid/LDH and organic polyacrylic acid. Electrostatic adherence is not the only way of interaction in such a LBL assembly. Polymeric units adhering to graphene by virtue of hydrophobic interactions have been known for a long time, for example, polyvinylpyrrolidone.[177] As a matter of fact not only simple 2D films, but also porous 2D heterostructure films (Fig. 11c and d) with superior control over the morphology, thickness and packing geometry have already been achieved.[176] Such porous structures can be achieved through colloidal template assisted LBL assembly. In this method, a colloidal monolayer was spin-coated with SnO_2 using the LBL technique. After drying and annealing, the resulting structure was a 3D interconnected porous structure of ordered SnO_2 layers. The extension of this method for creating heterostructures was also shown by alternating deposition of In_2O_3 and Fe_2O_3 (Fig. 11d).

As far as graphene is concerned, there are many reports of graphene nanosheets being deposited using LBL techniques. However, most of the techniques demonstrated use polyelectrolyte electrostatic glue.[177–179] This might inherently impose certain limitations on the application of 2DM films prepared. Also, the technique hasn't been extended well to graphene based 2D/2D heterostructures. This may be due to the fact that the surface interactions between all 2DMs are not strong. The functionalization of 2DMs for inducing charge may be a good option to overcome this issue by enhancing interfacial interaction.

5. Characterization

After preparing materials, it is important to be able to observe it closely through a "looking glass". Along with the evolution of 2DMs and heterostructures, the concept of this looking glass has evolved. All the techniques, direct and indirect that allow scientists to draw inferences about materials and the corresponding devices, are known as characterization techniques. The techniques have evolved so fast and into such a giant entity that a separate review section would be required to cover every technique and its nuances. For example, Raman spectra alone can give information about geometric defects, mechanical strain, doping levels, material identification, number of layers, thickness of 2DMs, and all different inferences made only from the observations of Raman peaks.[180] Therefore, to keep this review concise, this section will deal only with heterostructure characterization. First, we will discuss different techniques relevant to the characterization of the 2DMs. Then, we will turn our attention towards the techniques relevant to studying 2D heterostructures in particular and outline their different characteristics that show up while using those techniques. Finally, we will discuss some recent novel techniques that could be useful for future studies.

5.1. Different techniques

After a 2DM has been prepared, it is important to know its size, thickness, number and stacking order of layers. Subsequently, we should also have an idea about the quality of the material which is determined by the defect characterization and chemical composition. Next comes the characterization of specific properties in relation with the device in which the 2DM will be incorporated. Often, it is not necessary to perform all the

characterization on a single material but the above-mentioned ones are important because they give information that is vital for any kind of application. Therefore, this presents us with a good starting point to commence our discussion about indispensable characterization techniques.

5.1.1. Scanning probe-based techniques. They involve a range of techniques that have a physical probe which relies on a stimulus-feedback mechanism for obtaining information about surface and physical properties by raster scanning over the material. Scanning probe-based techniques typically include atomic force microscopy (AFM) and scanning tunnelling microscopy (STM), which are invaluable in electronic application and fundamental studies of 2DMs and heterostructures. As the name suggests AFM allows the atomic level of resolution, and not only does it allow the observation of thicknesses merely a single monolayer high but also gives a clear picture about the orientation of 2D layers with respect to each other. It also serves as a suitable approach for determining the smoothness of the surface.[181–183] In addition, AFM can also be used to apply force on any desired area on a 2DM by pointing the probe on a suitable location. This allows the study of the mechanical strength and strain of 2DMs. Such operations are invaluable when it comes to observing strain-induced effects like piezoelectricity in ultra-thin materials.[184] Lattice mismatch can cause Moire patterns with varying periodicity depending on the angle of rotation between the layers. This also causes strain along the plane of 2DMs, leading to interesting phenomena like commensurate–incommensurate phase transition, accompanied by the formation of domain walls in 2D heterostructures. This has been studied using AFM of graphene on h-BN.[185]

AFM alone can provide a wealth of information about 2DMs and heterostructures, but the inferences from such observations need to be cross-checked with other characterization tools to draw rational conclusions and avoid errant inferences. The STM technique was used to test the theory developed from AFM observations.[185] The results were in agreement and the theory for the existence of commensurate–incommensurate states with different strain distributions was verified. STM uses a probe to scan the surface of any given material. A voltage is applied between the 2DM and STM probe tip. The medium between them acts as a quantum barrier. As is known from theories of quantum mechanics, tunnelling current depends on the barrier width. This mechanism of tunnelling can be used for both microscopy and spectroscopy.[186] While providing an image of the surface, it can also be used to study the defects. Not only that, by ionizing the defects with an electric field prior to scanning tunnelling spectroscopy, the Coulomb potential and dielectric properties of the film can be studied. This could ultimately give a better picture about the excitonic binding energy of 2DMs,[187] which can be used to design high performance optoelectronic devices. Very recently, STM has also been used as a method to probe mechanical properties by utilizing the interaction between the probe and 2DMs without causing any indentation. This enabled the application of a force below 10^{-9} N on a monolayer of graphene.[188] Both AFM and STM provide sub-nanometer level precision in a dry air medium.

While these two methods discussed above are used almost for every obtained 2DM and heterostructure, some probe-based techniques are used for specific purposes, for example, kelvin probe force microscopy (KPFM). The KPFM technique can be considered as an extension of conductive AFM. By measuring the contact potential difference between the probe and sample, a map of surface potential and work function can be created. Thus, it provides a suitable method for probing the electronic properties of 2DMs, making it the choice of characterization in a range of applications in organic devices, multi-junction heterostructures, and solar cells. A detailed review of KPFM has been provided by Melitz *et al.*,[189] which may be very useful for readers interested in learning the underlying mechanism in detail. Since the magnetism is not the main topic of discussion of this paper, we won't discuss in depth about magnetic force microscopy (MFM) which gives an accurate picture of the magnetic and non-magnetic responses with a nanometer scale precision. The first report of MFM used to probe the magnetism in 2DMs like graphene and MoS_2 was made by Li *et al.*[190] This work may act as a starting point for readers interested in magnetic studies of 2DMs.

5.1.2. Electron diffraction-based techniques. There are several techniques that fall under the umbrella term of electron diffraction based techniques. These techniques generally involve a source that produces an electron beam which is incident on the sample after passing through an electromagnetic lens. The scattered electrons are then detected by suitable detectors. The kind of interaction that electrons have with the system before being detected gives us a way of categorizing different methods and the application of any method for the characterization of material largely depends on the end goal. Here without getting into the details of the mechanism, we will mention the main techniques that are routinely used in heterostructure characterization. The first electron microscope was a TEM in which an electron beam passes through a thin sample to a detector. To obtain high resolution, the energy of the electron beam needs to be high, but such a high energy can result in charring of materials (usually non-metals), reducing the range of application. Fortunately, in recent times low voltage equipment has been developed along with aberration correction tools, which enable high resolution without damage to the sample. TEM can be fitted with an additional tool to measure the loss of kinetic energy of electrons after passing through a sample. This technique is known as electron energy loss spectroscopy. It can provide information about the thickness of 2DMs, bandgap and chemical composition.[191] Scanning TEM (STEM) involves moving the beam in a raster pattern over the sample. This can give information not only about the surface but also about interfaces and changes in chemical composition.[192] As we will see later this feature is very important for the detailed characterization of 2D heterostructures. Along with these, high resolution TEM (HRTEM) is often employed to observe minute details of nanostructures with a sub nanometer level precision.[193] High angle annular dark field STEM (HAADF-STEM) is particularly useful for studying lateral heterostructures due to its Z-contrast imaging proportional to the

atomic number, providing a clear picture of the heterointerface.[194]

While TEM detects transmitted electrons, a scanning electron microscope (SEM) detects backscattered and secondary electrons. The resolution from backscattered electrons is generally better than that obtained from secondary electrons. Since the mean free path of secondary electrons is low, most of the information obtained from SEM is surface related. With 5–30 keV source energy, this technique provides a resolution of nearly 10 angstroms.

5.1.3. X-ray based techniques. These are the techniques that use an X-ray source to illuminate the sample and then draw the inference from the interaction of X-rays with the sample. The most popular use of X-rays for characterization is in the form of X-ray diffraction (XRD). Following Bragg's law, it is well known that a periodic lattice acts like a diffraction grating for X-ray beams that produce a reciprocal lattice, from which the crystal structure and a plethora of information can be determined. This is also applied to 2DMs but only if they have a large size.[195] While XRD is not a surface specific method, there is another important X-ray based technique, X-ray photoelectron spectroscopy (XPS), which can provide surface information. The principle involves recording photoelectron emission spectra (with characteristic peaks corresponding to particular atoms or states) after the sample has been irradiated with X-rays, and thus it can provide information about the elemental composition, chemical state, *etc.* For 2DMs, XPS is particularly useful to probe chemical bonds and study interfaces.[196]

5.1.4. Raman spectroscopy. Raman spectroscopy is perhaps the most ubiquitously used technique for graphene, other 2DMs and their heterostructure characterization, and is the most intensively studied characterization technique. Raman spectroscopy detects the vibrational and rotational modes of oscillations in materials and shows results in the form of peaks, which is essentially like creating a fingerprint for a specific material. By studying the peaks carefully in relation to other known fingerprints of the same or different materials, one can reach conclusions about the crystal structure, electronic structure, phonon modes, flake thickness, stacking sequence and many more characteristics.[197]

In Fig. 12(c–f), the different types of Raman spectra are shown to demonstrate the power of this technique. Raman spectra for graphene grown on different substrates show different I_D/I_G intensity ratios of G band and 2D band (Fig. 12c). With a decrease in the number of layers, a peak shift to a lower frequency can be observed for MoS_2. The reason for this is the weak coupling between electronic transition and A_{1g} phonons in lower two dimensions compared to the bulk (Fig. 12d). Heterostructures show distinct spectra compared to the individual components (Fig. 12e). Moreover, the method of preparation

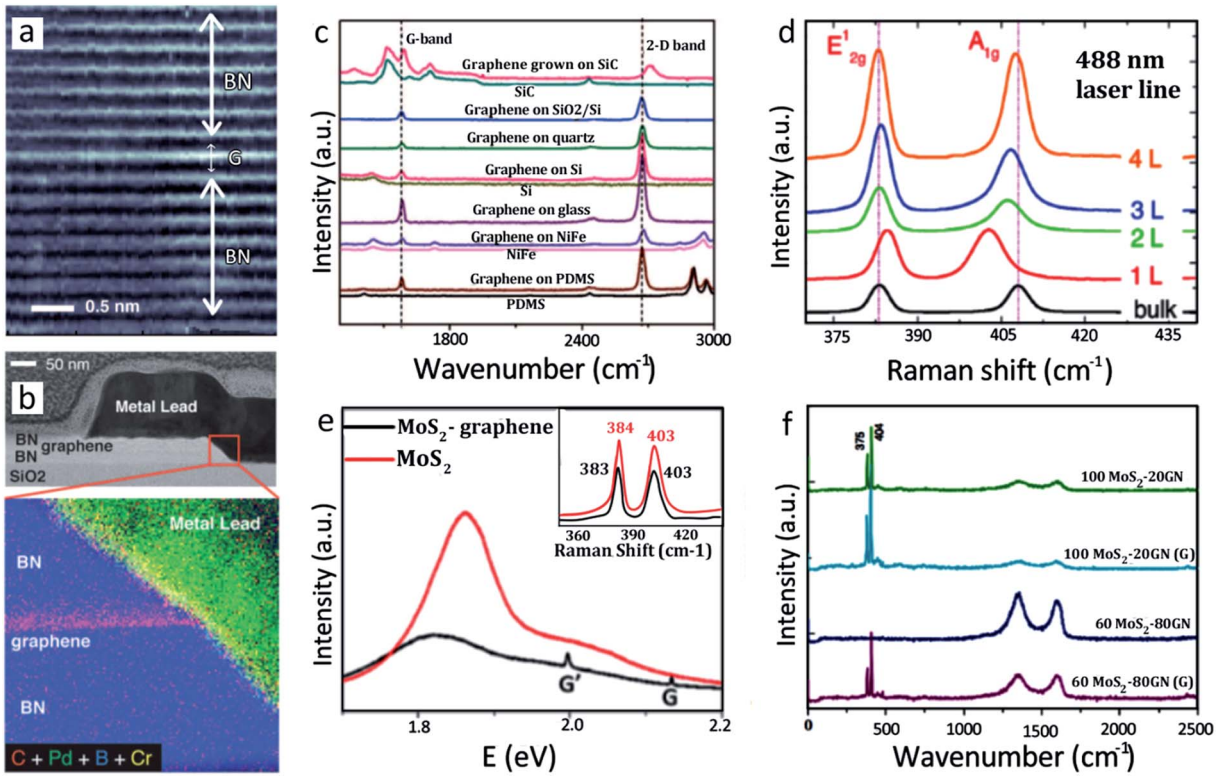

Fig. 12 (a) HAADF-STEM image of graphene/BN layers that are nearly indistinguishable. (b) EELS of graphene/BN layers, showing a clear difference between the compositions.[60] Copyright 2013, The American Association for Advancement of Science. (c) Raman spectra of graphene on different substrates.[198] Copyright 2008, American Chemical Society. (d) Raman spectra of MoS_2 layers from a monolayer to bulk.[199] Copyright 2012, Wiley-VCH Verlag GmbH & Co. KgaA. (e) Raman spectra of a CVD-grown MoS_2/graphene heterostructure and MoS_2.[108] Copyright 2014, American Chemical Society. (f) Raman spectra of MoS_2/graphene heterostructures prepared by a solution based method. GN represents graphene nanosheet.[139] Copyright 2013, Electrochemical Society.

and composition also affects the intensity of peaks, as can be seen by comparing Fig. 12e and f.

5.2. Understanding heterostructures by characterization

The first heterostructure created by Dean *et al.*[47] used AFM for physical characterization. In the early days of 2DM deposition, optical contrast was used to confirm the presence of the 2DM on the substrate. Height distribution determined by tapping mode AFM was used to observe the surface roughness of graphene deposited on h-BN sheets. However, graphene was indistinguishable from h-BN. The thickness of h-BN was roughly 14 nm.

SEM was used to first locate the interface.[60] The HAADF-STEM image shows the formation of well-defined layers, but it is easily seen that graphene and h-BN cannot be differentiated from this picture (Fig. 12a). This shortcoming can be overcome by using electron energy loss spectroscopy (EELS), which is an excellent way for compositional mapping (Fig. 12b).[60,160] Additionally, EELS also gives an insight into the mechanism of heterostructure assembly. As mentioned before, HAADF-STEM could be very useful for TMDC/TMDC based heterostructures where different TMDCs are composed of different atoms while the overall material shows similar properties. The HAADF signal is proportional to $Z^{1.7}$ where Z is the atomic number.[200] Therefore, this could be used to identify whether the obtained material is an alloy or a true heterostructure.

While dealing with CVD-grown heterostructures, to identify whether the heterostructure is a vertically stacked heterostructure or in-plane, the most effective way is AFM.[101] In Fig. 13b and c just by looking at the SEM images of in-plane h-BN–graphene (h-BN–G) and vertically stacked graphene/h-BN (G/h-BN) heterostructures, we can notice a slight difference in contrast, but it is not very reliable. The best approach is to create a height profile using AFM (Fig. 13d–g). In the case of the in-plane h-BN–G heterostructure, there will be a characteristic single peak distribution in the height histogram, whereas for the vertically stacked G/h-BN there will be a two-peak distribution with a certain height difference depending on the materials grown (in this case of G/h-BN ~0.93 nm). However, SEM is useful to observe differently shaped growths over a larger area, which suggests that CVD growth of 2D heterostructures is strongly dependent on substrate facets.[101] In most liquid based approaches for synthesizing heterostructures, multiple layers get stacked together. These layers manifest in the form of dark fringes in TEM images. By counting the fringes one can determine the number of layers.[138] In conjunction with elemental mapping, alternate stacks and their thickness as well as the

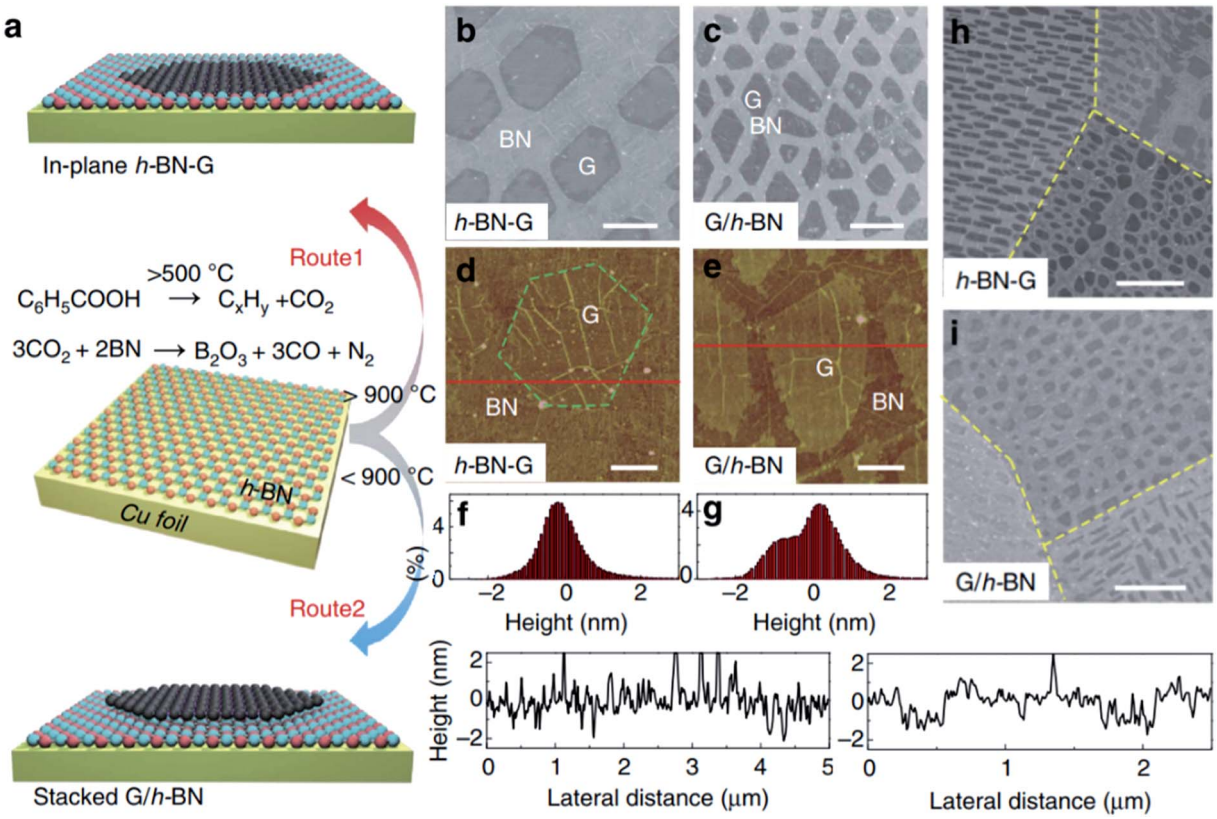

Fig. 13 Vertically stacked and horizontal in-plane graphene/h-BN heterostructures. (a) Schematic of the temperature-dependent switching between horizontal in-plane h-BN–graphene (h-BN–G, route 1) and stacked graphene/h-BN (G/h-BN, route 2) heterostructures. (b) SEM image of h-BN–G. (c) SEM image of G/h-BN. (d–g) AFM height profiles of (d) h-BN–G and (e) G/h-BN, and corresponding height histograms of (f) h-BN–G and G/h-BN. (h and i) SEM images showing the facet-dependent growth of (h) h-BN–G and (i) G/h-BN on copper substrates.[101] Copyright 2015, Nature Springer.

expansion and intercalation of layers can be determined accordingly.

Spectroscopic information can provide insight for detailed understanding of heterostructures. For example, single point Raman spectroscopy over the heterostructure can reveal whether the as-grown layers are monolayers or multilayers. Monolayer graphene has a sharp and symmetric 2D peak with an intensity ratio of 2D : G > 1. This will be retained even when graphene forms heterostructures.[101] XPS can be used to determine the spatial distribution of different components of heterostructures. By comparing the spectra of a pristine 2DM and the corresponding heterostructures, we can get a clear picture of coverage of the 2DM which enables us to infer about the type of heterostructure. This could also give us an idea about the mechanism of heterostructure formation. For example, the XPS map of Boron 1 s in an in-plane heterostructure shows "holes" with the same shape as the graphene observed by SEM.[101] This suggests that the formation of the in-plane h-BN–G heterostructure proceeds *via* etching of h-BN from the substrate. In addition, by observing peak shifts in XPS spectra, one can deduce information about interactions between 2DMs in heterostructures.[201] Apart from chemical characterization, spectroscopic techniques like Raman spectroscopy can also be used to directly observe the spatial maps of particular Raman modes. This could provide insight into other interesting properties. For example, E_{2g} and A_{1g} modes are strain dependent. Therefore, a spatial map of these modes can offer useful information about local strains that are so commonly exhibited near heterostructure interfaces.[125]

5.3. Other advanced characterization techniques

Every report on the fabrication of 2DMs or heterostructures is attached with a detailed characterization technique. However, there are some reports that focus on making the characterization of heterostructures simpler and more accurate by giving a baseline of observation in a control environment. The characterization of physical and chemical properties of heterostructures from scratch can be a tedious task, particularly when the focus is on device application, rather than component identification. At such times, a baseline to judge the quality and distinguish the components can save a lot of time and effort. For example, a baseline or "fingerprint" has been established by Zhou *et al.*[202] for studying MoS_2 based van der Waals heterostructures. It exploited the sensitivity of Raman modes (E^1_{2g} and A_{1g}) to interfacial strain and quality of contact between the components, providing a high throughput method to assist device fabrication (Fig. 14).

Very recently, an optical trapping approach to manipulate flakes in liquid exfoliated 2DMs has been developed. The mechanism behind such a unique approach is the conservation of electromagnetic momentum when light interacts with matter which could be used either for trapping or pushing nanosheets in

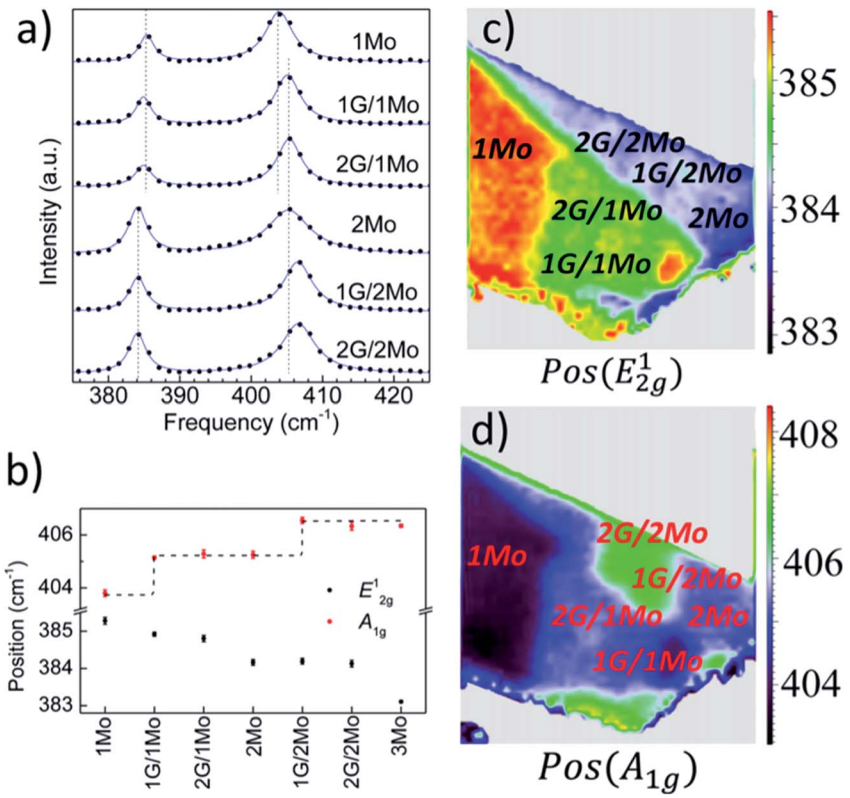

Fig. 14 (a) Raman spectra of MoS_2 in a *x*G/*y*Mo heterostructure on Si/SiO_2 ($x = 1, 2$; $y = 1, 2$). (b) Raman peak positions of MoS_2 extracted from the spectra in (a). (c and d) Raman maps of (c) E^1_{2g} and (d) A_{1g} positions for the heterostructures. Red and green regions in (c) correspond to bare MoS_2 and encapsulated MoS_2, respectively. In (d), the dark blue region corresponds to bare monolayer MoS_2 (1Mo) and the light blue region represents encapsulated MoS_2, which also extends to bilayer MoS_2 (2Mo).[202] Copyright 2014, American Chemical Society.

a liquid medium. This when combined with spectroscopic tools can provide a contact/transfer free method of characterization,[203] giving us a more accurate picture about the metrology of obtained materials without any undue contamination caused by the usual transfer process. However, this method hasn't been explored in terms of heterostructure characterization. Nevertheless, with more optimization this could become a powerful technique for the *in situ* characterization of 2D heterostructures.

In situ techniques have always been attractive because they can provide the information of synthesis, diffusion and other dynamic processes without transferring the materials after each step. This makes the understanding of the growth mechanism in real-time possible which can provide a less complicated guide to creating better materials. *In situ* Raman spectroscopy in conjunction with isotope labelling has been used to provide information of graphene layer interaction with other graphene layers as well as its environment. The isotopic engineering suggested in this research is particularly beneficial in understanding the effect of the environment. This method is potentially a powerful tool for investigating heterostructures as well.[204] Such isotopic engineering may not be possible in all materials but other methods to create "identifiers" could be explored. *In situ* Raman spectroscopy in conjunction with photoluminescence spectroscopy and theoretical calculations also provides a way of studying the transition of the bandgap from direct to indirect in monolayer MoS_2 achieved by out-of-plane compression induced strain engineering (~0.5 GPa).[205] There are other *in situ* techniques but they are more suitable for characterizing the device performance and understanding the mechanism.

No single characterization technique can claim to reveal all the features of a given 2D heterostructure. It can't even claim to be accurate all the time. But from the plethora of research that is being reported, the scientists have a bag full of resources available to them. The rational mix and match of different characterization techniques is undeniably important for reaching the right conclusion that neatly ties all the observations into a comprehensive theory (Fig. 15).

6. Energy storage and conversion of 2D heterostructures

2D heterostructures have proved their competence time and again by outperforming devices made from single 2DMs. As discussed earlier, this improvement is attributed to synergistic effects caused by close interaction between different components which may result in significant changes in physical as well as chemical properties that ultimately allow us to tune or activate certain features useful for different applications. In this section we will discuss some emerging applications of 2D heterostructures that boosted the specific performance.

It should be noted that unlike electronic application the aim of 2D heterostructures for energy storage and conversion is not to obtain large continuous nanosheets with high quality *via* methods such as CVD growth but to obtain relatively small nanosheets that form 2D heterostructures at the nanoscale level. As energy related performances are very sensitive to electrolyte-exposed active edge sites,[213–217] surfaces,[15,242] porosity,[227] *etc.*, it is more advantageous to focus on solution-based techniques to obtain hetero-structured nanosheets. Therefore, for energy storage and conversion, solution-based techniques hold special importance. Furthermore, CVD based techniques present additional scope for studying electrochemical mechanisms by virtue of high quality heterostructures obtainable from them. This will be discussed further in the following subsections. Also, it should be noted that, keeping the material

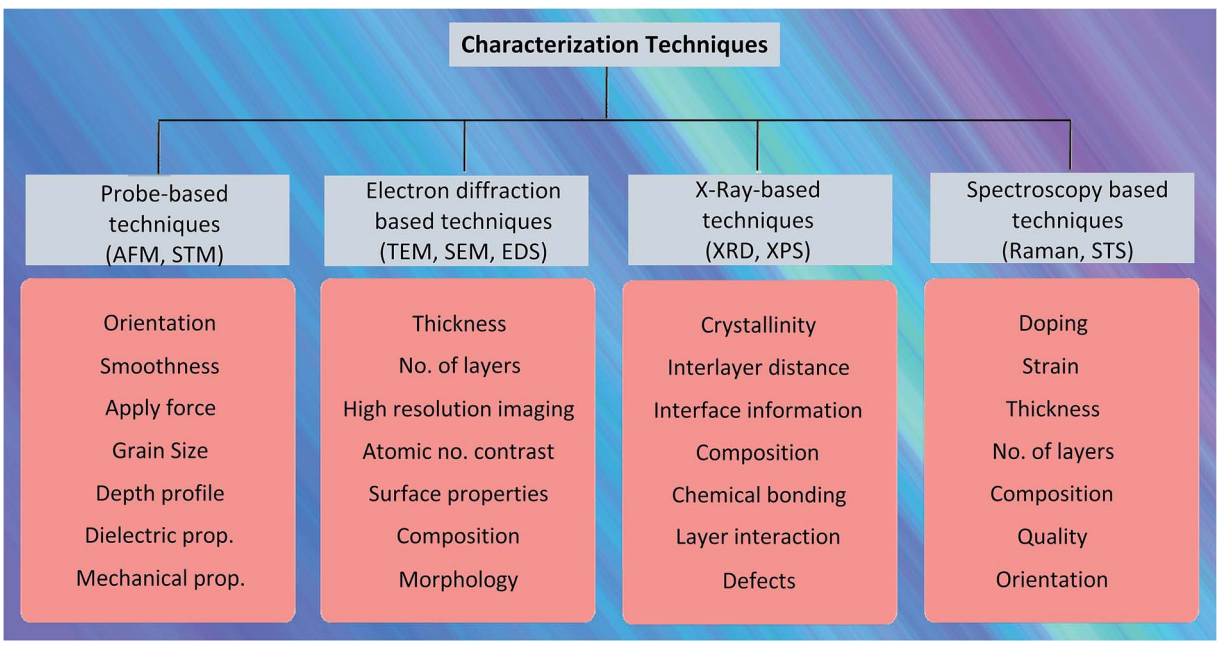

Fig. 15 Different characterization techniques and their specialities.

the same, we can achieve enhanced performances by designing devices with suitable architectures. In addition, we will also go over some such innovations related to the device architecture.

6.1. Catalysis

An energy conversion process entails a large pool of useful reactions, *e.g.*, hydrogen evolution reaction (HER), oxygen evolution reaction (OER), and oxygen reduction reaction (ORR). However, these reactions suffer from high activation barriers (or loss in overpotential). To overcome these intractable problems, one effective route is the use of catalysts. Catalysts without participating in the reaction essentially change the reaction rate and in many cases can substantially improve the selectivity. For example, platinum (Pt), the most effective catalyst for the HER and ORR (acidic media), is a rare and precious metal, but suffers from high cost. To this end, non-precious metal and metal-free materials have been intensively explored.[206–208] Among them, 2DMs have already proven their merits in this field starting from graphene[39,209,210] to the TMDC[211,212] family with different modifications (doping and hybrid) in the form of electrocatalysts, photocatalysts, *etc.* Major parameters used to characterize catalytic activity are the overpotential (lower is better), Tafel slope (lower is better) and durability (large number of cycles is better). Heterostructures provide an additional parameter controllable by stacking 2DMs of different work functions. Layered materials are particularly attractive for catalysis (*e.g.*, OER) because the large interlayer spacing acts as a good region for water and ion intercalation and significantly facilitates redox reactions.[213] Moreover, when 2D heterostructures are created, these layers can be finely separated to expose more catalytic active sites in them. Such heterostructures have been realized using GO/iron–nickel LDH, showing improved catalytic performance compared to their pristine 2DMs. This performance can further be increased by reducing GO to rGO. As a result, high conductive rGO corresponds to improved charge transport and further reduces the overpotential to as low as 0.195 V for OER.[14] The performances exhibited by the above-mentioned heterostructures are better than that of the usual Ir-based catalysts. 2D heterostructures have also benefited the HER at the complementary cathode. In 2011, Li *et al.* demonstrated the outstanding HER catalytic activity of MoS_2 nanoplates deposited on graphene sheets,[214] showing an overpotential of nearly 100 mV (*vs.* the Standard Hydrogen Electrode) while a Pt electrode shows nearly 0 mV overpotential under the same conditions. Also, the HER performance of this MoS_2/graphene heterostructure was far better than that of individual MoS_2 and graphene, indicative of their synergistic effect. On one hand, MoS_2 nanoplates were small in lateral size, well-dispersed and their aggregation was prevented by the interaction with graphene. On the other hand, the conductive network of graphene facilitated rapid electron transport. The density of active edge sites is one of the most important factors in determining the catalytic activity in this example. This has been further confirmed by Kong *et al.* using their vertically aligned MoS_2 nanowalls grown on various substrates by using a vapor deposition method.[215] Vertical alignment exposes maximal edge sites and the architecture with respect to the current collector enables charge transfer along individual layers (Fig. 16). The impressive overpotential (<200 mV) and Tafel slope (~86 mV dec^{-1}) obtained for this structure evidenced a direct correlation between the exchange current density and exposed edge sites. The density of edge sites was varied using the degree of annealing, and current density was obtained by fitting the linear region of the Tafel plot to the Tafel equation. However, this isn't a real example of 2D heterostructures. Later the same group went on to create vertically aligned heterostructures of MoS_2 and WSe_2,[216] presenting a promising application in terms of photocatalytic activity and combining the light absorption capability of WSe_2 and catalytic activity of MoS_2. Having a high activity at a high rate of H_2 evolution is an important performance index desired from catalysts. On this front, Pt/C catalysts become ineffective due to their smooth surface. By contrast, MoS_2/rGO heterostructures performed better by showing an increase in activity with increasing rate, assigned to the presence of a large number of edge sites.[217] These results also show a rate of 35 times higher than that of single MoS_2. Since the performance of catalytic electrodes is dependent on the availability of active edge sites, 3D porous heterostructures are a promising way of enhancing performance. A two-step CVD growth of a graphene/MoS_2 system showed enhanced electrocatalytic activity with a fast HER and remarkable OER/ORR by virtue of its mesoporous structure and van der Waal interaction between the faces that enabled strain, interface and electronic engineering.[256] All the above-discussed systems exhibit high durability, making them suitable for industrial consideration once they're scaled up (Fig. 16).

Another mechanism for catalysis is *via* the photo-absorption route. Various heterostructures have been explored, including carbon nitride (C_3N_4)/h-BN, $ZnIn_2S_4$/$MoSe_2$, and MoS_2/WS_2. For photocatalysts, the composition is an important parameter. The composition should be optimized such that the photocatalytically active sites are not blocked by the other component while still having sufficient interaction for electron–hole separation. This was verified by He *et al.* in their HER from methanol catalysed by C_3N_4 loaded on h-BN nanosheets.[220] The quantity of C_3N_4 could be enhanced by increasing the loading of the urea precursor, and to a certain extent this improved the performance by efficient charge separation. However, beyond a certain point, the activity is reduced due to light shielding.[220] Apart from the composition, the shape of the heterostructures also plays an important role in increasing catalysis, as confirmed from the studies on flower-like $ZnIn_2S_4$/$MoSe_2$ heterostructures.[201] This kind of hierarchical architecture and ultrathin nature of the "petals" aids in reducing charge transfer resistance by shortening the charge carrier diffusion paths, thus making active sites more accessible. Once again, this study also emphasises the role of composition with an optimum loading of $ZnIn_2S_4$ to $MoSe_2$ loading of 2%, which could stably operate for 17.5 hours without any visible change in activity, suggesting their remarkable durability. Another important consideration when dealing with vertically stacked heterostructure based photocatalysts is the stacking sequence. The stacking sequence

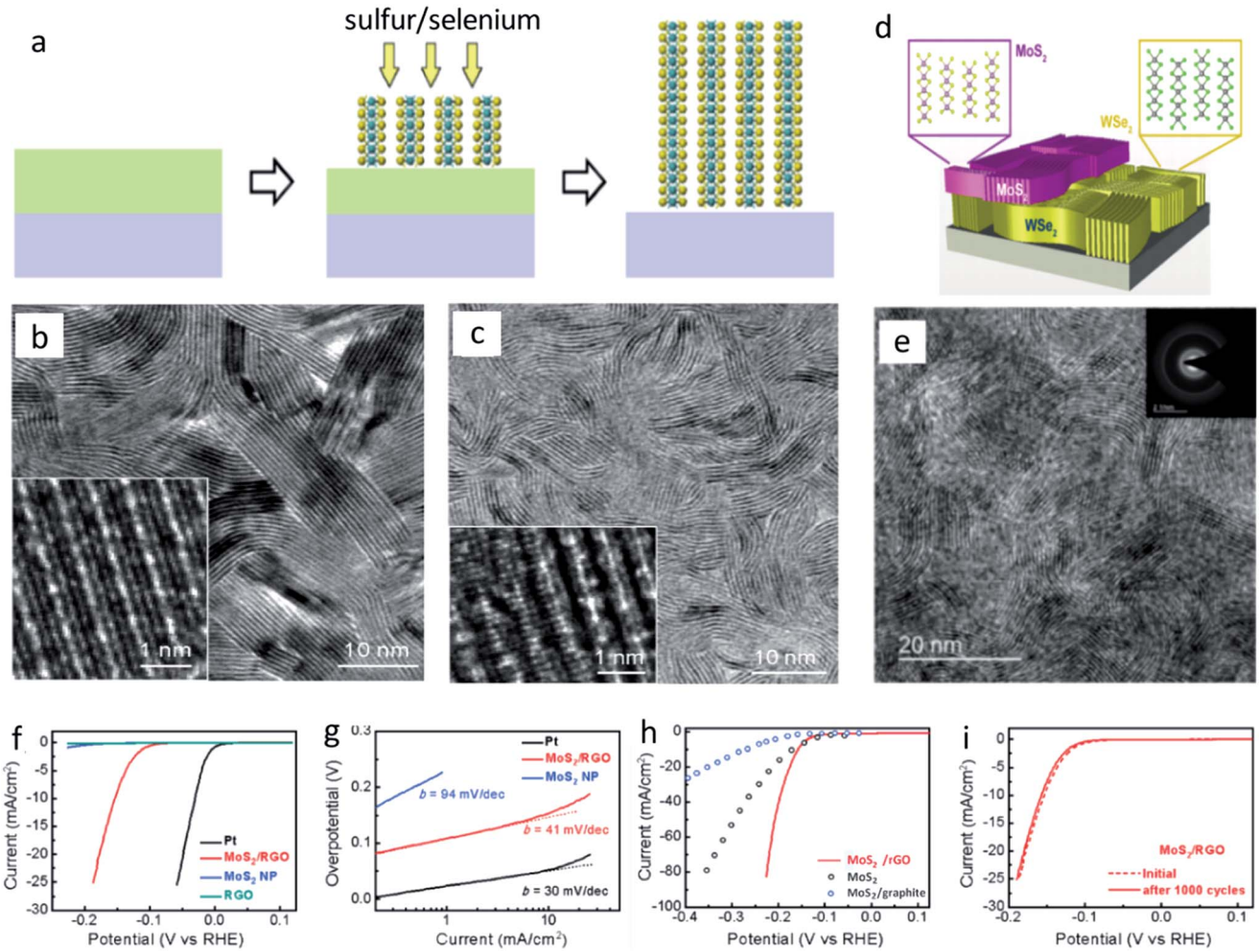

Fig. 16 (a) Diffusion of S/Se into Mo layers leads to the formation of vertically aligned sulphide/selenide nanowall structures. (b and c) TEM images of vertically aligned (b) $MoSe_2$ and (c) MoS_2.[215] Copyright 2013, American Chemical Society. (d) Schematic and (e) HRTEM image of the vertically aligned MoS_2/WSe_2 heterostructure, showing a well-defined vertically aligned structure.[216] Copyright 2015, American Chemical Society. (f) *I*–*V* curves and (g) Tafel plots of the MoS_2/rGO heterostructure, MoS_2 nanoparticles (MoS_2 NPs), rGO and Pt. (h) Performance comparison of the MoS_2/rGO heterostructure with previously reported MoS_2 (ref. 218) and MoS_2/graphite.[219] (i) Durability test of the MoS_2/rGO heterostructure.[214]

with respect to the metal contact is important because it decides the band alignment which in turn affects the activation voltage. For instance, the MoS_2/WS_2/Au electrode showed an overpotential of 192 mV while WS_2/MoS_2/Au needed a large overpotential of 252 mV to activate the HER.[107] And the hydrogen evolution rate is also higher for the MoS_2/WS_2/Au heterostructure. This can be explained by considering that photogenerated electron–hole pairs get separated into different layers. Electrons can reduce H^+ while holes neutralize electrons at the respective electrodes. Therefore, the availability of electrons at the surface is desirable for increasing the HER performance. With the WS_2/MoS_2/Au electrode, the electrons move to MoS_2 since it has a lower conduction band. This means fewer electrons are available at the surface to catalyse hydrogen evolution and the electron kinetics from the electrode to active sites is sluggish (Table 3).

From the above discussion, it is demonstrated that 2D heterostructures are making rapid strides in performance benchmarks and possess the potential to revolutionize the catalytic frontier with their gradual fall in overpotential and Tafel slope and increase in durability.

6.2. Energy storage

As pointed out above, 2D heterostructures can help to overcome the shortcomings of individual 2DMs, evident from the myriad of supercapacitor and battery performance enhancements achieved recently. As we know from a Ragone plot (energy density *vs.* power density), supercapacitors offer high power density and low energy density while batteries show the reverse trend. So the target for study on 2D heterostructures in relation to energy storage has been to close the gap between the two devices or even produce a device with both high densities. In this section, we will discuss some recent advances in 2D heterostructures for batteries and supercapacitors to recount their promising potential in this field.

Table 3 A summary of the OER and HER performance of 2D heterostructure catalysts

Heterostructure	Type of reaction	Overpotential (V)	Tafel slope (mV dec^{-1})	Durability (seconds or cycles)	Ref.
LDH/rGO	OER	0.19	39.0	High	14
$Ni_{0.67}Fe_{0.33}$/C	OER	0.21	35.1	High	213
NiFe graphene/LDH*	OER	0.23	42.0	High	221
NiFe graphene/LDH#	OER	0.21	40.0	High	221
NiFe graphene/LDH	HER	0.2	—	High	221
MoS_2–rGO	HER	0.1	41.0	High	214
MoS_2 nano-flake/graphene	HER	0.27	35	High	217
WS_2/rGO	HER	0.15	58	High	222
MoS_2/$CoSe_2$	HER	0.11	36	High	223

* mixture of 2DMs, # heterostructure.

6.2.1. Batteries. In general, conventional LIBs used graphite as the anode but they were prone to fatigue and low-power density, leading the researchers to focus on 2DMs, *e.g.*, graphene. However, graphene appears to have moderate capacity, unavailable voltage platform, and low coulombic efficiency. To this end, 2D heterostructures of graphene with TMDCs would be more effective in terms of enhanced capacity and in curbing the irreversible capacity of graphene and improving the conductivity of TMDCs, originating from the formation of a solid-electrolyte interface (SEI).[146] MoS_2 nanosheets using cyclic voltammetry (CV) measurements show a high initial charge discharge capacity of 1280 and 1040 mA h g^{-1} but show a coulombic efficiency of only ~81% and cycle performance is only ~58% after 200 cycles. With a MoS_2/graphene heterostructure, all the performances were improved significantly, with charge and discharge capacities of 1403 and 1185 mA h g^{-1}, 85% coulombic efficiency, and >90% capacity retention after 200 cycles.[146] The electrochemical impedance spectrum (EIS) provided insightful information showing low charge transfer resistance. The presence of a conductive component, *e.g.*, graphene, improves the rate capability significantly. It should be noted that similar to heterostructure-based catalysts here the composition is also important. For example, a composition of MoS_2 greater than 90% leads to the restacking and performance loss. Such results of synergy in graphene/TMDC heterostructures have also been observed by other groups.[35,224–226] Furthermore, enhancing the porosity as a whole, *e.g.*, MoS_2 deposited on 3D graphene foam, also has a positive effect on battery performance in terms of high capacity, in which the presence of the 3D graphene backbone can completely eliminate the use of a conductive metal-based current collector.[227] Apart from MoS_2, tin based dichalcogenide and oxide based heterostructures have also been explored with respect to LIBs with enhanced performance.[228,229] However, researchers are still trying to overcome the issue of high irreversible capacity caused by the formation of a SEI.

With the fast development of portable electronics and electrical vehicles, LIBs are facing great challenges taking into consideration the high price, limited lithium resources and low energy density. Some post-LIBs, *e.g.*, sodium ion batteries (SIBs),[230] lithium sulfur (Li–S) batteries,[231] potassium ion batteries[232] *etc.* are considered as alternatives to LIBs. Recently, attention has turned towards SIBs partly because of their relative abundance and low cost. However, Na^+ ions are bigger than Li^+ ions which hinders their immediate application to conventional 2DMs as they will be pulverized by repeated large volume contraction and expansion. In such a situation, 2D heterostructures remain as a viable and reliable option. Luo *et al.* demonstrated SnS_2/rGO heterostructures, with control over the orientation of SnS_2 over graphene, for both SIBs and LIBs.[233] The parallel orientation showed an initial reversible capacity of 704 mA h g^{-1} for sodiation, much higher compared to 338 mA h g^{-1} in MoS_2/graphene for SIBs reported by David *et al.*[234] However, in SnS_2/rGO, the coulombic efficiency was 69%,[233] which is lower compared to the 83% of MoS_2/rGO reported.[234] Also, MoS_2/rGO showed better cycling performance than SnS_2/graphene. It is worth noting that the cycling performance of SnS_2/rGO electrodes was improved to ~87% by coating them with carbon particles due to the re-consolidation of strength. Fig. 17 shows the schematic preparation of MoS_2/rGO heterostructure paper, exhibiting excellent coulombic efficiency and a possible mechanism for sodiation–desodiation in such a heterostructure. Black phosphorus (BP) is a very promising material for SIBs due to its high capacity for sodium storage, but sodium insertion can cause a large volume change (300%) which degrades the capacity rapidly. To counter this, a binder-free BP-graphene 2D heterostructure prepared by electrostatic dispersion followed by electrophoretic deposition has been reported. The intimate interaction between the two materials allowed graphene to act as a volume buffer while maintaining BP's high capacity. A very high discharge capacity of 2365 mA h g^{-1} could be achieved with stable cycling performance (Fig. 18a–c).[258]

Lithium sulfur (Li–S) batteries are theoretically better than LIBs with energy density in the order of 2600 W h kg^{-1}, based on the redox reaction between elemental sulfur and $Li(S_8 + 16Li \leftrightarrow 8Li_2S)$. However, Li–S batteries present some key issues of low electrical and Li^+ ionic conductivity of sulfur and solid sulfides (Li_2S_2 and Li_2S), a large volume expansion up to 80% from sulfur to Li_2S, and a serious shuttle effect pertaining to the soluble nature of polysulfides (Li_2S_x, $4 < x < 8$).[231] To address these issues regarding Li–S batteries, sulfur being an insulator generally needs to be bounded using a conductive polymer or

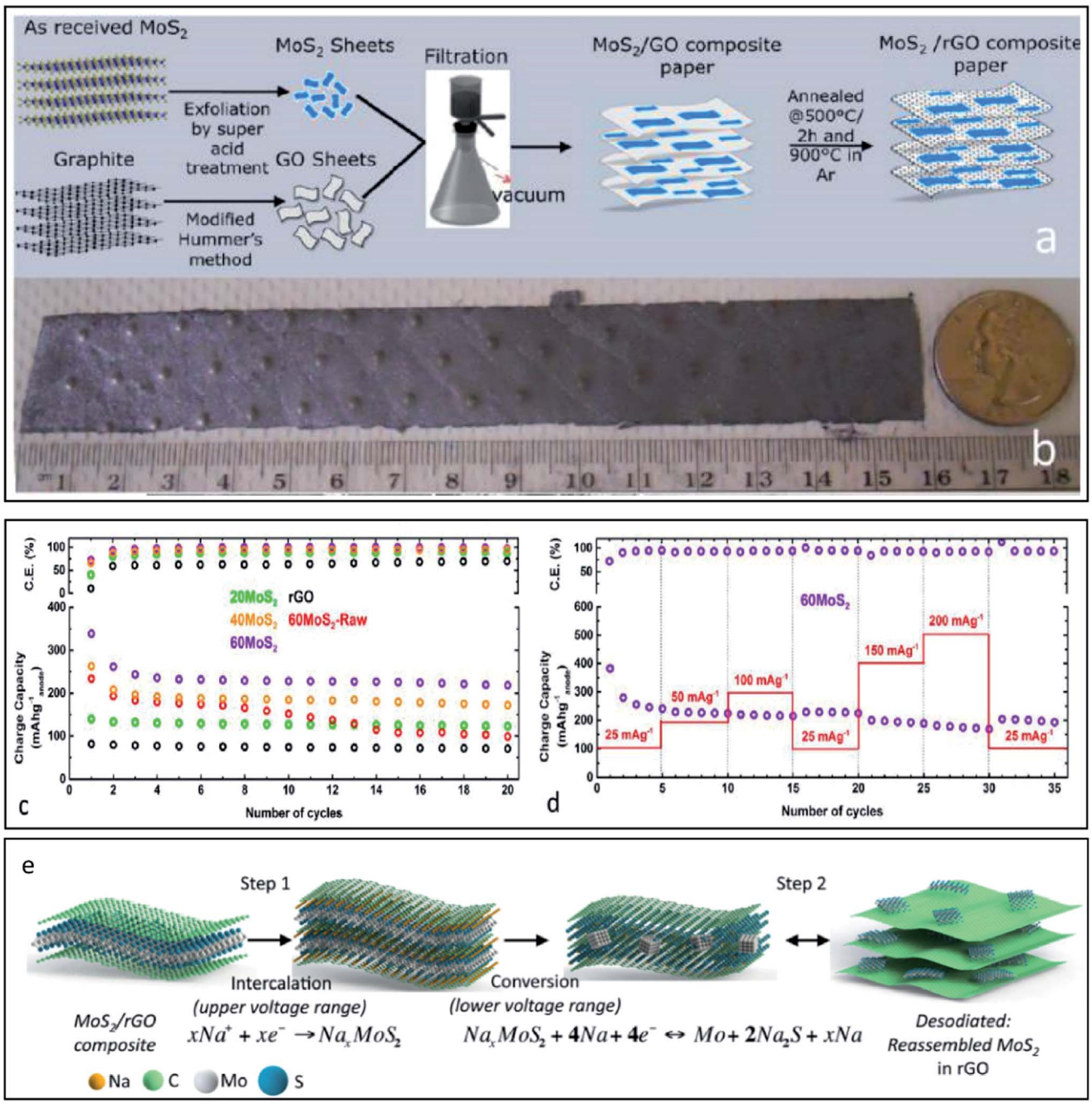

Fig. 17 (a) Schematic showing the synthesis of MoS_2/rGO heterostructure paper. (b) Photograph showing MoS_2/rGO paper prepared by vacuum filtration and subsequent annealing. (c) Sodium ion charge capacity of the paper electrode prepared with different MoS_2 loadings. Here 20, 40, and 60 MoS_2 represent the percentage of MoS_2 loading by weight in the corresponding MoS_2/rGO papers, respectively. (d) Coulombic efficiency of the 60 MoS_2/rGO heterostructure. (e) Proposed mechanism of sodium insertion and extraction with the MoS_2/rGO heterostructured electrode.[234] Copyright 2014, American Chemical Society.

nanocarbons. Previous studies using ordered nanocarbon and sulfur pushed energy density to as high as 1320 mA h g^{-1} bringing this cathode material into the limelight in this field.[228] A CVD-grown graphene foam-rGO heterostructure validates the synergistic effect by combining several advantages of two different morphologies on one platform, a 3D porous structure, high conductivity and effective prevention of polysulfide shuttling. This kind of unique structure allows a high sulfur loading of 83% and imparts a high areal capacity of 10.3 mA h cm^{-2}. Remarkably, this structure is able to retain 63.8% capacity even at such a high sulfur loading (Fig. 18d–f).[257] Besides graphene, MXenes are emerging 2DMs with exceptional properties for energy storage devices supported by theoretical calculations and experiments.[9,235–237] However, there are very few reports about MXene based heterostructures delivering high energy density for batteries. Nevertheless, a computational approach

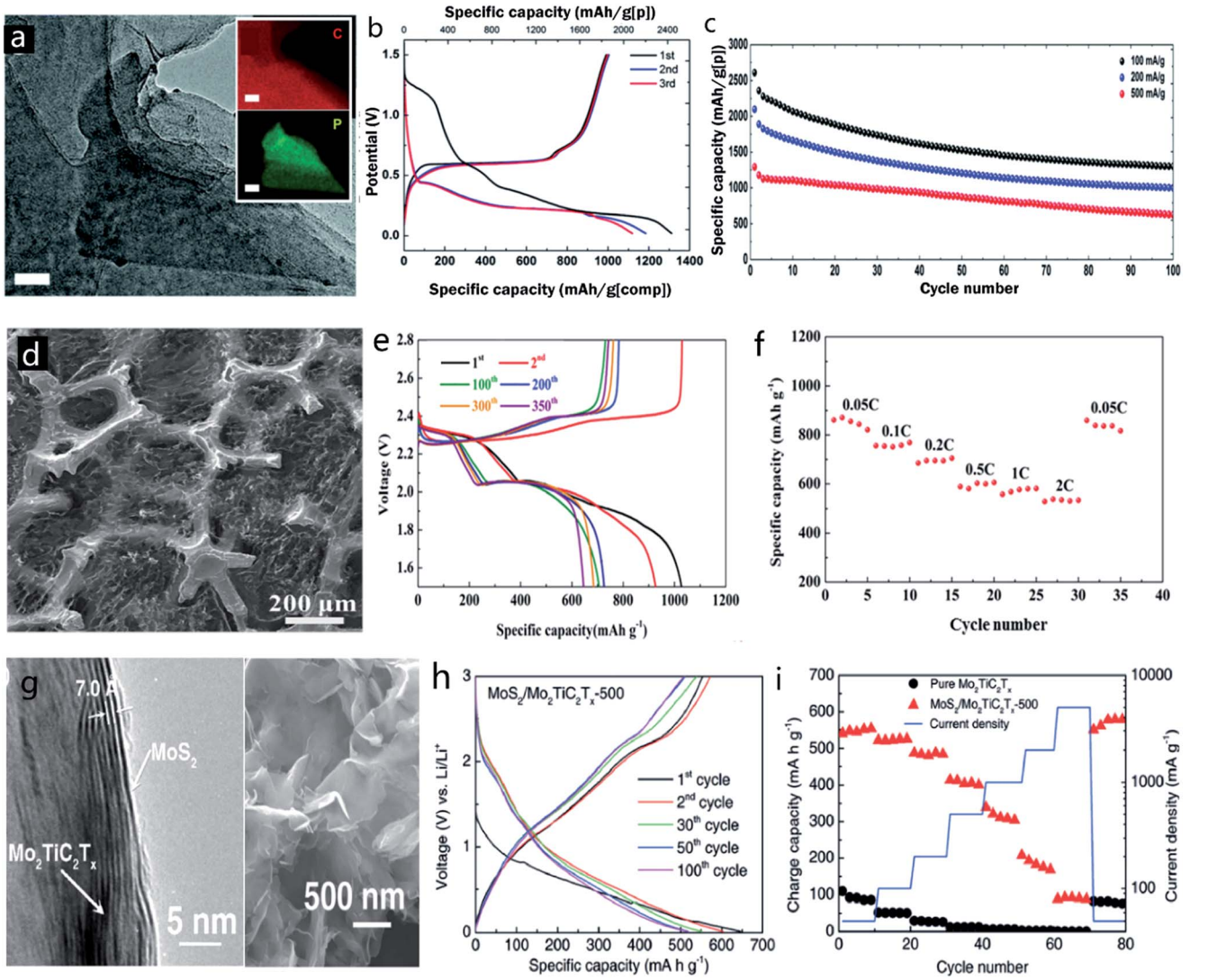

Fig. 18 (a) HRTEM image of a BP/graphene heterostructure (inset shows EDS elemental mapping) (scale bars: 5 μm). (b) Galvanostatic charge and discharge profile of the BP/graphene heterostructure at 100 mA h g_P^{-1}. (c) Cycling performance up to 100 cycles with different current densities.[258] Copyright 2018, The Royal Society of Chemistry. (d) SEM image of a graphene foam/rGO heterostructure. (e) Galvanostatic charge and discharge profile, and (f) rate performance of the graphene foam/rGO heterostructure.[257] Copyright 2015, Wiley-VCH Verlag GmbH & Co. KgaA. (g) HRTEM (left) and SEM (right) images of $MoS_2/Mo_2TiC_2T_x$ heterostructures. (h) Galvanostatic charge and discharge curve of $MoS_2/Mo_2TiC_2T_x$ heterostructures. (i) Rate performance of the heterostructures compared with the pristine material showing a remarkable improvement in performance.[154] Copyright 2015, Wiley-VCH Verlag GmbH & Co. KgaA.

suggests that MXene/graphene heterostructures due to the combined lower molecular weight and higher conductivity are promising candidates for LIBs.[238] While choosing a potential component, a trade-off between capacity and kinetics is inevitable. For a $MoS_2/Mo_2TiC_2T_x$ heterostructure,[154] the initial discharge capacity (646 mA h g^{-1} at 100 mA g^{-1}) was higher compared to pristine $Mo_2TiC_2T_x$ (134 mA h g^{-1}), accompanied by an improved cycling stability of nearly 92%. This synergy between the components provides a suitable host for accommodating the Li_2S intermediate formed during the cathodic process, thus enhancing the cycling stability (Fig. 18g–i). A recent study of a $Ti_3C_2T_x$/rGO/S ternary heterostructure system with a high sulfur loading (~70%)[239] showed high capacity and excellent cycling stability (984 mA h g^{-1} after 100 cycles), pointing towards the promising potential of MXene based heterostructures. One disadvantage of Li–S batteries is the insulating nature of sulfur that could be possibly avoided with lithium–selenium (Li–Se) batteries which possess similar energy and power density to Li–S batteries. Focused research in this direction is quite recent but given the advantages compared to Li–S batteries it is a promising direction to pursue. Recently, several reports have showcased the potential of Li–Se batteries. Since sulfur and selenium are so similar in their atomic properties, and have the same set of problems like active material loss in the form of poly-selenides,[259] as expected, research for Li–Se batteries has taken the same route as Li–S batteries and several nanocomposites, encapsulation, *etc.* have been reported to mitigate this issue.[260] This opens good opportunities for using 2D heterostructures for Li–Se systems to achieve enhanced performance like Li–S systems.

6.2.2. Supercapacitors. In supercapacitors, the application of 2D heterostructures, *e.g.*, graphene/MO and graphene/TMDC, may change the mechanism of energy storage from electric double layer capacitors (EDLCs) to redox pseudocapacitors. For instance, the CV of a graphene electrode for EDLCs shows non-faradaic peaks while a low loading of the TMDC (MoS_2) onto it shows redox shoulders, derived from the faradaic reaction of the TMDC. With a medium and high loading of MoS_2, redox peaks start to appear in the near rectangular feature, suggesting the addition of pseudocapacitance.[142] The specific capacitance of 265 F g^{-1} for the medium loading (17.6% by weight) obtained is higher than that of the pure MoS_2 electrode (20 F g^{-1}) at 50 mV s^{-1}. Also, similar to batteries, the ratio of components is important as observed from the performance improvement with increasing MoS_2 loading and then decrease beyond the optimum loading. Such heterostructures have also shown a lower level of self-discharge compared to their 2D counterparts by reducing faradaic leakage and charge

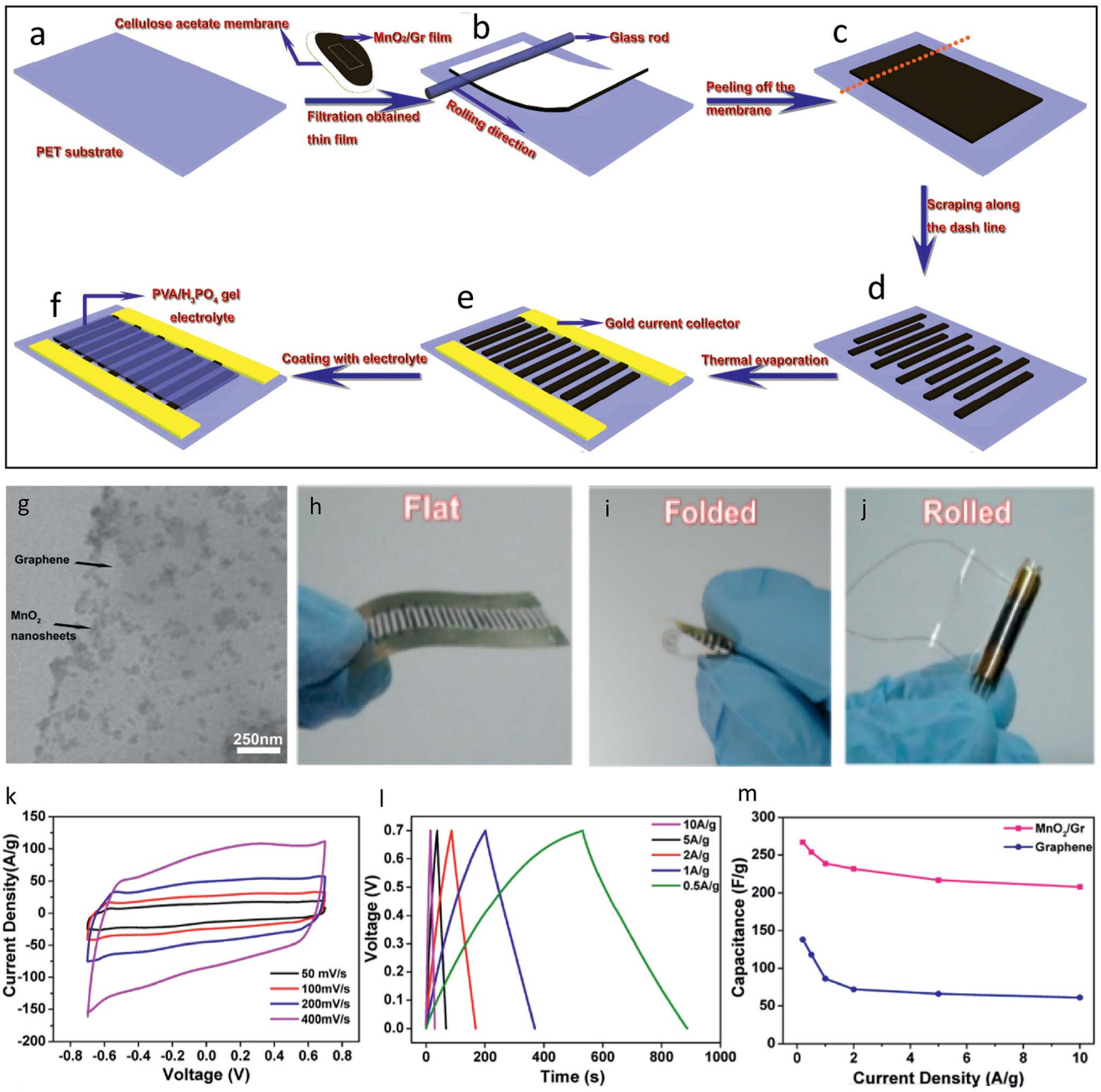

Fig. 19 (a–f) Schematic representation of the process involved in the fabrication of a planar supercapacitor with finger-like electrodes synthesized using MnO_2/graphene heterostructures. (g) TEM image showing MnO_2 nanoplates on graphene nanosheets. (h–j) Photograph of the planar supercapacitor in different bending states of flat, folded and rolled, respectively. (k) CV with different scan rates, (l) galvanostatic charge and discharge curves at different current densities, and (m) performance comparison of the MnO_2/graphene heterostructure with purely graphene based planar supercapacitors.[149] Copyright 2013, American Chemical Society.

redistribution.[240] The synergistic effect is more pronounced in heterostructures than that in simply mixed composites. This can be clearly observed from the remarkably stable cyclability up to 50 000 cycles and a high specific capacitance of 415 F g^{-1} at 1000 mA g^{-1} of the MoS_2/graphene heterostructure.[241] Similarly, a heterostructure of MnO_2/graphene not only shows a high capacitance of 254 F g^{-1} but also superior rate capability with a capacitance as high as 208 F g^{-1} at a current density 10 A g^{-1}.[149] This is because when MnO_2 is integrated with graphene, the resulting heterostructure could provide a unique way of tuning the distance between the conducting graphene sheets and also provide active sites for the adsorption of ions that is essential for improving the supercapacitive mechanism. Fig. 19 shows the fabrication of such planar micro-supercapacitors with inter-digital electrodes made of MnO_2/rGO heterostructures. The planar structure enables superior flexibility while retaining excellent electrochemical performance.

From an application point of view, all-solid-state supercapacitors are highly desirable for constructing flexible and wearable electronic devices. Recently, a stacked-layer heterostructure film (denoted as TP/EG) assembled from thiophene (TP, a thickness of ~3.5 nm) nanosheets and electrochemically exfoliated graphene (EG, thickness of ~1.0 nm) using an alternating deposition technique was first reported by Wu *et al.* for all-solid-state flexible micro-supercapacitors (TP/EG-MSCs, Fig. 20).[242] Such a rationally designed heterostructure could be operated at a high rate of up to 1000 V s^{-1} and offered ultrahigh rate capability with an areal capacitance of 1.30 mF cm^{-2} and

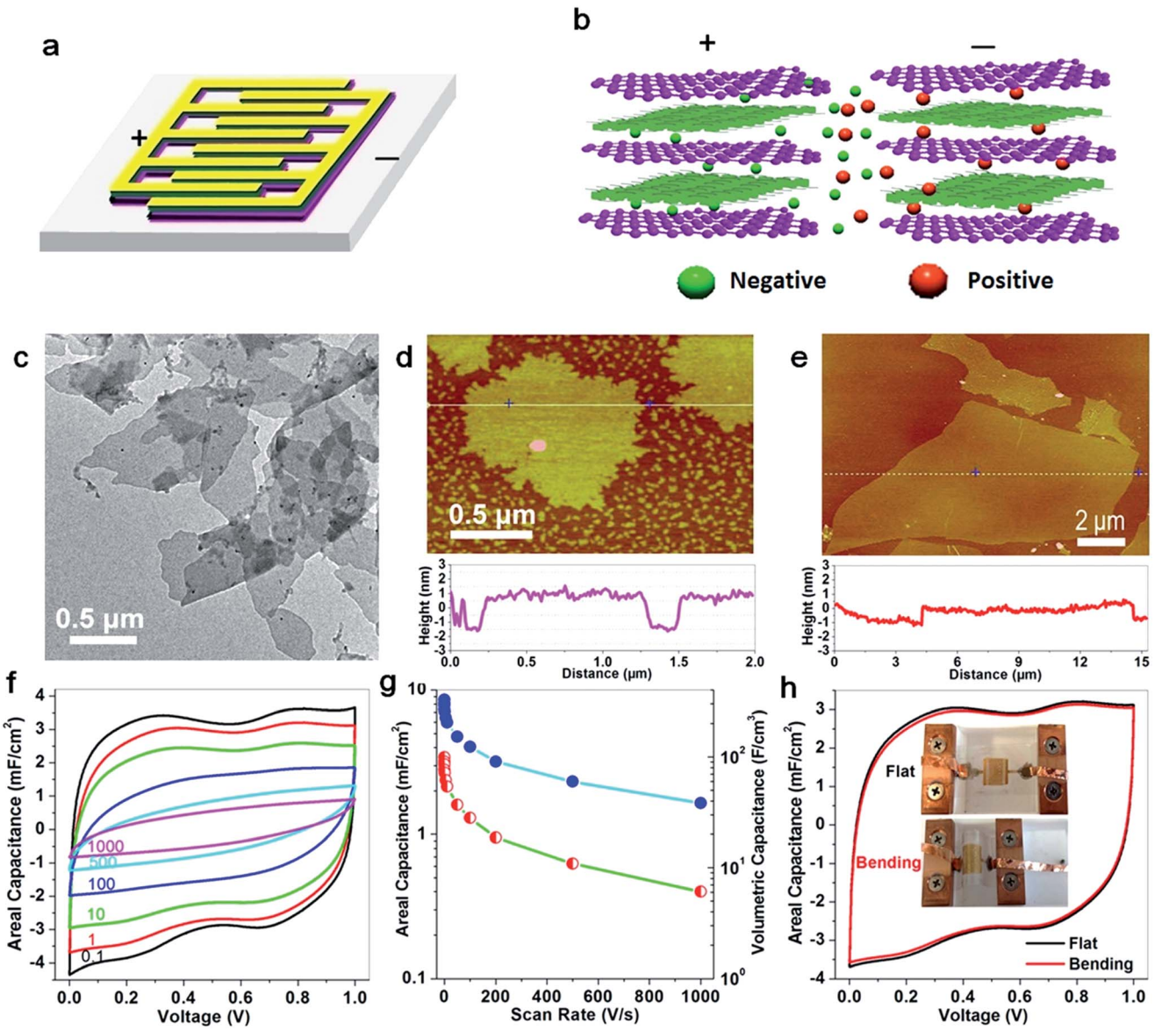

Fig. 20 (a and b) Scheme of (a) the planar TP/EG-MSCs from the top view and (b) side view of the charging state, respectively. (c) TEM image of a TP nanosheet. (d) AFM image and height profile of the TP nanosheet. (e) AFM image and height profile of EG nanosheets. (f) CV curves of TP/EG-MSCs obtained at scan rates from 0.1 to 1000 V s^{-1}. (g) The areal capacitance and volumetric capacitance of TP/EG-MSCs as a function of the scan rate. (h) CV curves of TP/EG-MSCs under flat and bending states. Inset: photographs of TP/EG-MSCs under flat and bending states.[242]

a volumetric capacitance of 123 F cm^{-3} at 100 V s^{-1}. Also, the performance showed no significant degradation even with high bending angles, highlighting the clear advantage of ultrathin polymer pseudo-capacitance having a synergistic effect with graphene's conductivity in the heterostructure film that guarantees fast ion diffusion and electron transport throughout the binder-free compact film electrode (Fig. 20).[242] This strategy of assembling stacked-layer heterostructure films will open up a novel possibility for realizing 2D graphene and analogous redox nanosheets for new-concept thin-film energy storage devices.

While liquid-based techniques are favorable for fabricating electrodes, CVD growth has also been reported to produce porous 3D graphene structures using a foam-based template for these applications. This not only provides a high conductivity network for electronic transport but also serves as a platform for synthesizing 2D heterostructures molded into a 3D configuration.[255] Using a $Ni(NO_3)_2$ electrolyte a high capacitance of 816 F g^{-1} (5 mV s^{-1}) was achieved.

Besides graphene based architectures, a unique heterostructure of MXene derived carbon (MDC) and ordered mesoporous carbon (OMC) showed incredible rate capability and cycling stability in KOH electrolyte. For instance, even at a high current density of 40 A g^{-1}, it shows a specific capacitance as high as 188 F g^{-1}. And only 2% loss of capacitance is observed after 7000 cycles at a high current density of 4 A g^{-1}. This ultrahigh performance is due to the increased accessibility of the active surface area and fast electrolyte transport through the carbon networks.[15] This provides a good opportunity to fabricate MXene-based heterostructures for hybrid supercapacitors, micro-supercapacitors, and asymmetric supercapacitors with high capacitance.[243] In particular, a heterostructure of MnO_2/MXene has also been reported to be a good supercapacitor electrode with a high capacitance of 390 F g^{-1} at a scan rate of 100 mV s^{-1} and excellent durability with a capacity retention of 93% after 6000 cycles,[244] due to the perfect combination of the high electrochemical activity of MnO_2 and the high conductivity of MXenes. Therefore, 2D heterostructures based on graphene and other 2D nanosheets hold great potential for developing high-performance and flexible energy storage devices.

7. Challenges and prospects

In summary, we have reviewed the state-of-the-art advances in the synthesis and characterization of 2D heterostructures for advanced energy storage and conversion, including catalysts (*e.g.*, HER, OER, and ORR), batteries (LIBs, SIBs, and Li–S), supercapacitors and micro-supercapacitors. Although great progress has been made so far, there are still greater challenges to the entire realization of 2DMs and particularly heterostructures in widespread applications, partly because they are difficult to handle and partly because of the lack of fundamental understanding as to how exactly does the synergy work. In this section we will discuss some of these challenges and provide our perspectives on future directions that may be fruitful in propelling the understanding and applications of 2D heterostructures.

The first important issue lies in the controllable design and precise fabrication of 2D heterostructures. With the number of 2DMs available in our inventory, we should have hundreds of varieties of heterostructures with each one having different properties to the other through different synergistic interactions. However, we still have only a handful of 2D heterostructures with graphene, h-BN, TMDCs and MXenes dominating the scene. Preparing vertically stacked heterostructures by mechanical stacking is rather facile but not scalable, and horizontal in-plane heterostructures need special care due to the lattice matching criteria. Not all 2DMs can be grown into heterostructures by CVD methods. To overcome this problem, we need to look for modified 2DMs and innovative ways of creating 2D heterostructures through solution-based methods. Solution based methods provide a way of modifying the characteristics of 2DMs during the growth process and revert back the changes after heterostructures have been formed. Although this is not a perfect method and could introduce defects, this method could still give us hope for creating novel 2D heterostructures to understand the synergistic interaction between the new 2DMs. Understanding the interactions is of great importance because then we can optimize the heterostructures for specific applications. Recent studies on novel heterostructures developed by CVD processes, followed by a transfer step, gave hope for the electronic study of heterostructures.[245] Also, developing in-plane heterostructures using solution based methods, *e.g.*, organic-based bottom-up strategy, although difficult but very promising,[160] provides us with more options to work with. New design and precise stacking of 2DMs in sequence, inspired from nature, could be a suitable way to explore new materials of 2DM based heterostructures.[246]

Second, characterization techniques become more and more important for the observation of 2D heterostructures and understanding of their growth mechanism as well as creation of 2D heterostructure-based devices, which in turn could provide a new insightful guide to creating better heterostructure materials. In particular, when it comes to understanding the mechanism of devices (especially in energy storage), *in situ* characterization techniques offer real-time monitoring of devices during operation. This allows us to determine not only structural evolution but also chemical changes, hence providing insights into the structural durability and reaction mechanism.[247] These techniques become more relevant while considering devices fabricated from heterostructures, because with an increasing number of components a pronounced mixture of mechanisms takes place. Also, the structural evolution in heterostructure based electrodes should be observed in real time. And newly developed *in situ* characterization techniques for studying 2DM electrodes[248,249] could be extended to heterostructure based systems for a comprehensive study of transformations and transitions occurring during operation. For instance, a single nanowire electrode was used to reach important conclusions about the mechanism of capacity fading in V_2O_5 based batteries.[248] By replacing that with 2D heterostructures we may gain insight into unprecedented mechanisms.

Third, an all-CVD growth of high-quality 2D heterostructures, consisting of designable shapes and components of varying 2DMs with covalently bonded interfaces, is a high priority for fundamental research and electronic applications, but is still underdeveloped. Currently most CVD based techniques for heterostructure fabrication still rely on the transfer of as-grown 2DMs from one substrate to another, which inherently introduces the shortcomings (*e.g.*, defects and indeterminate control on size) of the mechanical stacking method to this otherwise efficient route. Therefore, it is necessary that an all-CVD growth be sought for retaining high quality of covalently bonded heterostructures. It is optimistic that researchers are trying to employ multiple steps of CVD growth to avoid transfers.[125,126] Pushing in this direction, through better understanding of its fundamental mechanism, may lead to the ultimate realization of 2D heterostructures for large scale electronic application.

Fourth, the realization of certain 2D heterostructures will unveil new opportunities for novel devices with unprecedented performance. It has been observed before that greater potential of 2DMs can be realized in devices by creating newer device architectures for the complete integration of electronics and energy storage on a single substrate.[250–252] Therefore, it can be argued that applying these device architectures could lead to better utilization of heterostructure properties. For example, vertically aligned graphene on a current collector has been used to boost greatly the power density of existing electrodes. This could be a promising device architectural template for creating heterostructure-based electrodes with enhanced performance.[251]

Fifth, computational simulation is highly necessary to precisely build 2D heterostructures, which should go hand in hand with experiments. Experiments provide useful data for computation and computation offers useful insights into mechanisms and gives direction for future research. When 2D heterostructures are considered, computational work becomes even more vital given the complexity of the system. To make an accurate judgement about the mechanism of devices and the factor that makes heterostructures perform better, characterization techniques must be accompanied by computation. First principles studies are the sought-after methods currently and they have been successful so far in predicting new materials and combinations for effective applications.[238,253] The role of computational studies will become even more important in the coming times if next-generation heterostructures are to be predicted and understood. However, characterizing next-generation heterostructures may be a mammoth task for the present level of computational power and efficiency commonly employed. It may need extraordinary efforts to find viable and applicable heterostructures to move into the next generation.

Seeing the rapid progress, it is not too bold to suggest that in the near future 2DMs and heterostructures will reach their full potential. So, we should have plans for further research to create next-generation heterostructures. One way of realizing this could be to combine vertical and in-plane heterostructures. As we have already seen from the previous discussions that 2DM synergy can result in unprecedented properties. Therefore, it is quite reasonable to assume that the different types of heterostructures could also create synergistic effects to result in something unthinkable. This would give us an additional control parameter to modify the properties of each section of novel yet complicated 2D heterostructures. This could lead to an all-in-one integration system of electronics and energy storage, leading to the ultimate miniaturization and modularization. This concept may not be too ambitious given the success already achieved in creating difficult heterostructure patterns and structures.[119,254] This could also provide us with a way of studying different geometries and morphologically periodic effects of 2D heterostructures. All in all, we indeed hope that this review will shed light on the intriguing opportunities, prospects and challenges that would be possibly addressed by the introduction of 2D heterostructures into varying applications from batteries, supercapacitors to fuel cells and other electronics.

Conflicts of interest

There are no conflicts of interest to declare.

Acknowledgements

This work was financially supported by the National Key R&D Program of China (Grant 2016YFA0200200 and 2016YFB0100100), National Natural Science Foundation of China (Grant 51572259), Natural Science Foundation of Liaoning Province (Grant 201602737), Recruitment Program of Global Expert (1000 Talent Plan), DICP (DICP ZZBS201708), DICP & QIBEBT (Grant DICP & QIBEBT UN201702), Dalian National Laboratory For Clean Energy (DNL), CAS, and Exploratory Research Program of Shaanxi Yanchang Petroleum (Group) CO., LTD & DICP. Mr P. Das is grateful to the CAS-TWAS President's Fellowship (Fellowship No. 2017CTF018).

References

1 R. L. Anderson, *Solid-State Electron.*, 1962, **5**, 341–351.
2 Y. Huang, E. J. Kramer, A. J. Heeger and G. C. Bazan, *Chem. Rev.*, 2014, **114**, 7006–7043.
3 J. Kesters, P. Verstappen, M. Kelchtermans, L. Lutsen, D. Vanderzande and W. Maes, *Adv. Energy Mater.*, 2015, **5**, 1500218.
4 E. Wang, W. Mammo and M. R. Andersson, *Adv. Mater.*, 2014, **26**, 1801–1826.
5 K. S. Novoselov, A. K. Geim, S. V. Morozov, D. Jiang, Y. Zhang, S. V. Dubonos, I. V. Grigorieva and A. A. Firsov, *Science*, 2004, **306**, 666–669.
6 A. K. Geim and K. S. Novoselov, *Nat. Mater.*, 2007, **6**, 183–191.
7 H. Li, J. Wu, Z. Yin and H. Zhang, *Acc. Chem. Res.*, 2014, **47**, 1067–1075.
8 Y. Dong, Z. S. Wu, S. Zheng, X. Wang, J. Qin, S. Wang, X. Shi and X. Bao, *ACS Nano*, 2017, **11**, 4792–4800.
9 Y. Dong, S. Zheng, J. Qin, X. Zhao, H. Shi, X. Wang, J. Chen and Z. S. Wu, *ACS Nano*, 2018, **12**, 2381–2388.

10 H. Xiao, Z. S. Wu, L. Chen, F. Zhou, S. Zheng, W. Ren, H. M. Cheng and X. Bao, *ACS Nano*, 2017, **11**, 7284–7292.
11 J. R. Brent, N. Savjani, E. A. Lewis, S. J. Haigh, D. J. Lewis and P. O'Brien, *Chem. Commun.*, 2014, **50**, 13338–13341.
12 K. Vaklinova, A. Hoyer, M. Burghard and K. Kern, *Nano Lett.*, 2016, **16**, 2595–2602.
13 C. Xu, S. Song, Z. Liu, L. Chen, L. Wang, D. Fan, N. Kang, X. Ma, H.-M. Cheng and W. Ren, *ACS Nano*, 2017, **11**, 5906–5914.
14 X. Long, J. Li, S. Xiao, K. Yan, Z. Wang, H. Chen and S. Yang, *Angew. Chem., Int. Ed.*, 2014, **53**, 7584–7588.
15 J. Wang, J. Tang, B. Ding, V. Malgras, Z. Chang, X. Hao, Y. Wang, H. Dou, X. Zhang and Y. Yamauchi, *Nat. Commun.*, 2017, **8**, 15717.
16 K. Wang, K. De Greve, L. A. Jauregui, A. Sushko, A. High, Y. Zhou, G. Scuri, T. Taniguchi, K. Watanabe, M. D. Lukin, H. Park and P. Kim, *Nat. Nanotechnol.*, 2018, **13**, 128–132.
17 P. Tassin, T. Koschny, M. Kafesaki and C. M. Soukoulis, *Nat. Photonics*, 2012, **6**, 259.
18 D. G. Papageorgiou, I. A. Kinloch and R. J. Young, *Prog. Mater. Sci.*, 2017, **90**, 75–127.
19 L. Liao and X. Duan, *Mater. Today*, 2012, **15**, 328–338.
20 J. Li, L. Niu, Z. Zheng and F. Yan, *Adv. Mater.*, 2014, **26**, 5239–5273.
21 D. Li, W. Y. Lai, Y. Z. Zhang and W. Huang, *Adv. Mater.*, 2018, **30**, 1704738.
22 Z. S. Wu, Y. Z. Tan, S. Zheng, S. Wang, K. Parvez, J. Qin, X. Shi, C. Sun, X. Bao, X. Feng and K. Mullen, *J. Am. Chem. Soc.*, 2017, **139**, 4506–4512.
23 S. Zheng, X. Tang, Z. S. Wu, Y. Z. Tan, S. Wang, C. Sun, H. M. Cheng and X. Bao, *ACS Nano*, 2017, **11**, 2171–2179.
24 K. Zhang, X. Yang and D. Li, *J. Energy Chem.*, 2018, **27**, 1–5.
25 K. S. Novoselov, A. K. Geim, S. V. Morozov, D. Jiang, M. I. Katsnelson, I. V. Grigorieva, S. V. Dubonos and A. A. Firsov, *Nature*, 2005, **438**, 197–200.
26 G. Liu, S. Ahsan, A. G. Khitun, R. K. Lake and A. A. Balandin, *J. Appl. Phys.*, 2013, **114**, 154310.
27 K. Tang, R. Qin, J. Zhou, H. Qu, J. Zheng, R. Fei, H. Li, Q. Zheng, Z. Gao and J. Lu, *J. Phys. Chem. C*, 2011, **115**, 9458–9464.
28 Z. S. Wu, K. Parvez, X. Feng and K. Mullen, *Nat. Commun.*, 2013, **4**, 2487.
29 H.-W. Wang, Z.-A. Hu, Y.-Q. Chang, Y.-L. Chen, Z.-Y. Zhang, Y.-Y. Yang and H.-Y. Wu, *Mater. Chem. Phys.*, 2011, **130**, 672–679.
30 Y. Wang, J. W. Shan and G. J. Weng, *J. Appl. Phys.*, 2015, **118**, 065101.
31 M. Lundie, Ž. Šljivančanin and S. Tomić, *J. Mater. Chem. C*, 2015, **3**, 7632–7641.
32 D. Jariwala, V. K. Sangwan, L. J. Lauhon, T. J. Marks and M. C. Hersam, *ACS Nano*, 2014, **8**, 1102–1120.
33 L. Peng, Y. Zhu, D. Chen, R. S. Ruoff and G. Yu, *Adv. Energy Mater.*, 2016, **6**, 1600025.
34 M. Chhowalla, H. S. Shin, G. Eda, L. J. Li, K. P. Loh and H. Zhang, *Nat. Chem.*, 2013, **5**, 263–275.
35 K. Chang and W. Chen, *ACS Nano*, 2011, **5**, 4720–4728.
36 E. Pomerantseva and Y. Gogotsi, *Nat. Energy*, 2017, **2**, 17089.
37 X. Cai, T. C. Ozawa, A. Funatsu, R. Ma, Y. Ebina and T. Sasaki, *J. Am. Chem. Soc.*, 2015, **137**, 2844–2847.
38 Y. Yao, Q. Fu, Y. Y. Zhang, X. Weng, H. Li, M. Chen, L. Jin, A. Dong, R. Mu, P. Jiang, L. Liu, H. Bluhm, Z. Liu, S. B. Zhang and X. Bao, *Proc. Natl. Acad. Sci. U. S. A.*, 2014, **111**, 17023–17028.
39 J. Deng, P. Ren, D. Deng and X. Bao, *Angew. Chem., Int. Ed.*, 2015, **54**, 2100–2104.
40 D. Deng, K. S. Novoselov, Q. Fu, N. Zheng, Z. Tian and X. Bao, *Nat. Nanotechnol.*, 2016, **11**, 218–230.
41 L.-Y. Gan, Q. Zhang, C.-S. Guo, U. Schwingenschlögl and Y. Zhao, *J. Phys. Chem. C*, 2016, **120**, 2119–2125.
42 G. Wang, J. Zhang, S. Yang, F. Wang, X. Zhuang, K. Müllen and X. Feng, *Adv. Energy Mater.*, 2018, **8**, 1702254.
43 Z. Liao, N. Gauquelin, R. J. Green, S. Macke, J. Gonnissen, S. Thomas, Z. Zhong, L. Li, L. Si, S. Van Aert, P. Hansmann, K. Held, J. Xia, J. Verbeeck, G. Van Tendeloo, G. A. Sawatzky, G. Koster, M. Huijben and G. Rijnders, *Adv. Funct. Mater.*, 2017, **27**, 1606717.
44 Y. C. Huang, X. Chen, C. Wang, L. Peng, Q. Qian and S. F. Wang, *Nanoscale*, 2017, **9**, 8616–8622.
45 Q. H. Wang, K. Kalantar-Zadeh, A. Kis, J. N. Coleman and M. S. Strano, *Nat. Nanotechnol.*, 2012, **7**, 699–712.
46 K. F. Mak, C. Lee, J. Hone, J. Shan and T. F. Heinz, *Phys. Rev. Lett.*, 2010, **105**, 136805.
47 C. R. Dean, A. F. Young, I. Meric, C. Lee, L. Wang, S. Sorgenfrei, K. Watanabe, T. Taniguchi, P. Kim, K. L. Shepard and J. Hone, *Nat. Nanotechnol.*, 2010, **5**, 722.
48 T. Ando, *J. Phys. Soc. Jpn.*, 2006, **75**, 074716.
49 A. H. Castro Neto, F. Guinea, N. M. R. Peres, K. S. Novoselov and A. K. Geim, *Rev. Mod. Phys.*, 2009, **81**, 109–162.
50 K. Nomura and A. H. MacDonald, *Phys. Rev. Lett.*, 2007, **98**, 076602.
51 E. H. Hwang, S. Adam and S. D. Sarma, *Phys. Rev. Lett.*, 2007, **98**, 186806.
52 S. Fratini and F. Guinea, *Phys. Rev. B: Condens. Matter Mater. Phys.*, 2008, **77**, 195415.
53 J.-H. Chen, C. Jang, S. Xiao, M. Ishigami and M. S. Fuhrer, *Nat. Nanotechnol.*, 2008, **3**, 206.
54 G. F. Schneider, V. E. Calado, H. Zandbergen, L. M. Vandersypen and C. Dekker, *Nano Lett.*, 2010, **10**, 1912–1916.
55 P. J. Zomer, S. P. Dash, N. Tombros and B. J. van Wees, *Appl. Phys. Lett.*, 2011, **99**, 232104.
56 H. W. Hu, G. Haider, Y. M. Liao, P. K. Roy, R. Ravindranath, H. T. Chang, C. H. Lu, C. Y. Tseng, T. Y. Lin, W. H. Shih and Y. F. Chen, *Adv. Mater.*, 2017, **29**, 1703549.
57 S. Deng and V. Berry, *Mater. Today*, 2016, **19**, 197–212.
58 V. E. Calado, G. F. Schneider, A. M. M. G. Theulings, C. Dekker and L. M. K. Vandersypen, *Appl. Phys. Lett.*, 2012, **101**, 103116.
59 A. Castellanos-Gomez, M. Buscema, R. Molenaar, V. Singh, L. Janssen, H. S. J. van der Zant and G. A. Steele, *2D Mater.*, 2014, **1**, 011002.
60 L. Wang, I. Meric, P. Y. Huang, Q. Gao, Y. Gao, H. Tran, T. Taniguchi, K. Watanabe, L. M. Campos, D. A. Muller,

J. Guo, P. Kim, J. Hone, K. L. Shepard and C. R. Dean, *Science*, 2013, **342**, 614.
61 W. M. Haynes, *Handbook of Chemistry and Physics*, CRC Press, Boca Raton, 2014.
62 S. Wang, S. Suzuki and H. Hibino, *Nanoscale*, 2014, **6**, 13838–13844.
63 Q. Liu, Y. Gong, J. S. Wilt, R. Sakidja and J. Wu, *Carbon*, 2015, **93**, 199–206.
64 N. F. Santos, U. Zubets, A. F. Carvalho, A. J. S. Fernandes, L. Pereira and F. M. Costa, *Carbon*, 2017, **122**, 726–736.
65 H. Q. Ta, D. J. Perello, D. L. Duong, G. H. Han, S. Gorantla, V. L. Nguyen, A. Bachmatiuk, S. V. Rotkin, Y. H. Lee and M. H. Rummeli, *Nano Lett.*, 2016, **16**, 6403–6410.
66 C. H. Naylor, W. M. Parkin, Z. Gao, J. Berry, S. Zhou, Q. Zhang, J. B. McClimon, L. Z. Tan, C. E. Kehayias, M. Q. Zhao, R. S. Gona, R. W. Carpick, A. M. Rappe, D. J. Srolovitz, M. Drndic and A. T. C. Johnson, *ACS Nano*, 2017, **11**, 8619–8627.
67 J. Chen, X. Zhao, G. Grinblat, Z. Chen, S. J. R. Tan, W. Fu, Z. Ding, I. Abdelwahab, Y. Li, D. Geng, Y. Liu, K. Leng, B. Liu, W. Liu, W. Tang, S. A. Maier, S. J. Pennycook and K. P. Loh, *Adv. Mater.*, 2018, **30**, 1704674.
68 M. O'Brien, N. McEvoy, T. Hallam, H. Y. Kim, N. C. Berner, D. Hanlon, K. Lee, J. N. Coleman and G. S. Duesberg, *Sci. Rep.*, 2014, **4**, 7374.
69 Z. Yan, J. Lin, Z. Peng, Z. Sun, Y. Zhu, L. Li, C. Xiang, E. L. Samuel, C. Kittrell and J. M. Tour, *ACS Nano*, 2012, **6**, 9110–9117.
70 G. Lu, T. Wu, Q. Yuan, H. Wang, H. Wang, F. Ding, X. Xie and M. Jiang, *Nat. Commun.*, 2015, **6**, 6160.
71 J. Lee, S. Pak, P. Giraud, Y. W. Lee, Y. Cho, J. Hong, A. R. Jang, H. S. Chung, W. K. Hong, H. Y. Jeong, H. S. Shin, L. G. Occhipinti, S. M. Morris, S. Cha, J. I. Sohn and J. M. Kim, *Adv. Mater.*, 2017, **29**, 1702206.
72 Z. Li, P. Wu, C. Wang, X. Fan, W. Zhang, X. Zhai, C. Zeng, Z. Li, J. Yang and J. Hou, *ACS Nano*, 2011, **5**, 3385–3390.
73 T. Wu, G. Ding, H. Shen, H. Wang, L. Sun, Y. Zhu, D. Jiang and X. Xie, *Nanoscale*, 2013, **5**, 5456–5461.
74 Y. Xue, B. Wu, L. Jiang, Y. Guo, L. Huang, J. Chen, J. Tan, D. Geng, B. Luo, W. Hu, G. Yu and Y. Liu, *J. Am. Chem. Soc.*, 2012, **134**, 11060–11063.
75 B. Luo, E. Gao, D. Geng, H. Wang, Z. Xu and G. Yu, *Chem. Mater.*, 2017, **29**, 1022–1027.
76 L. Song, L. Ci, H. Lu, P. B. Sorokin, C. Jin, J. Ni, A. G. Kvashnin, D. G. Kvashnin, J. Lou, B. I. Yakobson and P. M. Ajayan, *Nano Lett.*, 2010, **10**, 3209–3215.
77 S. M. Eichfeld, L. Hossain, Y. C. Lin, A. F. Piasecki, B. Kupp, A. G. Birdwell, R. A. Burke, N. Lu, X. Peng, J. Li, A. Azcatl, S. McDonnell, R. M. Wallace, M. J. Kim, T. S. Mayer, J. M. Redwing and J. A. Robinson, *ACS Nano*, 2015, **9**, 2080–2087.
78 K. Kang, S. Xie, L. Huang, Y. Han, P. Y. Huang, K. F. Mak, C.-J. Kim, D. Muller and J. Park, *Nature*, 2015, **520**, 656.
79 S. Lee, K. Lee and Z. Zhong, *Nano Lett.*, 2010, **10**, 4702–4707.
80 S. Bhaviripudi, X. Jia, M. S. Dresselhaus and J. Kong, *Nano Lett.*, 2010, **10**, 4128–4133.
81 M. P. Lavin-Lopez, J. L. Valverde, M. C. Cuevas, A. Garrido, L. Sanchez-Silva, P. Martinez and A. Romero-Izquierdo, *Phys. Chem. Chem. Phys.*, 2014, **16**, 2962–2970.
82 Q. Zhang, B. Han, X. Tang, K. Heier, J. X. Li, J. Hoffman, M. Lin, S. L. Britton, A. Derecskei-Kovacs and H. Cheng, *J. Phys. Chem. C*, 2012, **116**, 16522–16531.
83 N. Zhan, G. Wang and J. Liu, *Appl. Phys. A: Mater. Sci. Process.*, 2011, **105**, 341–345.
84 J. Hwang, M. Kim, D. Campbell, H. A. Alsalman, J. Y. Kwak, S. Shivaraman, A. R. Woll, A. K. Singh, R. G. Hennig, S. Gorantla, M. H. Rummeli and M. G. Spencer, *ACS Nano*, 2013, **7**, 385–395.
85 B. Hu, Z. Wei, H. Ago, Y. Jin, M. Xia, Z. Luo, Q. Pan and Y. Liu, *Sci. China: Chem.*, 2014, **57**, 895–901.
86 X. Zhou, J. Shi, Y. Qi, M. Liu, D. Ma, Y. Zhang, Q. Ji, Z. Zhang, C. Li, Z. Liu and Y. Zhang, *ACS Nano*, 2016, **10**, 3461–3468.
87 Y. Zhang, Y. Zhang, Q. Ji, J. Ju, H. Yuan, J. Shi, T. Gao, D. Ma, M. Liu, Y. Chen, X. Song, H. Y. Hwang, Y. Cui and Z. Liu, *ACS Nano*, 2013, **7**, 8963–8971.
88 A. Sanne, R. Ghosh, A. Rai, H. C. P. Movva, A. Sharma, R. Rao, L. Mathew and S. K. Banerjee, *Appl. Phys. Lett.*, 2015, **106**, 062101.
89 J. D. Cain, F. Shi, J. Wu and V. P. Dravid, *ACS Nano*, 2016, **10**, 5440–5445.
90 Y. H. Lee, X. Q. Zhang, W. Zhang, M. T. Chang, C. T. Lin, K. D. Chang, Y. C. Yu, J. T. Wang, C. S. Chang, L. J. Li and T. W. Lin, *Adv. Mater.*, 2012, **24**, 2320–2325.
91 B. Li, Y. Gong, Z. Hu, G. Brunetto, Y. Yang, G. Ye, Z. Zhang, S. Lei, Z. Jin, E. Bianco, X. Zhang, W. Wang, J. Lou, D. S. Galvao, M. Tang, B. I. Yakobson, R. Vajtai and P. M. Ajayan, *Angew. Chem., Int. Ed.*, 2016, **55**, 10656–10661.
92 X. Ling, Y. H. Lee, Y. Lin, W. Fang, L. Yu, M. S. Dresselhaus and J. Kong, *Nano Lett.*, 2014, **14**, 464–472.
93 L. Chen, B. Liu, M. Ge, Y. Ma, A. N. Abbas and C. Zhou, *ACS Nano*, 2015, **9**, 8368–8375.
94 J. Shi, X. Zhang, D. Ma, J. Zhu, Y. Zhang, Z. Guo, Y. Yao, Q. Ji, X. Song, Y. Zhang, C. Li, Z. Liu, W. Zhu and Y. Zhang, *ACS Nano*, 2015, **9**, 4017–4025.
95 K. Hayashi, S. Sato, M. Ikeda, C. Kaneta and N. Yokoyama, *J. Am. Chem. Soc.*, 2012, **134**, 12492–12498.
96 S. Chaitoglou and E. Bertran, *J. Mater. Sci.*, 2017, **52**, 8348–8356.
97 A. A. Koos, A. T. Murdock, P. Nemes-Incze, R. J. Nicholls, A. J. Pollard, S. J. Spencer, A. G. Shard, D. Roy, L. P. Biro and N. Grobert, *Phys. Chem. Chem. Phys.*, 2014, **16**, 19446–19452.
98 B. Liu, M. Fathi, L. Chen, A. Abbas, Y. Ma and C. Zhou, *ACS Nano*, 2015, **9**, 6119–6127.
99 N. Selvakumar, B. Vadivel, D. V. S. Rao, S. B. Krupanidhi and H. C. Barshilia, *Appl. Phys. A: Mater. Sci. Process.*, 2016, **122**, 943.
100 J. C. Koepke, J. D. Wood, Y. Chen, S. W. Schmucker, X. Liu, N. N. Chang, L. Nienhaus, J. W. Do, E. A. Carrion, J. Hewaparakrama, A. Rangarajan, I. Datye, R. Mehta, R. T. Haasch, M. Gruebele, G. S. Girolami, E. Pop and J. W. Lyding, *Chem. Mater.*, 2016, **28**, 4169–4179.

101 T. Gao, X. Song, H. Du, Y. Nie, Y. Chen, Q. Ji, J. Sun, Y. Yang, Y. Zhang and Z. Liu, *Nat. Commun.*, 2015, **6**, 6835.
102 Q. Li, Z. Zhao, B. Yan, X. Song, Z. Zhang, J. Li, X. Wu, Z. Bian, X. Zou, Y. Zhang and Z. Liu, *Adv. Mater.*, 2017, **29**, 1701325.
103 W. Xu, D. Kozawa, Y. Liu, Y. Sheng, K. Wei, V. B. Koman, S. Wang, X. Wang, T. Jiang, M. S. Strano and J. H. Warner, *Small*, 2018, **14**, e1703727.
104 Y. Gong, J. Lin, X. Wang, G. Shi, S. Lei, Z. Lin, X. Zou, G. Ye, R. Vajtai, B. I. Yakobson, H. Terrones, M. Terrones, B. K. Tay, J. Lou, S. T. Pantelides, Z. Liu, W. Zhou and P. M. Ajayan, *Nat. Mater.*, 2014, **13**, 1135–1142.
105 Y. Gong, S. Lei, G. Ye, B. Li, Y. He, K. Keyshar, X. Zhang, Q. Wang, J. Lou, Z. Liu, R. Vajtai, W. Zhou and P. M. Ajayan, *Nano Lett.*, 2015, **15**, 6135–6141.
106 Y. Xue, Y. Zhang, Y. Liu, H. Liu, J. Song, J. Sophia, J. Liu, Z. Xu, Q. Xu, Z. Wang, J. Zheng, Y. Liu, S. Li and Q. Bao, *ACS Nano*, 2016, **10**, 573–580.
107 J. Shi, R. Tong, X. Zhou, Y. Gong, Z. Zhang, Q. Ji, Y. Zhang, Q. Fang, L. Gu, X. Wang, Z. Liu and Y. Zhang, *Adv. Mater.*, 2016, **28**, 10664–10672.
108 L. Yu, Y. H. Lee, X. Ling, E. J. Santos, Y. C. Shin, Y. Lin, M. Dubey, E. Kaxiras, J. Kong, H. Wang and T. Palacios, *Nano Lett.*, 2014, **14**, 3055–3063.
109 T. Georgiou, R. Jalil, B. D. Belle, L. Britnell, R. V. Gorbachev, S. V. Morozov, Y. J. Kim, A. Gholinia, S. J. Haigh, O. Makarovsky, L. Eaves, L. A. Ponomarenko, A. K. Geim, K. S. Novoselov and A. Mishchenko, *Nat. Nanotechnol.*, 2013, **8**, 100–103.
110 K. Roy, M. Padmanabhan, S. Goswami, T. P. Sai, G. Ramalingam, S. Raghavan and A. Ghosh, *Nat. Nanotechnol.*, 2013, **8**, 826–830.
111 P. T. Loan, W. Zhang, C. T. Lin, K. H. Wei, L. J. Li and C. H. Chen, *Adv. Mater.*, 2014, **26**, 4838–4844.
112 J. Shi, M. Liu, J. Wen, X. Ren, X. Zhou, Q. Ji, D. Ma, Y. Zhang, C. Jin, H. Chen, S. Deng, N. Xu, Z. Liu and Y. Zhang, *Adv. Mater.*, 2015, **27**, 7086–7092.
113 T. Chen, Y. Zhou, Y. Sheng, X. Wang, S. Zhou and J. H. Warner, *ACS Appl. Mater. Interfaces*, 2018, **10**, 7304–7314.
114 C. R. Dean, L. Wang, P. Maher, C. Forsythe, F. Ghahari, Y. Gao, J. Katoch, M. Ishigami, P. Moon, M. Koshino, T. Taniguchi, K. Watanabe, K. L. Shepard, J. Hone and P. Kim, *Nature*, 2013, **497**, 598–602.
115 C. Jin, J. Kim, J. Suh, Z. Shi, B. Chen, X. Fan, M. Kam, K. Watanabe, T. Taniguchi, S. Tongay, A. Zettl, J. Wu and F. Wang, *Nat. Phys.*, 2016, **13**, 127–131.
116 D. Fu, X. Zhao, Y. Y. Zhang, L. Li, H. Xu, A. R. Jang, S. I. Yoon, P. Song, S. M. Poh, T. Ren, Z. Ding, W. Fu, T. J. Shin, H. S. Shin, S. T. Pantelides, W. Zhou and K. P. Loh, *J. Am. Chem. Soc.*, 2017, **139**, 9392–9400.
117 A. Yan, J. Velasco Jr, S. Kahn, K. Watanabe, T. Taniguchi, F. Wang, M. F. Crommie and A. Zettl, *Nano Lett.*, 2015, **15**, 6324–6331.
118 P. Sutter, Y. Huang and E. Sutter, *Nano Lett.*, 2014, **14**, 4846–4851.
119 Z. Liu, L. Ma, G. Shi, W. Zhou, Y. Gong, S. Lei, X. Yang, J. Zhang, J. Yu, K. P. Hackenberg, A. Babakhani, J. C. Idrobo, R. Vajtai, J. Lou and P. M. Ajayan, *Nat. Nanotechnol.*, 2013, **8**, 119–124.
120 L. Ci, L. Song, C. Jin, D. Jariwala, D. Wu, Y. Li, A. Srivastava, Z. F. Wang, K. Storr, L. Balicas, F. Liu and P. M. Ajayan, *Nat. Mater.*, 2010, **9**, 430–435.
121 S. M. Kim, A. Hsu, P. T. Araujo, Y. H. Lee, T. Palacios, M. Dresselhaus, J. C. Idrobo, K. K. Kim and J. Kong, *Nano Lett.*, 2013, **13**, 933–941.
122 L. Liu, J. Park, D. A. Siegel, K. F. McCarty, K. W. Clark, W. Deng, L. Basile, J. C. Idrobo, A.-P. Li and G. Gu, *Science*, 2014, **343**, 163.
123 P. Sutter, R. Cortes, J. Lahiri and E. Sutter, *Nano Lett.*, 2012, **12**, 4869–4874.
124 Y. Gao, Y. Zhang, P. Chen, Y. Li, M. Liu, T. Gao, D. Ma, Y. Chen, Z. Cheng, X. Qiu, W. Duan and Z. Liu, *Nano Lett.*, 2013, **13**, 3439–3443.
125 M.-Y. Li, Y. Shi, C.-C. Cheng, L.-S. Lu, Y.-C. Lin, H.-L. Tang, M.-L. Tsai, C.-W. Chu, K.-H. Wei, J.-H. He, W.-H. Chang, K. Suenaga and L.-J. Li, *Science*, 2015, **349**, 524.
126 H. Li, P. Li, J. K. Huang, M. Y. Li, C. W. Yang, Y. Shi, X. X. Zhang and L. J. Li, *ACS Nano*, 2016, **10**, 10516–10523.
127 M. Mahjouri-Samani, M. W. Lin, K. Wang, A. R. Lupini, J. Lee, L. Basile, A. Boulesbaa, C. M. Rouleau, A. A. Puretzky, I. N. Ivanov, K. Xiao, M. Yoon and D. B. Geohegan, *Nat. Commun.*, 2015, **6**, 7749.
128 S. J. Yun, G. H. Han, H. Kim, D. L. Duong, B. G. Shin, J. Zhao, Q. A. Vu, J. Lee, S. M. Lee and Y. H. Lee, *Nat. Commun.*, 2017, **8**, 2163.
129 S.-S. Lee, K.-H. Choi, S.-H. Kim and S.-Y. Lee, *Adv. Funct. Mater.*, 2018, **28**, 1705571.
130 K.-H. Choi, H.-W. Kim, S.-S. Lee, J. Yoo, D.-G. Lee and S.-Y. Lee, *Adv. Sustainable Syst.*, 2018, **2**, 1700132.
131 W. S. Hummers, *J. Am. Chem. Soc.*, 1958, **80**, 1339.
132 C.-Y. Su, A.-Y. Lu, Y. Xu, F.-R. Chen, A. N. Khlobystov and L.-J. Li, *ACS Nano*, 2011, **5**, 2332–2339.
133 S. Yang, S. Bruller, Z. S. Wu, Z. Liu, K. Parvez, R. Dong, F. Richard, P. Samori, X. Feng and K. Mullen, *J. Am. Chem. Soc.*, 2015, **137**, 13927–13932.
134 K. Parvez, Z. S. Wu, R. Li, X. Liu, R. Graf, X. Feng and K. Müllen, *J. Am. Chem. Soc.*, 2014, **136**, 6083–6091.
135 T. Liu, X. Zhang, K. Liu, Y. Liu, M. Liu, W. Wu, Y. Gu and R. Zhang, *Nanotechnology*, 2018, **29**, 095401.
136 A. B. Bourlinos, V. Georgakilas, R. Zboril, T. A. Steriotis, A. K. Stubos and C. Trapalis, *Solid State Commun.*, 2009, **149**, 2172–2176.
137 G. Ma, H. Peng, J. Mu, H. Huang, X. Zhou and Z. Lei, *J. Power Sources*, 2013, **229**, 72–78.
138 C. Zhao, X. Wang, J. Kong, J. M. Ang, P. S. Lee, Z. Liu and X. Lu, *ACS Appl. Mater. Interfaces*, 2016, **8**, 2372–2379.
139 Y. Hu, X. Li, A. Lushington, M. Cai, D. Geng, M. N. Banis, R. Li and X. Sun, *ECS J. Solid State Sci. Technol.*, 2013, **2**, M3034–M3039.
140 K.-J. Huang, L. Wang, Y.-J. Liu, Y.-M. Liu, H.-B. Wang, T. Gan and L.-L. Wang, *Int. J. Hydrogen Energy*, 2013, **38**, 14027–14034.

141 X. Xie, Z. Ao, D. Su, J. Zhang and G. Wang, *Adv. Funct. Mater.*, 2015, **25**, 1393–1403.
142 E. G. da Silveira Firmiano, A. C. Rabelo, C. J. Dalmaschio, A. N. Pinheiro, E. C. Pereira, W. H. Schreiner and E. R. Leite, *Adv. Energy Mater.*, 2014, **4**, 1301380.
143 E. G. Firmiano, M. A. Cordeiro, A. C. Rabelo, C. J. Dalmaschio, A. N. Pinheiro, E. C. Pereira and E. R. Leite, *Chem. Commun.*, 2012, **48**, 7687–7689.
144 K. Chang and W. Chen, *Chem. Commun.*, 2011, **47**, 4252–4254.
145 X. Yan, Y. Wang, C. Liu, M. Guo, J. Tao, J. Cao, D. Fu, L. Dai and X. Yang, *J. Energy Chem.*, 2018, **27**, 176–182.
146 L. Jiang, B. Lin, X. Li, X. Song, H. Xia, L. Li and H. Zeng, *ACS Appl. Mater. Interfaces*, 2016, **8**, 2680–2687.
147 X. Xu, C. S. Rout, J. Yang, R. Cao, P. Oh, H. S. Shin and J. Cho, *J. Mater. Chem. A*, 2013, **1**, 14548.
148 K. Shiva, H. S. S. Ramakrishna Matte, H. B. Rajendra, A. J. Bhattacharyya and C. N. R. Rao, *Nano Energy*, 2013, **2**, 787–793.
149 L. Peng, X. Peng, B. Liu, C. Wu, Y. Xie and G. Yu, *Nano Lett.*, 2013, **13**, 2151–2157.
150 P. Xia, B. Zhu, B. Cheng, J. Yu and J. Xu, *ACS Sustainable Chem. Eng.*, 2017, **6**, 965–973.
151 J. Xu, D. Li, Y. Chen, L. Tan, B. Kou, F. Wan, W. Jiang and F. Li, *Nanomaterials*, 2017, **7**(12), 450.
152 M. Naguib, O. Mashtalir, J. Carle, V. Presser, J. Lu, L. Hultman, Y. Gogotsi and M. W. Barsoum, *ACS Nano*, 2012, **6**, 1322–1331.
153 X. Zhang, Z. Zhang and Z. Zhou, *J. Energy Chem.*, 2018, **27**, 73–85.
154 C. Chen, X. Xie, B. Anasori, A. Sarycheva, T. Makaryan, M. Zhao, P. Urbankowski, L. Miao, J. Jiang and Y. Gogotsi, *Angew. Chem., Int. Ed.*, 2018, **57**, 1846–1850.
155 P. Yasaei, A. Behranginia, T. Foroozan, M. Asadi, K. Kim, F. Khalili-Araghi and A. Salehi-Khojin, *ACS Nano*, 2015, **9**, 9898–9905.
156 L. Chen, G. Zhou, Z. Liu, X. Ma, J. Chen, Z. Zhang, X. Ma, F. Li, H. M. Cheng and W. Ren, *Adv. Mater.*, 2016, **28**, 510–517.
157 G. Wang, W. J. Slough, R. Pandey and S. P. Karna, *2D Mater.*, 2016, **3**, 025011.
158 Y. Lin, Y. Pan and J. Zhang, *Int. J. Hydrogen Energy*, 2017, **42**, 7951–7956.
159 H. U. Lee, S. C. Lee, J. Won, B. C. Son, S. Choi, Y. Kim, S. Y. Park, H. S. Kim, Y. C. Lee and J. Lee, *Sci. Rep.*, 2015, **5**, 8691.
160 J. Wang, D. Liu, H. Huang, N. Yang, B. Yu, M. Wen, X. Wang, P. K. Chu and X. F. Yu, *Angew. Chem., Int. Ed.*, 2018, **57**, 2600–2604.
161 A. A. Mamedov, N. A. Kotov, M. Prato, D. M. Guldi, J. P. Wicksted and A. Hirsch, *Nat. Mater.*, 2002, **1**, 190.
162 P. T. Hammond, *Adv. Mater.*, 2004, **16**, 1271–1293.
163 F. Geng, R. Ma, Y. Ebina, Y. Yamauchi, N. Miyamoto and T. Sasaki, *J. Am. Chem. Soc.*, 2014, **136**, 5491–5500.
164 R. Chalasani, A. Gupta and S. Vasudevan, *Sci. Rep.*, 2013, **3**, 3498.
165 L. Li, R. Ma, Y. Ebina, K. Fukuda, K. Takada and T. Sasaki, *J. Am. Chem. Soc.*, 2007, **129**, 8000–8007.
166 J. L. Gunjakar, T. W. Kim, H. N. Kim, I. Y. Kim and S.-J. Hwang, *J. Am. Chem. Soc.*, 2011, **133**, 14998–15007.
167 R. Chalasani, A. Gupta and S. Vasudevan, *Sci. Rep.*, 2013, **3**, 3498.
168 W. Ma, R. Ma, C. Wang, J. Liang, X. Liu, K. Zhou and T. Sasaki, *ACS Nano*, 2015, **9**, 1977–1984.
169 Y. Taguchi, R. Kimura, R. Azumi, H. Tachibana, N. Koshizaki, M. Shimomura, N. Momozawa, H. Sakai, M. Abe and M. Matsumoto, *Langmuir*, 1998, **14**, 6550–6555.
170 M. Muramatsu, K. Akatsuka, Y. Ebina, K. Wang, T. Sasaki, T. Ishida, K. Miyake and M. A. Haga, *Langmuir*, 2005, **21**, 6590–6595.
171 S. Patil, A. Harle, S. Sathaye and K. Patil, *CrystEngComm*, 2014, **16**, 10845–10855.
172 R. E. Schaak and T. E. Mallouk, *Chem. Mater.*, 2002, **14**, 1455–1471.
173 K. Saruwatari, H. Sato, T. Idei, J. Kameda, A. Yamagishi, A. Takagaki and K. Domen, *J. Phys. Chem. B*, 2005, **109**, 12410–12416.
174 C. Ziegler, S. Werner, M. Bugnet, M. Wörsching, V. Duppel, G. A. Botton, C. Scheu and B. V. Lotsch, *Chem. Mater.*, 2013, **25**, 4892–4900.
175 R. Gao, D. Yan, D. G. Evans and X. Duan, *Nano Res.*, 2017, **10**, 3606–3617.
176 L. Jia, W. Cai and H. Wang, *J. Mater. Chem.*, 2009, **19**, 7301.
177 F. Xiang, D. Parviz, T. M. Givens, P. Tzeng, E. M. Davis, C. M. Stafford, M. J. Green and J. C. Grunlan, *Adv. Funct. Mater.*, 2016, **26**, 2143–2149.
178 K. Hu, M. K. Gupta, D. D. Kulkarni and V. V. Tsukruk, *Adv. Mater.*, 2013, **25**, 2301–2307.
179 D. D. Kulkarni, I. Choi, S. S. Singamaneni and V. V. Tsukruk, *ACS Nano*, 2010, **4**, 4667–4676.
180 J.-B. Wu, M.-L. Lin, X. Cong, H.-N. Liu and P.-H. Tan, *Chem. Soc. Rev.*, 2018, **47**, 1822–1873.
181 A. Mohsin, L. Liu, P. Liu, W. Deng, I. N. Ivanov, G. Li, O. E. Dyck, G. Duscher, J. R. Dunlap, K. Xiao and G. Gu, *ACS Nano*, 2013, **7**, 8924–8931.
182 P. H. Jacobse, A. Kimouche, T. Gebraad, M. M. Ervasti, J. M. Thijssen, P. Liljeroth and I. Swart, *Nat. Commun.*, 2017, **8**, 119.
183 H. Ghorbanfekr-Kalashami, K. S. Vasu, R. R. Nair, F. M. Peeters and M. Neek-Amal, *Nat. Commun.*, 2017, **8**, 15844.
184 J. Qi, Y. W. Lan, A. Z. Stieg, J. H. Chen, Y. L. Zhong, L. J. Li, C. D. Chen, Y. Zhang and K. L. Wang, *Nat. Commun.*, 2015, **6**, 7430.
185 C. R. Woods, L. Britnell, A. Eckmann, R. S. Ma, J. C. Lu, H. M. Guo, X. Lin, G. L. Yu, Y. Cao, R. V. Gorbachev, A. V. Kretinin, J. Park, L. A. Ponomarenko, M. I. Katsnelson, Y. N. Gornostyrev, K. Watanabe, T. Taniguchi, C. Casiraghi, H. J. Gao, A. K. Geim and K. S. Novoselov, *Nat. Phys.*, 2014, **10**, 451–456.
186 O. Deniz, C. Sánchez-Sánchez, T. Dumslaff, X. Feng, A. Narita, K. Müllen, N. Kharche, V. Meunier, R. Fasel and P. Ruffieux, *Nano Lett.*, 2017, **17**, 2197–2203.

187 H. Liu, H. Zheng, F. Yang, L. Jiao, J. Chen, W. Ho, C. Gao, J. Jia and M. Xie, *ACS Nano*, 2015, **9**, 6619–6625.
188 B. Uder, H. Gao, P. Kunnas, N. de Jonge and U. Hartmann, *Nanoscale*, 2018, **10**, 2148–2153.
189 W. Melitz, J. Shen, A. C. Kummel and S. Lee, *Surf. Sci. Rep.*, 2011, **66**, 1–27.
190 H. Li, X. Qi, J. Wu, Z. Zeng, J. Wei and H. Zhang, *ACS Nano*, 2013, **7**, 2842–2849.
191 R. F. Egerton, *Rep. Prog. Phys.*, 2009, **72**, 016502.
192 D. A. Muller, *Nat. Mater.*, 2009, **8**, 263–270.
193 X. Ling, Y. Lin, Q. Ma, Z. Wang, Y. Song, L. Yu, S. Huang, W. Fang, X. Zhang, A. L. Hsu, Y. Bie, Y. H. Lee, Y. Zhu, L. Wu, J. Li, P. Jarillo-Herrero, M. Dresselhaus, T. Palacios and J. Kong, *Adv. Mater.*, 2016, **28**, 2322–2329.
194 X. Q. Zhang, C. H. Lin, Y. W. Tseng, K. H. Huang and Y. H. Lee, *Nano Lett.*, 2015, **15**, 410–415.
195 S. B. Desai, S. R. Madhvapathy, M. Amani, D. Kiriya, M. Hettick, M. Tosun, Y. Zhou, M. Dubey, J. W. Ager 3rd, D. Chrzan and A. Javey, *Adv. Mater.*, 2016, **28**, 4053–4058.
196 K. Zhang, N. J. Borys, B. M. Bersch, G. R. Bhimanapati, K. Xu, B. Wang, K. Wang, M. Labella, T. A. Williams, M. A. Haque, E. S. Barnard, S. Fullerton-Shirey, P. J. Schuck and J. A. Robinson, *Sci. Rep.*, 2017, **7**, 16938.
197 X. Zhang, Q. H. Tan, J. B. Wu, W. Shi and P. H. Tan, *Nanoscale*, 2016, **8**, 6435–6450.
198 Y. y. Wang, Z. h. Ni, T. Yu, Z. X. Shen, H. m. Wang, Y. h. Wu, W. Chen and A. T. Shen Wee, *J. Phys. Chem. C*, 2008, **112**, 10637–10640.
199 H. Li, Q. Zhang, C. C. R. Yap, B. K. Tay, T. H. T. Edwin, A. Olivier and D. Baillargeat, *Adv. Funct. Mater.*, 2012, **22**, 1385–1390.
200 O. L. Krivanek, M. F. Chisholm, V. Nicolosi, T. J. Pennycook, G. J. Corbin, N. Dellby, M. F. Murfitt, C. S. Own, Z. S. Szilagyi, M. P. Oxley, S. T. Pantelides and S. J. Pennycook, *Nature*, 2010, **464**, 571–574.
201 D. Zeng, L. Xiao, W. J. Ong, P. Wu, H. Zheng, Y. Chen and D. L. Peng, *ChemSusChem*, 2017, **10**, 4624–4631.
202 K. G. Zhou, F. Withers, Y. Cao, S. Hu, G. Yu and C. Casiraghi, *ACS Nano*, 2014, **8**, 9914–9924.
203 M. G. Donato, E. Messina, A. Foti, T. J. Smart, P. H. Jones, M. A. Iati, R. Saija, P. G. Gucciardi and O. M. Marago, *Nanoscale*, 2018, **10**, 1245–1255.
204 O. Frank, M. S. Dresselhaus and M. Kalbac, *Acc. Chem. Res.*, 2015, **48**, 111–118.
205 M. Pena-Alvarez, E. del Corro, A. Morales-Garcia, L. Kavan, M. Kalbac and O. Frank, *Nano Lett.*, 2015, **15**, 3139–3146.
206 Y. P. Zhu, C. Guo, Y. Zheng and S.-Z. Qiao, *Acc. Chem. Res.*, 2017, **50**, 915–923.
207 C. Hu and L. Dai, *Angew. Chem., Int. Ed.*, 2016, **55**, 11736–11758.
208 L. Zhang, X. Luo and Y. Li, *J. Energy Chem.*, 2018, **27**, 243–249.
209 E. Antolini, *Appl. Catal., B*, 2012, **123–124**, 52–68.
210 D. Deng, L. Yu, X. Pan, S. Wang, X. Chen, P. Hu, L. Sun and X. Bao, *Chem. Commun.*, 2011, **47**, 10016–10018.
211 T. F. Jaramillo, K. P. Jørgensen, J. Bonde, J. H. Nielsen, S. Horch and I. Chorkendorff, *Science*, 2007, **317**, 100.
212 X. Chia, A. Y. Eng, A. Ambrosi, S. M. Tan and M. Pumera, *Chem. Rev.*, 2015, **115**, 11941–11966.
213 S. Yin, W. Tu, Y. Sheng, Y. Du, M. Kraft, A. Borgna and R. Xu, *Adv. Mater.*, 2018, **30**, 1705106.
214 Y. Li, H. Wang, L. Xie, Y. Liang, G. Hong and H. Dai, *J. Am. Chem. Soc.*, 2011, **133**, 7296–7299.
215 D. Kong, H. Wang, J. J. Cha, M. Pasta, K. J. Koski, J. Yao and Y. Cui, *Nano Lett.*, 2013, **13**, 1341–1347.
216 J. H. Yu, H. R. Lee, S. S. Hong, D. Kong, H. W. Lee, H. Wang, F. Xiong, S. Wang and Y. Cui, *Nano Lett.*, 2015, **15**, 1031–1035.
217 H. Huang, J. Huang, W. Liu, Y. Fang and Y. Liu, *ACS Appl. Mater. Interfaces*, 2017, **9**, 39380–39390.
218 B. Hinnemann, P. G. Moses, J. Bonde, K. P. Jørgensen, J. H. Nielsen, S. Horch, I. Chorkendorff and J. K. Nørskov, *J. Am. Chem. Soc.*, 2005, **127**, 5308–5309.
219 T. F. Jaramillo, J. Bonde, J. Zhang, B.-L. Ooi, K. Andersson, J. Ulstrup and I. Chorkendorff, *J. Phys. Chem. C*, 2008, **112**, 17492–17498.
220 Z. He, C. Kim, L. Lin, T. H. Jeon, S. Lin, X. Wang and W. Choi, *Nano Energy*, 2017, **42**, 58–68.
221 W. Ma, R. Ma, C. Wang, J. Liang, X. Liu, K. Zhou and T. Sasaki, *ACS Nano*, 2015, **9**, 1977–1984.
222 J. Yang, D. Voiry, S. J. Ahn, D. Kang, A. Y. Kim, M. Chhowalla and H. S. Shin, *Angew. Chem., Int. Ed.*, 2013, **52**, 13751–13754.
223 M. R. Gao, J. X. Liang, Y. R. Zheng, Y. F. Xu, J. Jiang, Q. Gao, J. Li and S. H. Yu, *Nat. Commun.*, 2015, **6**, 5982.
224 Z. Wang, T. Chen, W. Chen, K. Chang, L. Ma, G. Huang, D. Chen and J. Y. Lee, *J. Mater. Chem. A*, 2013, **1**, 2202–2210.
225 H. Li, K. Yu, H. Fu, B. Guo, X. Lei and Z. Zhu, *J. Phys. Chem. C*, 2015, **119**, 7959–7968.
226 Y. Ge, C. Wang, Y. Zhao, Y. Liu, Y. Chao, T. Zheng and G. G. Wallace, *Small*, 2018, **14**, 1703096.
227 J. Wang, J. Liu, D. Chao, J. Yan, J. Lin and Z. X. Shen, *Adv. Mater.*, 2014, **26**, 7162–7169.
228 H.-E. Wang, X. Zhao, X. Li, Z. Wang, C. Liu, Z. Lu, W. Zhang and G. Cao, *J. Mater. Chem. A*, 2017, **5**, 25056–25063.
229 Y. Yang, X. Zhao, H.-E. Wang, M. Li, C. Hao, M. Ji, S. Ren and G. Cao, *J. Mater. Chem. A*, 2018, **6**, 3479–3487.
230 J. Mei, T. Liao and Z. Sun, *J. Energy Chem.*, 2018, **27**, 117–127.
231 Y. Dong, Z.-S. Wu, W. Ren, H.-M. Cheng and X. Bao, *Sci. Bull.*, 2017, **62**, 724–740.
232 T. Li and Q. Zhang, *J. Energy Chem.*, 2018, **27**, 373–374.
233 B. Luo, Y. Hu, X. Zhu, T. Qiu, L. Zhi, M. Xiao, H. Zhang, M. Zou, A. Cao and L. Wang, *J. Mater. Chem. A*, 2018, **6**, 1462–1472.
234 L. David, R. Bhandavat and G. Singh, *ACS Nano*, 2014, **8**, 1759–1770.
235 Y. Xie, Y. Dall'Agnese, M. Naguib, Y. Gogotsi, M. W. Barsoum, H. L. Zhuang and P. R. Kent, *ACS Nano*, 2014, **8**, 9606–9615.
236 D. Er, J. Li, M. Naguib, Y. Gogotsi and V. B. Shenoy, *ACS Appl. Mater. Interfaces*, 2014, **6**, 11173–11179.
237 Q. Tang, Z. Zhou and P. Shen, *J. Am. Chem. Soc.*, 2012, **134**, 16909–16916.

238 Y. Aierken, C. Sevik, O. Gülseren, F. M. Peeters and D. Çakır, *J. Mater. Chem. A*, 2018, **6**, 2337–2345.
239 W. Bao, X. Xie, J. Xu, X. Guo, J. Song, W. Wu, D. Su and G. Wang, *Chemistry*, 2017, **23**, 12613–12619.
240 M. A. Bissett, I. A. Kinloch and R. A. Dryfe, *ACS Appl. Mater. Interfaces*, 2015, **7**, 17388–17398.
241 A. Gigot, M. Fontana, M. Serrapede, M. Castellino, S. Bianco, M. Armandi, B. Bonelli, C. F. Pirri, E. Tresso and P. Rivolo, *ACS Appl. Mater. Interfaces*, 2016, **8**, 32842–32852.
242 Z. S. Wu, Y. Zheng, S. Zheng, S. Wang, C. Sun, K. Parvez, T. Ikeda, X. Bao, K. Mullen and X. Feng, *Adv. Mater.*, 2017, **29**, 1602960.
243 Z. Ling, C. E. Ren, M.-Q. Zhao, J. Yang, J. M. Giammarco, J. Qiu, M. W. Barsoum and Y. Gogotsi, *Proc. Natl. Acad. Sci. U. S. A.*, 2014, **111**, 16676.
244 W. Liu, Z. Wang, Y. Su, Q. Li, Z. Zhao and F. Geng, *Adv. Energy Mater.*, 2017, **7**, 1602834.
245 D. Geng, X. Zhao, Z. Chen, W. Sun, W. Fu, J. Chen, W. Liu, W. Zhou and K. P. Loh, *Adv. Mater.*, 2017, **29**, 1700072.
246 A. J. Molina-Mendoza, E. Giovanelli, W. S. Paz, M. A. Nino, J. O. Island, C. Evangeli, L. Aballe, M. Foerster, H. S. van der Zant, G. Rubio-Bollinger, N. Agrait, J. J. Palacios, E. M. Perez and A. Castellanos-Gomez, *Nat. Commun.*, 2017, **8**, 14409.
247 M. Hu, Z. Li, T. Hu, S. Zhu, C. Zhang and X. Wang, *ACS Nano*, 2016, **10**, 11344–11350.
248 L. Mai, Y. Dong, L. Xu and C. Han, *Nano Lett.*, 2010, **10**, 4273–4278.
249 N. Shpigel, M. D. Levi, S. Sigalov, L. Daikhin and D. Aurbach, *Acc. Chem. Res.*, 2018, **51**, 69–79.
250 S. Wang, Z. S. Wu, S. Zheng, F. Zhou, C. Sun, H. M. Cheng and X. Bao, *ACS Nano*, 2017, **11**, 4283–4291.
251 S. Zheng, Z. Li, Z. S. Wu, Y. Dong, F. Zhou, S. Wang, Q. Fu, C. Sun, L. Guo and X. Bao, *ACS Nano*, 2017, **11**, 4009–4016.
252 X. Shi, Z. S. Wu, J. Qin, S. Zheng, S. Wang, F. Zhou, C. Sun and X. Bao, *Adv. Mater.*, 2017, **29**, 1703034.
253 G. C. Guo, D. Wang, X. L. Wei, Q. Zhang, H. Liu, W. M. Lau and L. M. Liu, *J. Phys. Chem. Lett.*, 2015, **6**, 5002–5008.
254 T. M. Dinh, A. Achour, S. Vizireanu, G. Dinescu, L. Nistor, K. Armstrong, D. Guay and D. Pech, *Nano Energy*, 2014, **10**, 288–294.
255 X. Cao, Y. Shi, W. Shi, G. Lu, X. Huang, Q. Yan, Q. Zhang and H. Zhang, *Small*, 2011, **7**, 3163–3168.
256 C. Tang, L. Zhong, B. Zhang, H. F. Wang and Q. Zhang, *Adv. Mater.*, 2018, **30**, 1705110.
257 G. Hu, C. Xu, Z. Sun, S. Wang, H. M. Cheng, F. Li and W. Ren, *Adv. Mater.*, 2016, **28**, 1603–1609.
258 M. Li, N. Muralidharan, K. Moyer and C. L. Pint, *Nanoscale*, 2018, **10**, 10443–10449.
259 A. Abouimrane, D. Dambournet, K. W. Chapman, P. J. Chupas, W. Weng and K. Amine, *J. Am. Chem. Soc.*, 2012, **134**, 4505–4508.
260 J. Xu, J. Ma, Q. Fan, S. Guo and S. Dou, *Adv. Mater.*, 2017, **29**, 1606454.